

MOLECULAR MODELING OF L-TYPE

CA²⁺ CHANNEL WITH LIGANDS

**MOLECULAR MODELING OF L-TYPE
CALCIUM CHANNEL WITH CALCIUM IONS
AND LIGANDS**

By

EKATERINA FOLKMAN, B.Sc. M.Sc.

A thesis Submitted to School of Graduate Studies
In Partial Fulfillment of the Requirements
For the Degree
Master of Science

Department of Biochemistry
McMaster University

©Copyright by Ekaterina Folkman, May 2001

MASTER OF SCIENCE (2001)

McMaster University

(Biochemistry)

Hamilton, Ontario

TITLE: Molecular Modeling of L-Type Calcium Channel with Calcium Ions and
Ligands.

AUTHOR : Ekaterina Folkman, B.Sc. M.Sc. in Physics (St.Petersburg State Technical
University, Russia)

SUPERVISOR: Professor V.S.Ananthanarayanan

NUMBER OF PAGES: xiv, 160

Abstract

In the absence of X-ray structure of L-type Ca^{2+} channel (LCC), we have built a homology model of LCC based on the crystal structure of KcsA channel and have performed a series of docking simulations. The search for lowest-energy conformations was performed by the Monte Carlo energy-minimization method. To obtain the conformation with the lowest energy where dihydropyridine (DHP) ligand forms optimal contacts with the DHP-sensing residues of the channel, we have tested different sequence alignments between KcsA and LCC, and have docked the ligand inside the pore of the channel as well as into the interface between repeats IIIS5-IIIS6-IVS6. The LCC ligand tetrandrine was used during the studies of the selectivity filter of the channel. Conformational studies of the drug and its interaction with Ca^{2+} ions in a non-polar solution were performed by NMR spectroscopy. These experiments have demonstrated the binding of Ca^{2+} ions to the ligand.

In the model based on the alignment proposed by Lipkind and Fozzard (2000), the DHP ligand nifedipine fits inside the pore and forms favorable contacts with several hydrophobic DHP-sensing residues, and forms hydrogen bonds with conserved tyrosines in repeats III and IV. These interactions stabilize the portside-down docking mode of nifedipine, in which this blocker exposes its hydrophobic methoxy group to the

bracelet of hydrophobic residues forming the gate of the channel near the crossing of the bundle of helices. This stabilizes the closed state of the channel. In contrast, the agonist has the hydrophilic group at its portside. The favorable interaction of this group with hydrated Ca^{2+} ion facilitates its permeation through hydrophobic gate. We have simulated the passage of the hydrated ion along the pore with the agonist bound inside and determined several residues crucial for this passage. The role of these residues can be tested experimentally.

Acknowledgements

I would like to express my gratitude to my scientific supervisor Dr. V.S.Ananthanarayanan for guiding me during this project. I highly appreciate the great help of Dr. B.S. Zhorov in all modeling studies. I thank Dr. D.W.Hughes who trained me and helped in acquisition of NMR spectra, as well as Dr. A.D.Bain for his interesting and useful suggestions. In addition, I would like to thank the members of my supervisory committee, Dr. P.Berti and Dr. C.Y Kwan.

Table of contents

Abstractiii
Acknowledgementsv
Table of contentsvi
Abbreviationsix
List of illustrationsxi
List of tablesxiii
Chapter 1. Introduction	1
1.1. Ion Channels	1
1.2. Voltage-gated Ca ²⁺ channels	4
1.1.1 <i>Functions of voltage-gated Ca²⁺ channels</i>	4
1.1.2 <i>Types of voltage-gated Ca²⁺ channels</i>	5
1.1.3 <i>Subunit structure of Ca²⁺ channels</i>	7
1.1.4 <i>Ion selectivity of Ca²⁺ channels</i>	10
1.1.5 <i>Ca²⁺ channel modulation</i>	12
1.3. Ca ²⁺ -binding proteins	15
1.4. Ligands of L-type Ca ²⁺ channel	19
1.4.1 <i>Phenylalkylamines</i>	19

1.4.2. <i>Benzothiazepines</i>	20
1.4.3. <i>Dihydropyridines</i>	21
1.5. Objectives of current project ..	25
Chapter 2. Methods	28
2.1. Nomenclature and multiple sequence alignment	28
2.2. Molecular Modeling	30
2.3. Experimental methods ..	37
2.4. Nuclear Magnetic Resonance Spectroscopy	38
2.4.1. <i>Chemical shift</i>	38
2.4.2. <i>Coupling constant</i>	39
2.4.3. <i>One-dimensional and two-dimensional NMR experiments</i>	40
Chapter 3. Results	44
3.1. Initial Test Models based on alternative alignments ..	44
3.1.1. <i>Test Models</i>	44
3.1.2. <i>Docking of DHP into Test Models</i>	50
3.2. Conformational studies of tetrandrine	64
3.2.1. <i>Conformational analysis of tetrandrine</i>	67
3.2.2. <i>NMR studies of the drug</i>	71

3.2.3. Stochastically restrained MCM search	77
3.2.4. NMR of Ca^{2+} -bound tetrandrine in TFE	79
3.2.5. The modeling of tetrandrine interaction with Ca^{2+} ...	90
3.2.6. Tetrandrine docking into the model	92
3.3. Modeling of LCC selectivity filter with bound nifedipine	99
3.4. The docking of DHP ligands into the pore of LCC	106
3.4.1. Different binding modes of nifedipine	106
3.4.2. Docking of (R)- and (S)- enantiomers of Bay K 8644 into the model	115
3.5. Ca^{2+} permeation through agonist-bound pore	119
Chapter 4. Discussion	125
Chapter 5. Bibliography	137

Abbreviations

BTZ	-	benzothiazepine
COSY	-	correlation spectroscopy
DHP	-	dihydropyridine
GPCR	-	G-protein coupled receptor
KcsA	-	inwardly rectifying bacterial potassium channel of <i>Streptomyces lividans</i>
LA	-	local anesthetic drug
LCC	-	L-type calcium channel
M1(M2)	-	transmembrane segments of KcsA, homologous to S5 and S6 segments of VGICs
MCM	-	Monte Carlo Minimization
MEC	-	minimum-energy conformation
NCS	-	neuronal calcium sensors
NMR	-	Nuclear Magnetic Resonance
NOE	-	Nuclear Overhauser Effect
NOESY	-	Nuclear Overhauser Effect spectroscopy
ns	-	number of scans
ni	-	number of increments
PAA	-	phenylalkylamine
ROESY	-	rotating frame modification of NOESY
S1 to S6	-	membrane-spanning α -helical segments of voltage-gated ion channels

SNARE-	Soluble NSF attachment protein receptor
SR MCM -	stochastically restrained MCM search
TD -	(S,S)--(+)-tetrandrine
TFE -	trifluoroethanol
TM -	transmembrane
TOCSY -	total correlation spectroscopy
T-ROESY -	transverse-ROESY
VGICs -	voltage-gated ion channels
ZMM -	Zhorov Molecular Mechanics

List of Illustrations

Fig.1.1. Subunit structure of voltage-gated Ca ²⁺ channel	8
Fig.1.2. Structure of the α_1 -subunit of LCC	10
Fig. 1.3. Structures and activities of DHPs	23
Fig. 3.1. Dimensions of biologically active conformation of nifedipine	50
Fig. 3.2. Schemes of possible orientations of DHPs inside the pore of LCC	52
Fig. 3.3 A. The lowest-energy conformation of nifedipine bound inside the pore of Test Model 1	56
Fig. 3.3 B. Nifedipine bound in the interface III/V of Test Model I	58
Fig. 3.3 C. Nifedipine bound inside the pore of Test Model II	60
Fig. 3.3 D. Nifedipine in the III/IV interface of Test Model II	62
Fig. 3.4. Structural formula of (S,S) -(+) – tetrandrine	66
Fig.3.5. The 9-membered virtual cycle representation of tetrandrine.	67
Fig. 3.6. Superposition of triangle-shaped MECs and square-shaped MECs of TD	70
Fig.3.7. 1D proton spectrum of TD in CDCl ₃ processed with Gaussian Multiplication	71
Fig.3.8. T-ROESY spectrum of TD in CDCl ₃	73
Fig. 3.9. 1D ¹ H-NMR spectra of TD in TFE before and after addition of 1:1 molar ratio of Ca ²⁺	81
Fig. 3.10. Changes in chemical shifts of 1D proton spectra of TD in TFE after addition of Ca ²⁺	83

Fig.3.11 NOESY with Watergate Suppression spectrum of TD + Ca ²⁺ (1:1) in TFE . .	85
Fig.3.12. Lowest-energy triangular conformation of Ca ²⁺ - bound TD	91
Fig. 3.13. Side view of both lowest-energy conformations of TD	92
Fig. 3.14 Model 2 of TD in the selectivity filter of LCC	96
Fig. 3.15. Lowest-energy conformation of nifedipine bound inside the selectivity filter	104
Fig.3.16. Side view of MC-minimized model of nifedipine bound in portside-down mode in the pore of LCC	113
Fig.3.17. Side view of MC-minimized model of nifedipine bound in portside-up mode in the pore of LCC	114
Fig.3.18 A. Side view of MC-minimized model of antagonist R-Bay K 8644 bound in portside-down mode in the pore of LCC	117
Fig.3.18 B. Side view of MC-minimized model of agonist S-Bay K 8644 bound in portside-down mode in the pore of LCC	118
Fig.3.19. Passage of Ca ²⁺ ion surrounded by water molecules through the agonist-bound pore of LCC	121

List of Tables

Table 3.1. Aligned sequences of KcsA, L-type Ca ²⁺ channel and Na ⁺ channel	46
Table 3.2. Alignment of M2_KcsA with S6s of LCC used in Test Model II	46
Table 3.3. Effect of mutations in the cardiac L-type Ca ²⁺ channel on binding of DHPs	48
Table 3.4. Docking of nifedipine into the test models	53
Table 3.5. The energy and main torsion angles of the lowest-energy MECs of tetrandrine	69
Table 3.6. Chemical shifts of the protons in 1D spectrum of TD in CDCl ₃	72
Table 3.7. Proton-proton distance constraints, satisfied in low-energy conformations of TD	78
Table 3.8. Chemical shifts of protons of 1D spectrum of TD in TFE	82
Table 3.9. Proton-proton distance constraints, derived from the spectra of TD with Ca ²⁺ , satisfied in low-energy conformations of TD	89
Table 3.10. Starting orientations of TD in the selectivity filter and their energy after MC-minimization	95
Table 3.11. Different modes of nifedipine interaction with Ca ²⁺ ions chelated by acidic residues of selectivity filter	103
Table 3.12. Energy contribution of LCC residues to interaction with nifedipine	109
Table 3.13. Energy contributions of LCC residues to interaction with the aromatic ring of nifedipine	110

Table 3.14. Contact distances between Ca²⁺ ions and atoms of LCC and nifedipine in the portside-down binding mode 111

Table 3.15. Contact distances between Ca²⁺ ions and atoms of LCC and nifedipine in the portside-up binding mode.112

Chapter 1. Introduction

1.1 Ion channels

Ion channels compose a large superfamily of macromolecular proteins, controlling movement of ions, such as Na^+ , K^+ , Ca^{2+} and Cl^- , across the membranes of living cells. This movement is the basis of excitability of all nerve cells. Ion channels convert electrical signals in the cell membrane into the changes in intracellular ion concentrations, thereby activating such diverse crucial physiological processes as muscle contractions, neurotransmitter release at nerve terminals, proliferation of immune cells, regulation of enzymatic activities and gene expression (Hille, 1992). Ion channels can adopt either an open or closed state; the process of channel transition from one state to another is called “gating”. The changes of membrane potential, which is the difference in electric potential inside and outside the cell, increase the probability of the open state of voltage-gated ion channels (VGICs). Other ion channels’ gating can be governed by the binding of intracellular or extracellular ligands (ligand-gated channels) (Cockcroft, 1990), or by physical stimulation (mechano- and heat sensitive receptors) (Ghazi et al., 1998). Finally, there are voltage-independent channels that close and open randomly.

Voltage-gated ion channels are found in a wide range of procaryotic and eukaryotic organisms. They can assume at least three conformational states: closed, open and inactivated. Upon depolarization, the channels transfer from closed (resting) to open state in milliseconds, and then inactivate. Generally, the activation of Na^+ or Ca^{2+} channels results in cell depolarization and excitement, while the opening of Cl^- and K^+ channels will hyperpolarize and inhibit the cell.

The direction of transmembrane ion movement depends on the chemical gradient across the membrane. For example, the difference between millimolar levels of extracellular Ca^{2+} ions and micromolar levels of intracellular Ca^{2+} results in Ca^{2+} movement into the cell through open channel. The movement also depends on the channels' relative permeability to different ions determined by a number of different factors, one of which is the size compatibility of an ion and channel pore opening. However, channels are often able to discriminate effectively between the same size ions, such as Na^+ and Ca^{2+} , suggesting that there are some other mechanisms of ion selectivity.

Voltage-gated Na^+ , Ca^{2+} and K^+ channels share a common architecture. These channels often consist of several different subunits, called α , β , δ etc., but main channel functions are associated primarily with α -subunit. The α -subunits of the channels consist of four homologous domains (I to IV), each of these domains has six

membrane-spanning regions (S1 to S6), separated by hydrophilic intracellular and extracellular loops.

The S4 transmembrane (TM) region of all voltage-gated channels usually contains four to eight positively charged residues (lysine and/or arginine), separated from each other by two hydrophobic residues. It “senses” the changes in voltage across the membrane and regulates the channel gating according to these changes (Liman et al., 1991, Papazian et al., 1991). Cysteine- and histidine-scanning mutagenesis studies of this segment combined with fluorescence and electrophysiological experiments suggest the following model of sensor mechanism. Upon depolarization, the changes in membrane potential cause the repulsion of conserved basic residues. Resulting movement and rotation of S4 segments, observed experimentally (Baker et al., 1998, Cha et al., 1999), cause conformation changes, favoring the open state of the channel, without major distance changes between residues (Bezannila, 2000). The details of the changes remain unclear. These changes allow a channel to respond quickly to alteration of membrane potential.

There are some tetrameric ion channels found in both prokaryotes and eukaryotes. Each of their four domains has two TM segments, M1 and M2, homologous to segments S5 and S6 of oligomeric VGICs. The example of such channels is the inwardly rectifying bacterial K⁺ channel of *Streptomyces lividans* (KcsA). Recent crystallographic studies of this channel by Doyle et.al, (1998) have

confirmed the proposed general channel organization and features, such as the selectivity filter, pore and gate. They also reveal that the four repeats of two TM segments form the inverted teepee structure with the selectivity filter domain in its outer end. The dipoles of the pore-forming helices and the large water-filled cavity in the middle stabilize K^+ cations inside the pore (Doyle et.al, 1998).

1.2. Voltage-gated Ca^{2+} channels

1.2.1. Functions of voltage-gated Ca^{2+} channels

Increase of Ca^{2+} concentration inside the cell directly triggers a large number of vital physiological processes like muscle contraction, exocytosis, and release of hormones and neurotransmitters. Ca^{2+} entry may regulate cell growth and differentiation (Katz, 1996). The Ca^{2+} activation of signaling cascades is necessary for the gene expression and cell division. Therefore, many genetic diseases are linked to Ca^{2+} channel; the list of such known disorders is growing rapidly during the last years. For instance, patients with familial hemiplegic migraine and episodic ataxia type 2 were found to have mutations in genes coding α -subunit of Ca^{2+} channels (Ophoff et. al, 1996, Krauss et.al, 1998). Some types of paralysis and epilepsy are also linked to mutations in Ca^{2+} channel. The full understanding of these diseases and methods of their treatment requires deep knowledge about the mechanisms of channel activation and regulation, along with the three-dimensional structures of the different Ca^{2+} channels and major structural determinants of ligand-channel interaction.

1.2.2. Types of voltage-gated Ca^{2+} channels

Ca^{2+} channels are divided into several subtypes according to their electrophysiological and pharmacological properties (Hess 1990, Tsien 1987). Different α_1 -subunits are typical to each of these subtypes. The best-studied L-type (long-lasting) Ca^{2+} channels (LCC) are activated upon strong depolarization and have low deactivation and high inactivation rates. They are localized mostly in cardiac and skeletal muscle (α_{1C} and α_{1S} subunits). These channels are also found in some brain tissues such as neuronal soma and proximal dendrites (α_{1D}) (Bean 1989), in neuroendocrine system (α_{1D}) (Milani et.al, 1990), and in retina (α_{1F}) (Uchida and Iuvone, 1999). Their main functions include the excitation-contraction coupling in muscle cells, controlling of hormone secretion and mediating transcriptional events, which support learning and memory. The ion current through LCCs is modulated by dihydropyridines (DHPs), phenylalkylamines (PAAs) and benzothiazepines (BTZs) drugs. The blockers of Ca^{2+} currents are the most extensively used cardiovascular drugs worldwide (Wang et al., 1999). L-type Ca^{2+} channels are also regulated by second messenger-activated protein phosphorylation (Hess et al, 1984, Hymel et al, 1988).

In contrast to LCCs, some Ca^{2+} channels are activated at negative membrane potentials (depolarization near resting potential), inactivated rapidly and deactivated slowly, requiring strong depolarization, and have slow (about 8 pS) single

ion conductance (Pérez-Reyes, 1998). Such channels designated T-type Ca^{2+} channels for their transient kinetics. T-channels are localized in neurons and in cardiac and skeletal muscle cells. Their functions and regulation have not yet been analyzed in details; however, these channels may contribute to the pacemaking process which sets the rate and rhythm of the heartbeat (Triggle et al. 1997). T-type channels are insensitive to usual the Ca^{2+} antagonists. Some novel T-type Ca^{2+} channel blockers have been recently identified, such as aranidipine (Masumiya et.al, 2000), mibefradil (Roguin and Edoute, 1999) and kurtoxin-peptide from South African scorpion (Chuang et.al, 1998).

The voltage dependence of the third class, N-type Ca^{2+} channels, is intermediate; they inactivate faster than L-type, but slower than T-type. Located at nerve terminals and dendrites, these channels regulate neurotransmitter release. N-type Ca^{2+} channels are blocked by cone snail peptide ω -conotoxin (McCleskey et al, 1987, Tsien et al, 1987) and is insensitive to DHPs.

Neuronal P-, Q-, and R-type Ca^{2+} channels are activated under the strong depolarization and have slow inactivation rates. The primary function of all these channels is the release of neurotransmitters. These types of Ca^{2+} channels were initially distinguished by their pharmacological profiles. P-type channels are highly sensitive to spider toxin ω -agatoxin (Llinas et al, 1989). They are found in cerebellum, at nerve terminals and neuromuscular junctions. Q-type channels are also blocked by ω -

agatoxin, but with significantly lower affinity (Randall & Tsien, 1995). These channels show some sensitivity to ω -conotoxin MVIIIC. The locations of Q-type channels are cerebellar granule cells and hippocampal pyramidal neurons. Finally, R-type Ca^{2+} channels, resistant to most organic and peptide Ca^{2+} channels blockers, can be blocked by peptide SNX-482, from African tarantula (Newcomb et al, 1998).

1.2.3. Subunit structure of Ca^{2+} channels

Like all other VGICs, Ca^{2+} channels are multisubunit proteins (Fig.1.1). Expression of the main α_1 subunit produces protein retaining major electrophysiological and pharmacological properties of the heteromeric channels (Wei et al, 1991, Tanabe et al, 1988). However, these properties can be greatly modulated by auxiliary subunits (Felix, 1997). Specific combinations of the subunits contribute to functional diversity of Ca^{2+} channels.

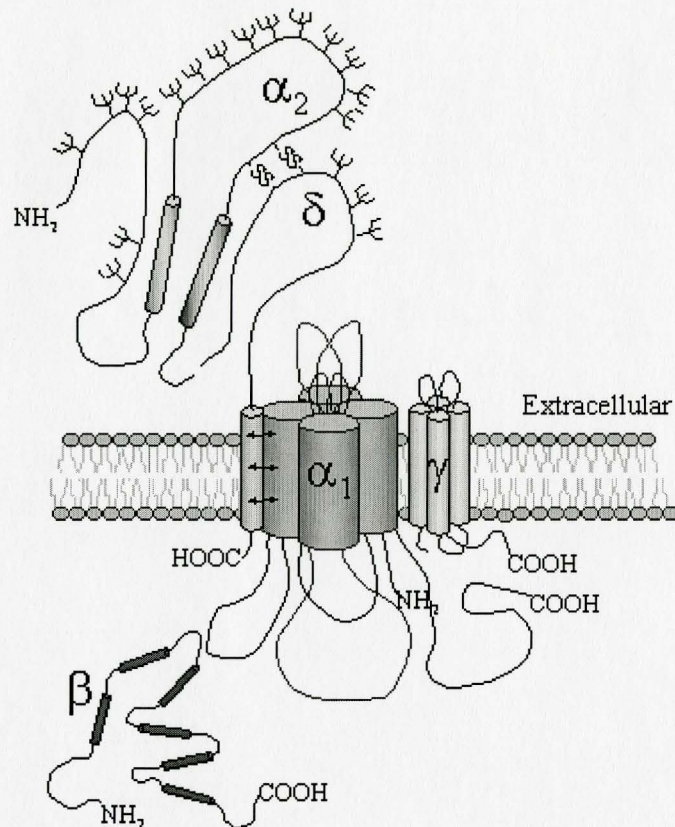


Fig.1.1. Subunit structure of voltage-gated Ca^{2+} channel (Based on Felix et al., 1997, Catterall, 1995, Isom et al., 1995)

The membrane-spanning $\alpha_2\delta$ auxiliary subunit plays a crucial role in assembling and regulation of α_1 subunit. This 140-170 kDa subunit is found in Ca^{2+} channels purified from skeletal muscle, heart and brain tissues. Both α_2 and δ are derived from the same gene and are post-translationally cleaved to yield two separate proteins that remain linked by disulfide bonds (De Jongh, 1990). The extracellular domain of $\alpha_2\delta$ is extensively glycosylated (Jay et al, 1991). It was shown that

coexpression of this subunit with α_1 increased the Ca^{2+} current by 10-fold. (Felix et al., 1997)

The intracellular β -subunit is usually 52-78 kDa in size and is specific for the heart, muscle, brain, lung, and kidney Ca^{2+} channels. It stimulates current amplitude, regulates the voltage dependence of activation and deactivation and the kinetics of ion entry (Gregg et al., 1996, Burgess et al., 1997). It also increases the functional expression of all six domains of the main α -subunit. Coexpression of β -subunit with α_1 -subunit dramatically increased its sensitivity to Ca^{2+} (Wallner et al., 1995). The β -subunit interacts with the conserved motif of cytoplasmic linker between repeats I and II of α_1 subunit and contains several cAMP-dependent protein kinase phosphorylation sites (Nunoki et al., 1989, Ruth et al., 1989)

The γ -subunit is specific for neuronal, skeletal muscle and lung Ca^{2+} channels. It is a 30 kDa glycosylated hydrophobic protein and is predicted to have four transmembrane domains. This subunit produces a small increase of Ca^{2+} current and channel activation rate and is associated with several neurological disorders, such as absence epilepsy (Letts et al., 1998).

The main pore-forming α_1 -subunit (160-273 kDa) of Ca^{2+} channel is composed of four internal homologous membrane-spanning domains (repeats I-IV), containing six α -helical TM segments S1-S6. (Fig.1.2). Membrane-diving P-loops, the

linkers between S5 and S6 segments, form the outer part of the pore and comprise the channel's selectivity filter (Kim et al., 1993).

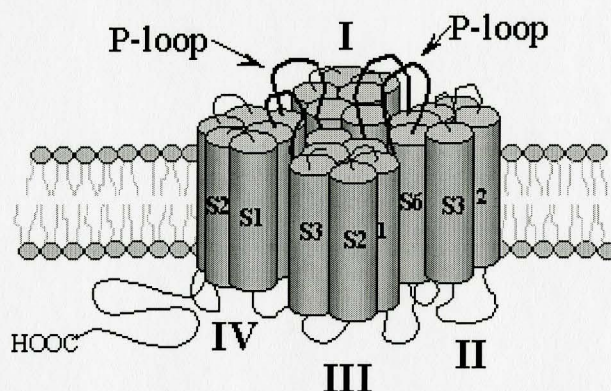


Fig.1.2. Structure of the α_1 -subunit of LCC. Pore-forming P-loops between S5 and S6 are shown in thick black lines. P-loops of repeats I and III are omitted for clarity.

1.2.4. Ion selectivity of Ca^{2+} channel

In order to perform properly their main functions, all ion channels have to effectively distinguish some specific ions, which are required to penetrate the cell, from all other ions in solution. In spite of increasing amount of experimental data, the mechanism of Ca^{2+} channel selectivity is not well understood yet. The X-ray structure of KcsA demonstrated some channel's features, important for understanding of selectivity mechanism (Doyle et al, 1998). The selectivity filter of KcsA is formed by

several rings of backbone oxygens of conserved residues, the inner diameter of which corresponds to the size of K^+ ions. However, these findings cannot be applied to voltage-gated Ca^{2+} channels. While K^+ channel separates ions by their size, allowing larger K^+ ions through, Ca^{2+} channels successfully differentiate, for example, Ca^{2+} and Na^+ ions, which have exactly the same size. Only in the absence of channel's "favorite" Ca^{2+} ions in solution can other ions permeate the channel (Almer and McCleskey, 1984). In addition, ions penetrate the channel with an impressive rate of 10^6 ions per second, so the process of ion selection is not only precise, but also very fast.

Experimental studies indicate that membrane-diving P-loops compose the outer mouth of the pore (Kim et al, 1993). Each of four P-loops contains conserved glutamate residues, which have been shown to form the "selectivity filter" of the channel, the so-called "EEEE-locus" (Yang, 1993, Mikala et al, 1993). The side-chains of all four glutamates interact directly with permeating cations, giving another reason in favor of different mechanisms of selectivity in Ca^{2+} and K^+ channels. Cysteine-scanning experiments have also shown that side-chains of these residues are accessible from outside the cell, and, therefore, face the pore (Koch et al., 2000). Recently, the probing of the other "ring" of conserved acidic residues, located downstream of the EEEE-motif, has demonstrated that they are also involved in the process of ion selectivity (Bahinski et al., 1997). Further mutational studies are required to reveal all residues in P-loop motives affecting ion permeability.

Recent theoretical studies suggest a possible mechanism of channel selectivity, employing the modeling system based on Poisson-Nernst-Planck equation (Nonner et al, 2000). Authors have theoretically predicted the binding curves for various ions in the selectivity filter. The work supports the proposed multiple-ion electroneutral pore with several Ca^{2+} binding sites (Zhorov and Ananthanarayanan, 1996).

1.2.5. Ca^{2+} channel modulation

After entering the cell, Ca^{2+} ions become tightly linked to various signal transduction processes. In many cases, the proteins involved in these pathways provide feedback regulation of Ca^{2+} channels in addition to voltage-dependent gating process.

One of the earliest reported examples of Ca^{2+} channel regulation is β -adrenergic stimulation of the slow inward Ca^{2+} currents. The experimental fact that β -adrenergic agonists induce increases in cardiac contractility and heart beat rate was widely used in medicine for a long time. It appears that this stimulation is mediated by cAMP and cAMP-dependent protein kinase (Reuter, 1974). β -adrenergic stimulation also plays an important role in transcriptional regulation of LCC (Fan et al, 2000).

cAMP-dependent protein kinase phosphorylation alone may cause the enhancement of LCC activation. The substrates for this phosphorylation are α_1 and β

subunits of the channel (Takahashi et al, 1987, Jahn et al, 1988). The phosphorylation increases the probability of channel's open state and, in cardiac channels, the conductance of the channel (Reuter and Scholz, 1977, Hess et al, 1984, Hymel et al, 1988, Davare et al., 2000).

Neuronal N and P/Q channels are regulated through multiple G-protein coupled pathways (Hille 1994, Jones and Elmslie, 1997). This regulation is important for controlling the synaptic transmission and hormone secretion. G-protein interaction with neuronal channels results in the shifting of channel's voltage-dependence to more positive membrane potentials, reducing the steepness of voltage-dependent activation and slowing rate of activation. Neuronal Ca^{2+} channels are regulated mainly by $G_{\beta\gamma}$ subunit of G-protein (Herlitze et al, 1996, Ikeda, 1996). $G_{\beta\gamma}$ was shown to obstruct the gating movement of S4 voltage sensors of Ca^{2+} channel (Jones et al, 1997). This effect can be overcome by prolonged depolarization to more positive membrane potentials to force the sensor movement. The possible sites of $G_{\beta\gamma}$ interaction with Ca^{2+} channels have been extensively studied by various site-directed mutagenesis experiments, construction and analysis of channel chimeras (Zamponi et al, 1998, Herlitze et al, 1997, Canti et al, 1999). Effective inhibition of Ca^{2+} currents by G-proteins may require additional proteins, such as SNARE protein syntaxin (Wiser et al, 1996).

Ca^{2+} ions, entering the cell, themselves effectively regulate Ca^{2+} currents. The channel inactivation caused by intracellular ion accumulation is, in fact, much

faster than the voltage-dependent one. In cardiac cells, such inactivation is the main determinant of the duration of ion current (Lee et al, 1985). Calmodulin, the protein that has a high affinity to Ca^{2+} ions, was found to be constitutively bound to C-termini of α_1 subunit. The binding of excessive intracellular Ca^{2+} ions to this protein initiates conformation changes that result in increasing the rate and degree of channel inactivation. (Zuhlke and Reuter, 1998, Peterson et al, 1999, Lee et al, 1999, 2000)

Ca^{2+} channels are also regulated by a number of proteins and protein complexes like the SNARE protein complex, interacting with neuronal channels through a large intracellular loop between domains II and III, shifting the voltage-dependence to the more-negative membrane potentials (Wiser et al, 1996, Bezprozvanny et al, 1995). Such channel inhibition may be important for the proper regulation of hormone and neuropeptide secretion, and cell exocytosis.

Pharmacological modulation of Ca^{2+} channels is widely used in medicine, mainly for the treatment of various cardiovascular disorders (Hockerman et al., 1997). Therapeutically available L-type Ca^{2+} channel antagonists are the best studied among all Ca^{2+} channel drugs; detailed review of these drugs is presented in following section. There are also several potent and selective antagonists of neuronal voltage-gated Ca^{2+} channels. It is well known that most of the deadliest natural toxins from various species target ion channels. In the case of neuronal Ca^{2+} channels, the scorpion, spider and cone snail venoms reportedly block the channel, causing

neurological damage (Llinas et al, 1989, Newcomb et al, 1998, Leao et al, 2000). All these toxins are extremely helpful and effective tools for experimental studies, assisting in our understanding of biological functions, pharmacological properties and the structure of ion channels.

1.3. Calcium-binding proteins

Ca^{2+} ions are involved in modulation of diverse physiological processes, such as neurotransmitter release, muscle contraction and gene expression (Hille, 1992). Intracellularly the effect of Ca^{2+} is mediated by several Ca^{2+} -binding proteins, most of which contain the so-called “EF-hand” motif - a widespread domain, currently found in 66 protein families (Lewit-Bentley and Rety, 2000). The classic EF-hand consists of about 30 amino acids forming a helix (E)-loop-helix (F) domain within which the Ca^{2+} ion is coordinated by α -helices on either side via the network of seven hydrogen bonds. The EF ligands coordinating Ca^{2+} ion are usually the side chains of Asp, Asn, Glu or Ser residues or a water molecule. There are two groups of Ca^{2+} -binding EF-hand proteins. The proteins of the first group do not undergo significant conformational changes upon binding of Ca^{2+} and serve as Ca^{2+} buffers or transporters, for example calbindin and parvalbumin. The binding of Ca^{2+} ion to the EF-containing proteins of the second group does result in the conformational transition of EF-hand to an “open” state allowing interaction with target proteins and consecutive mediation of signal

transmission (Houdusse and Cohen, 1996, Strynadka et al., 1997). The second group includes, for example, calmodulin and S100 proteins.

The best known EF-containing protein calmodulin is expressed in all eukaryotic cells and participates in signaling pathways regulating the movement, growth and proliferation (Chin and Means, 2000). This relatively small sensor protein of 148 residues responds to the changes of intracellular free Ca^{2+} concentration within a range of $10^{-7} - 10^{-6}$ M. The binding of Ca^{2+} ions initiates the structural rearrangement of two EF-hand motives and exposure of methionine-rich hydrophobic surface, making possible the hydrophobic interaction with target proteins (Meador et al., 1992, 1993). Among the target proteins for calmodulin are protein kinases (Yamamoto et al., 1997), phosphatases (Sobiechek et al., 1997, Moreno et al., 2000) and phosphodiesterases (Pichard et al., 1981). It has also been shown that calmodulin modulates ion channels (Peterson et al., 1999, Lee et al., 1999).

Another family of Ca^{2+} -binding proteins, neuronal calcium sensors (NCS), is found in retinal photoreceptors and neurons (Braunewell and Gundelfinger, 1999). Recoverin, neurocalcin δ and hippocalcin are some examples of NCS proteins. Their role in phototransduction, regulation of neurotransmitter release, control of gene expression, and regulation of ion channels has been recently confirmed (Braunewell and Gundelfinger, 1999). All members of the family possess four Ca^{2+} -binding EF-hand domains. Upon Ca^{2+} binding the NCS proteins undergo substantial conformational

changes, which indicates that they act as Ca^{2+} sensors and switches. These changes have been characterized by the crystallographic studies of recoverin, which demonstrate extensive structural rearrangements exposing the hydrophobic surface for interaction with target proteins (Ames et al., 1997). NCS proteins bind Ca^{2+} with an affinity not far above the resting free Ca^{2+} concentration (McFerran et al., 1998, Ladant, 1995), which is about a 10-fold higher than the affinity to Ca^{2+} binding to calmodulin (Cox et al., 1981). The presence of the diverse Ca^{2+} -binding proteins, which possess different Ca^{2+} binding affinities, in the same neuronal cells provides the dynamic range over which Ca^{2+} can regulate neuronal activities. This allows responses to small changes over the resting Ca^{2+} concentration of 100nM up to high-micromolar increases (Burgoyenne and Weiss, 2001).

In addition, there are several Ca^{2+} -binding proteins which do not contain EF-motif. Some of them are found in membrane, and others are intracellular. One of the best characterized Ca^{2+} -binding membrane proteins is sarcoplasmic reticulum Ca^{2+} pump, belonging to the family of cation transporters, P-type ATPases. It pumps the Ca^{2+} ions against the concentration gradient from the cytoplasm to the sarcoplasmic reticulum, which is necessary for the proper Ca^{2+} signaling (East, 2000). The pump can assume two different conformations, corresponding to the free and Ca^{2+} -binding forms of the protein. The 3D structure of the latter form has recently been solved by X-Ray crystallography (Toyoshima et al., 2000). Two Ca^{2+} ions were located on approximately

mid-way across the membrane bilayer, chelated by Asp/Asn and Glu residues of different α -helices of the pump.

One of the intracellular non-EF Ca^{2+} -binding proteins is annexin, which is found in plant and mammalian cells. Inside the cell annexin has several diverse functions, such as vesicle trafficking and phosphodiesterase activity. Of our special interest is that annexin modulates ion channel activity. In addition, it has been recently proposed that this protein itself may serve as an atypical ion channel, increasing membrane permeabilization for the Ca^{2+} ions (Lim et al., 1998). The X-Ray structure of the plant annexin showed that the protein is organized of four domains, each of which contains five α -helical segments arranged parallel and anti-parallel to each other and connected by several loops (Hoffmann et al., 2000). Several acidic residues located in the loops and in the helical segment IV are responsible for Ca^{2+} binding. Ca^{2+} -induced structural rearrangements of this protein result in exposure of the loops and their binding to the membrane by several membrane-penetrating aromatic residues.

All these examples of Ca^{2+} -binding proteins demonstrate that, in most cases, Ca^{2+} ions bind to proteins by interacting with several acidic residues, whether located in the EF-hand motif or at the α -helical transmembrane segments of Ca^{2+} pump. In the case of LCC, the EEEE-locus of P-loops serves as a Ca^{2+} -binding domain (Yang et al., 1993). These data are used during the modeling of LCC in this and other studies.

1.4. Ligands of L-type Ca^{2+} channel

The crucial role of LCCs in regulation of smooth and cardiac muscle contraction has made them the major therapeutical targets for treatment of different disorders of heart and blood vessels. Drugs which can effectively block contractions in depolarized cardiac and vascular muscles and thus help in treating cardiac failure and hypertension have been known for at least a century. The oldest discovered were diltiazem, verapamil and nifedipine, so-called “first-generation molecules” (Triggle, 1999). Most modern LCC drugs are derivatives of these earliest prototypes, divided, accordingly, into three structurally distinct classes: Benzothiazepines (BTZs), phenylalkylamines (PAAs) and dihydropyridines (DHPs).

1.4.1. Phenylalkylamines

Verapamil and its derivatives are tertiary amines, positively charged at physiological pH. Three best-studied PAAs: verapamil, desmethoxyverapamil (devapamil D888) and methoxyverapamil (D600), are structurally similar compounds, differing from each other in the number of methoxy groups on each of their phenyl rings. Interestingly, the (-) enantiomers were shown to be stronger blockers than (+) enantiomers (Ferry et al., 1984). Electrophysiological and binding studies suggested that the affinity of PAA binding depends on the channel state, with the inactivated state

having the highest affinity (McDonald et al, 1984, Herzig et al, 1992). As the ratio of open, closed and inactivated states of the channel is voltage-dependent, so is the PAA binding affinity. It was found that the blocking affinity depends also on the frequency of membrane potential; this important property of PAA binding results in their extensive use as antiarrhythmic drug (Johnson et al, 1996). The PAA blocking of L-type Ca^{2+} channels in both vascular smooth and cardiac muscles has been used for treatment of hypertension and arrhythmias. Unfortunately, there are a number of negative side effects, such as flushing, headache and constipation (Opie, 1988, Man in't Veld, 1989).

The photolabelling and mutational studies indicate that the PAA binding site is composed of several amino acids of segment S6 of repeats IV and III (Doring et al, 1996) and conserved glutamates at the pore loops between S5-S6 segments of repeat III and IV (Hockerman et al, 1997). Electrophysiological studies suggest that PAAs block the channel from the intracellular side, entering the cell in the uncharged lipid soluble form and reaching the receptor from inside (Varadi et al, 1995). The PAA binding site is allosterically linked with benzothiazepines and dihydropyridines binding sites. The fact that PAA binding inhibits other drugs' interactions with their receptor sites may indicate the competitive mechanism of channel blockage.

1.4.2. Benzothiazepines

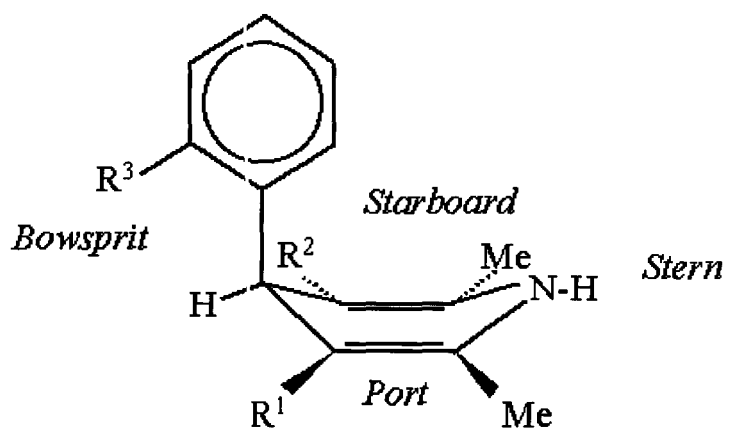
Diltiazem and the other BTZs contain a tertiary alkylamine side chain, which was found to be necessary for their interaction with receptor site (Kimball et al, 1993). The blocking of LCC by BTZs is intermediate, more frequency-dependent than DHPs, but less than PAAs. The tonic voltage-dependent block of LCC by diltiazem is stronger than that of verapamil derivatives and weaker than the DHP's block. BTZs block the Ca^{2+} channel from the extracellular side (Seydl et al, 1993, Hering et al, 1993). The BTZ binding site is less studied than the DHP and PAA ones, however, some experimental data suggested the binding site is partially composed of some amino acids of segment S6 of repeat IV and III (Kraus et al, 1996). This site is also allosterically linked to those of other L-type Ca^{2+} channel drugs. BTZ binding was shown to inhibit interaction of PAA with the channel, but stimulate DHP binding (Ferry and Glossmann, 1982, DePover et al, 1982). However, the binding sites of PAAs and BTZs are probably not identical since they access their binding domains from the opposite sides of membrane.

1.4.3. Dihydropyridines

DHPs are the most extensively studied LCC drugs. Compared to the other LCC ligands, 1,4-dihydropyridines are more potent and selective vasodilating drugs, effectively treating specific vascular disorders like cerebral vasospasm and

peripheral vascular disorder (Triggle, 1999). Channel modulation by DHPs is voltage-dependent (Bodi et al., 1997). DHP drugs consist of two structurally closely related groups of compounds, which are pharmacologically characterized as channel antagonists, favoring inactivated state of the channel, and agonists, favoring open state. DHP antagonists are widely used in medicine, while DHP agonists are important from the scientific point of view as a tool for probing of channel gating mechanism.

Theoretical and experimental studies suggest that in the lowest-energy conformation flattened-boat DHP ring is orthogonal to 4-aryl (phenyl) group at the “bowsprit” and the polar group at the phenyl ring tends to be maximally separated from NH group of the DHP ring (Fig.1.3) (Langs and Triggle, 1985, Govyryn and Zhorov, 1994, Goldmann and Stoltefuss, 1991). Interestingly, in case of some DHPs, both antagonist and agonist are enantiomers of the same compound, such as Bay K 8644 and PN-202 791, implying a complex mechanism of channel modulation by DHPs.



Compound	R ¹ port	R ² starboard	R ³	Effect
Nifedipine	COOMe	COOMe	NO ₂	Blocker
(R)-Bay K 8644	COOMe	NO ₂	CF ₃	Blocker
(S)-Bay K 8644	NO ₂	COOMe	CF ₃	Activator

Fig. 1.3. Structures and activities of DHPs

To determine the location of DHP receptor site a series of charged DHP derivatives were constructed by Bangalore et al.(1995), with DHP ring connected a head group by alkyl spacer chains of 2, 6, 8, 10 and 12 methylene groups. Applied extracellularly, such derivatives were found to be the most effective in channel blocking when having the spacer chain of 10 methylene groups, which corresponds to 11-14 Å. All derivatives, applied intracellularly, failed to block the channel, proving that the receptor site is accessible only from extracellular side (Bangalore et al, 1994, Kwan et al., 1995). Various photolabeling, chimeric and mutational studies have demonstrated that conserved residues, forming high-affinity DHP binding site, are located mostly at the IVS5, IVS6 and IIS5 transmembrane segments (Grabner et al, 1996, Striessnig et al, 1991, Peterson et al, 1996, Schuster et al.,1996, etc.). A number of conserved acidic residues located at the loops between S5 and S6 segments were also found to be important determinants of DHP binding (Yang et al, 1993). Recent studies have demonstrated that the reconstruction of highly sensitive DHP binding site requires additional, not yet identified amino acids, for instance, in IS6 segment (Lacinova et.al, 1999). Detailed analysis of all amino acids shown to be involved in DHP binding is presented in Chapter 3 (*Results*).

Binding of DHPs to calcium channel is Ca^{2+} -dependent (Peterson and Catterall, 1995; Mitterdorfer et al., 1995). Chelating of Ca^{2+} ions by electronegative atoms of DHPs was shown experimentally by NMR and spectroscopy studies. The drugs assume different conformations in the absence and presence of Ca^{2+} ions (Belciug

and Ananthanarayanan, 1994). A ternary complex of Ca^{2+} ions, DHP and some residues of DHP's binding site may be formed upon drug's binding to receptor (Ananthanarayanan, 1991, Zhorov, 1993).

1.5. Objectives of current project

Due to the unique properties of Ca^{2+} channels and their involvement in a wide range of physiological processes, they have become attractive targets for drug design. The blockers of Ca^{2+} channels are the major cardiovascular drugs, the worldwide sales of which are in a range of billions dollars per year (Wang et al., 1999). All these drugs, derived from the oldest prototypes: verapamil, diltiazem and nifedipine, are often associated with serious unwanted side effects (Opie, 1988). The search of the novel, more effective drugs with fewer side effects, requires in-depth knowledge of the structural organization of the channel.

Attempts to crystallize large transmembrane proteins, such as LCC, by traditional methods often fail due to protein insolubility in water solutions. That is why the X-Ray structure of any voltage-gated ion channel is yet to be acquired. Another powerful method of structure determination, NMR, is also ineffective when applied to the proteins like LCC, which has about 1400 residues. The method of homology modeling can form an alternative and help in understanding of major structural

determinants of the channel. This method has already demonstrated its potential during, for example, the modeling studies of μ -opioid receptor, a member of G-protein coupled receptor (GPCR) family (Zhorov and Ananthanarayanan, 1998, 2000), and chloride channels of glycine and GABA receptors (Zhorov and Bregestovski, 2000).

Interestingly, the recently solved X-ray structure of rhodopsin, another GPCR (Palczewski et al., 2000) has revealed the same structural features as those predicted theoretically for μ -opioid receptor using the homology modeling approach (Zhorov and Ananthanarayanan, 2000). Ca^{2+} and K^{+} voltage-gated ion channels share significant functional homology, thus we can use the known structure of KcsA as a template for the modeling studies.

The main objective of current project is to build a homology model of pore-forming S5-S6 segments of LCC based on the X-ray structure of corresponding KcsA segments, using available experimental data as additional constraints during the modeling. To test various modes of DHP binding, we will perform the ligand docking into the obtained model. The conclusion about the best ligand-binding mode is to be based on several criteria, such as the energy of ligand-receptor interaction and number of optimal contacts between the ligand and conserved residues, which have been shown experimentally to interact with DHPs (DHP-sensing residues). By docking of different DHP ligands, both antagonists and agonists, into the best obtained model, we will try to reveal the structural features of the drugs and their ability to modulate the ion flow in different manners.

As mentioned above, the folding of the pore-forming P-loops of LCC differs from that of KcsA due to specific mechanisms of ion selectivity in these channels. The complete rationale concerning this difference is presented in the sections below. Therefore, we cannot use homology-modeling approach to model these segments of LCC. Some LCC ligands, such as (S,S)-(+)-tetrandrine (TD), are known to bind the channel in the region of selectivity filter. We can use such ligands to find the approximate geometry of the pore mouth by shaping the flexible P-loops around the drug. In order to investigate the interaction of the drug with Ca^{2+} ions, we will perform the conformational studies of free and Ca^{2+} -bound TD, using NMR spectroscopy. Finally, we will explore the process of ion permeation inside the agonist-bound pore of the LCC by modeling the passage of a hydrated Ca^{2+} ion from the selectivity filter to the “gate” of the channel. This modeling simulation can help us to reveal the structural features of the channel pore and the ligands, important for the channel gating and for the modulation of the ion current through the channel.

Chapter 2. Methods

2.1. Nomenclature and multiple sequence alignment

In order to use the X-ray structure of KcsA in homology modeling, the atom coordinates of KcsA were downloaded from the Brookhaven Protein Data Bank (code *1BLB*). The amino acid sequence of L-type Ca^{2+} channel from rabbit cardiac muscle was taken from *SWISS-PROT* database, the entry code is *CICC_RABIT*. Since, in the present study, we modeled only S5-S6 transmembrane segments of LCC, we selected the corresponded fragments of *CICC_RABIT* sequence for aligning them with KcsA. The following nomenclature of the residues in TM segments was selected (Zhorov et al., 2001). The first residue from the N-terminus of every KcsA transmembrane segment was designated a relative number 1, and all other residues located downstream, in the direction to C-terminus, were numbered correspondingly. The designation of every LCC residue contains the number of repeat and TM segment, as well as the relative number of the corresponding homologous residue of KcsA. For example, the designation of $\text{Asn}^{\text{III}5.18}$ means that this residue is located in TM segment S5 of repeat III and aligned with the eighteenth residue of the corresponding TM segment of KcsA.

The extra- and intracellular linkers were not included in the model because of their remote location from the DHP binding site and selectivity filter of the channel. Only membrane-diving P-loops between S5 and S6, which form the outer vestibule of the pore, were aligned with homologous loops between M1 and M2 segments of KcsA. Because of different length of P-loops of LCC and KcsA, we cannot use the same approach to assign the residue's numbers as we did for S5 and S6 segments. Instead, the most conserved selectivity-filter-forming glutamate residues of LCC P-loops were assigned the relative number 50, and other loop residues located up- and downstream of these glutamates assumed numbers decreasing or increasing from 50. For example, Asp^{IP.54} is the aspartate, located four positions downstream of selectivity filter in P-loop of repeat I.

The initial multiple sequence alignment was performed automatically by *MULTALIN* server (Corpet, 1988). However, S5 and S6 segments of LCC do not show high sequence identity with corresponding TM segments of KcsA, and, therefore, a number of alternative alignments are possible as well. In this situation we considered some additional biases for sequence aligning, namely the orientation of DHP-sensing residues and alignments of LCC with other ion channels. In case of Na⁺ channel, which shares high sequence identity with LCC, the residues interacting with local anesthetic drugs were aligned with pore-facing residues of KcsA (Lipkind and Fozzard, 2000). Using the fact that DHP-sensing residues of LCC are found in similar positions, we have built the Model I based on multiple sequence alignment of S6 segment of LCC

with Na⁺ channel and KcsA (see Table 3.1 in Chapter 3 below). An alternative alignment, proposed by Huber et al. (2000), placed the DHP-sensing residues in positions where they are faced the interface between the segments IIIS5-IIIS6-IVS6 (hereafter called interface III/IV). This alignment became a basis for the Model II of current project (see Table 3.2 in Chapter 3 below). In both models, the DHP-sensing residues in S5 segments faced the interface III/IV.

2.2. Molecular Modeling

The homology models of LCC were built by using ZMM molecular modeling package. This set of programs allows users to perform a variety of computer modeling simulations: the building of complex molecular systems, energy minimization, ligand docking, exploring of behavior of ligands and ions, and some specific interpretation of two-dimensional NMR spectra (Zhorov, 1993, Zhorov and Ananthanarayanan, 1996, 1998, 2000, Zhorov and Bregestovski, 2000). The program package, currently consisting of about 20000 *FORTRAN* operators, was created and developed for more than 30 years by Dr. Boris Zhorov. The process of improving, adding of novel program blocks and optimizing of computational procedures of ZMM is still continuing.

ZMM performs the conformational search by minimizing the energy in the space of generalized coordinates, varying bond and torsion angles, bond lengths,

position and orientation of free molecules. The powerful method of energy minimization, which is realized in ZMM, was first developed by Li and Sheraga (1987). The combination of Monte Carlo procedure with the minimization of system energy (Monte Carlo Minimization, MCM) allows fast and effective search for the lowest-energy conformations. The MCM protocol is based on repetition of following steps:

1. Change a value of randomly selected coordinate G by $n\Delta G_{max}$, where n is a random number, $-1 < n \leq 1$, and ΔG_{max} is the step-size parameter. If, for example, G is a torsion angle, then $\Delta G_{max} = 180^\circ$.
2. Minimize the energy of the new acquired conformation, taking into account the new value of G . The methods of energy minimization, employed in ZMM, are described below.
3. Accept this conformation into the resulting MCM trajectory, if

$$\Delta E = E_i - E_{i-1} \leq 0;$$

where E_i is the energy of new minimum-energy conformation (MEC), E_{i-1} is the energy of previous MEC, or if

$$\rho \leq \exp\left(-\frac{\Delta E}{RT}\right),$$

ρ is a random number, $\rho \in (0,1)$.

Only if the energy of the new conformation is lower than the energy calculated at previous step can this conformation be included into resulting MCM trajectory. Occasional selection of conformation with higher energy is also possible due

to the second criteria, but the probability of such selection depends on size of energy gap between the current and previous MEC and decreases dramatically if the new calculated energy is too high. The trajectory is usually terminated if 500 consecutive energy minimizations do not yield any new accepted MEC.

The following methods of energy minimizations are realized in ZMM.

The method of steepest descent is employed for the fast lowering from the area of initial high energy. In this method, we determine the descent step size and direction at every iteration by calculating the negative derivative of the energy calculated during the previous step. Very effective Davidon method of energy minimization requires calculation of the matrix of the second derivatives. In case of large proteins, calculation of such huge matrices at every iteration is very inefficient and requires considerable resources of computer memory. Therefore, only the energy of small molecules is calculated by this method in ZMM. For the larger molecules, we use the method of conjugative gradient, which is similar to the steepest descent method, but direction of each descend step depends now not only on the negative derivative of current energy, but also on previous directions.

High speed of trajectory convergence was acquired by developing of the analytical vector method of calculation of the first and second-degree derivatives (Zhorov, 1981). In this method, each atom is presented as a vector model, and the energy is calculated in the space of torsion angles, and polar angles of these vectors.

All trajectories were calculated at $T = 600$ K; this temperature is optimal for the convergence of MCM trajectories (Abagyan and Argos, 1992). The initial conformations were built using the X-ray structures of corresponding aligned segments of KcsA as templates. Initially the program assigned the values of template's backbone and sidechain torsions to aligned residues of LCC. If the side chain of KcsA residue was shorter than that of LCC residue, the lacked LCC side chain torsions were assigned the value of 180° . In the case when LCC contains proline residues in positions, where KcsA has some other residues, the torsion values required for closing of proline ring were assigned to them. To keep the general topology of KcsA, the C_α atoms of LCC were constrained to the coordinates of C_α atoms of corresponding KcsA residues by “pins” - flat-bottom parabolic penalty functions. These constraints keep the difference r between coordinates of C_α atoms of KcsA and LCC within the boundaries $d_l < r < d_h$ (usually d_l is 0, $d_h = 1 \text{ \AA}$) by using the quasiparabolic function $E_r = s(r) * f(r)$, where $s(r)$ is switching operator :

$$s(r) = \begin{cases} 1 & \text{if } r \leq d_l - x, \\ [(d_l + x - r)^2 (d_l + x - 3(d_l - x) + 2r)] / (2x)^3 & \text{if } d_l - x < r \leq d_l + x, \\ 0 & \text{if } d_l + x < r \leq d_h - x, \\ [(d_h - x - r)^2 (x - d_h + 3(d_h + x) - 2r)] / (2x)^3 & \text{if } d_h - x < r \leq d_h + x, \\ 1 & \text{if } d_h + x < r, \end{cases}$$

and $f(r)$ is a penalty function, $f(r) = C(r - d_h/2 - d_l/2)^2$.

In this function x is a switching distance (0.2 \AA), and C – force constant, $C = 10 \text{ kcal mol}^{-1} \text{ \AA}^{-1}$).

The procedure of the energy minimization of every model consisted of three consecutive MCM trajectories. In the first trajectory, only side-chain torsions were allowed to vary. In the second and third, all torsions and then all generalized coordinates were sampled. These steps were necessary to avoid major movements of helices, which could occur due to a number of “bad “ contacts at initial stages of minimization. All atom-atom interactions were calculated in *AMBER* force field, the set of parameters allowing user to calculate the atom-atom interactions. (Weiner et al., 1984).

The ligand docking was performed in several stages, the lowest-energy conformation of the drug-LCC complex, obtained at every step, was used as the starting conformation during the next step. At the first stages of ligand docking, the drug was placed manually in the receptor model in such a way, that it could form the maximum number of contacts with DHP-sensing residues, or, in some cases, to satisfy other experimentally determined constraints. Then the energy was MC-minimized with the ligand and receptor kept rigid. This “manual” docking was performed by using *InsightII* program (Molecular Simulations inc., San Diego, USA). At the next stage of docking, all generalized coordinates of the ligand and LCC were allowed to vary. To overcome remaining bad contacts and to impose the preferred orientation of the ligand, several drug atoms were constrained to closest DHP-sensing residues by flat-bottom constraints, similar to “pin” constraints described earlier ($d_l = 2-3 \text{ \AA}$, $d_h = 3-5 \text{ \AA}$, $C = 100 \text{ kcal mol}^{-1}\text{\AA}^{-1}$). Finally, the complex was MC-minimized with all constraints,

except “pins”, eliminated. Such method of gradual relaxation allows ligand to find the best orientation in the space available inside the receptor, to form hydrogen bonds and hydrophobic interactions with LCC residues.

The procedure of stochastically restrained MCM search (SR MCM) was used to work with some NMR-derived data. In two-dimensional NOE experiments the spectral peaks represent the through-space proton-proton interaction. The intensity of NOE every peak is proportional to the distance d between these two protons,

$$I = d_{ref}^6 \frac{I_{ref}}{d^6}$$

where I – intensity of given peak, d_{ref} – reference distance, I_{ref} – intensity of reference peak.

Usually the known distance between two protons, which is expected to be the same in any conformation, is chosen to be the reference distance. For example, the distance of 2.43 Å between two aromatic protons is often selected for this role. Intensity of reference peak and of all other peaks of the spectrum is determined by manual extraction of volume integrals of all peaks.

These proton-proton distances can be used as additional flat-bottom constraints, similar to those described earlier, during the conformational studies of given molecule. Although if we applied all the derived distances as constraints

simultaneously, we would probably end up with some unrealistic “average” conformation. We should take into account the fact that the NOE distances may represent several different conformations of the molecule, which coexist in solution at given temperature. We did that by using the method of SR MCM, which was already shown to be effective for small molecules and peptides (Ananthanarayanan et al., 1996, Qi et al., 2000). This procedure randomly activates and inactivates several NOE constraints, taking them from the stock of all NOEs of given spectrum, at every step of MCM search. If some constraint is inconsistent with current conformation, obtained so far in MCM trajectory, the activation of this constraint will yield a high-energy MEC, which will not be accepted in resulting trajectory. At the next step of MCM that NOE will be inactivated. In contrary, if the activation of a NOE constraint does not significantly contradict with current geometry, this constraint is considered as having “matched the conformation” and stays activated during further MCM search. To ensure the acceptance of such constraint, we apply the energy benefit of -1 kcal mol^{-1} for every matched NOE's, thus directing MCM search towards NMR-consistent conformations.

The results of all MCM simulations were visualized using *InsightII* and *RasMol 4.0* programs. The ligands were assembled and the charges on atoms were calculated by *Builder and MOPAC* program blocks of *InsightII* (Molecular Simulations inc., San Diego, USA).

2.3. Experimental Methods

For experimental studies of LCC drug tetrandrine and its complex with Ca^{2+} , we employed one-dimensional and two-dimensional NMR techniques. At the initial stage of studies we received a sample of tetrandrine as a generous gift from Dr. Kwan (Department of Medicine, McMaster University). When during the following experiments the larger quantities of the drug were required, the tetrandrine was purchased from Sigma-Aldrich Canada Ltd. The molecular weight of tetrandrine is 622.77, mp 219-222°C. An organic solvent trifluoroethanol (TFE), which was used in most experiments, was also bought from Sigma-Aldrich Canada Ltd. During the experiments of titration of tetrandrine with Ca^{2+} ions, the solution of calcium perchlorate $[\text{Ca}(\text{ClO}_4)_2]$ in TFE was added and mixed with tetrandrine, in order to obtain the required molar ratios. Since the water molecules could prevent cations from interaction with the drug, the lyophilization of $\text{Ca}(\text{ClO}_4)_2 \cdot 4\text{H}_2\text{O}$ was necessary to dry the compound before the experiments.

Typical lyophilization procedure started with desolvation of 10g of “wet” $\text{Ca}(\text{ClO}_4)_2 \cdot 4\text{H}_2\text{O}$ in 20 ml of 99.99% pure methanol, containing less than 0.01 % of water. The rotating vapor instrument was used to “pull off” the solvent. Then the steps were repeated by adding 10 ml of dry methanol and evaporating the solvent. Before lyophilization another 10 ml of dry methanol were added, solution was frozen while rotated in liquid nitrogen, then it was put in lyophilizer for about 12 hours, overnight. Resulting product of dry $\text{Ca}(\text{ClO}_4)_2$ was dissolved in TFE and used in

titration experiments. The presence of water in solution was checked during the NMR experiments.

2.4. Nuclear Magnetic Resonance Spectroscopy

Nuclear Magnetic Resonance (NMR) spectroscopy methods were used in current project during the conformational studies of tetrandrine. NMR is a powerful technique of structural analysis of molecules, based on magnetic resonance phenomena. The nuclei, which possess spin angular momentum, experience the spin transition from the low-energy state to the high, when irradiated with electromagnetic radiation of proper frequency. Since all nuclei undergo the magnetic “shielding”, caused by their own electrons, as well as by electrons of neighboring atoms, the transition frequency of every nucleus depends on its properties and on presence and amount of neighbors. Therefore, a lot of structural information about given molecule can be extracted from its NMR spectrum (Silverstein et al., 1991)

2.4.1. Chemical shift

As a result of magnetic shielding, nuclei in electron-rich environment experience transition at higher applied magnetic field, than the nuclei in electron-poor environment. Resulting shift of NMR signal of given nuclei is called a *chemical shift*. The observed chemical shift, measuring in Hz, depends on the frequency of applied field, so in order to unify the shifting scale, a new unit of ppm (*parts per million*) was accepted.

$$\delta = \frac{\delta_{obs}}{\nu} * 10^6$$

where δ - chemical shift, in *ppm*, δ_{obs} –observed chemical shift, in *Hz*, ν - oscillator frequency, in *Hz*. The factor of 10^6 was added for convenience, to convert the scale into simple whole numbers.

A reference peak of tetramethyl silane (TMS, $(\text{CH}_3)_4\text{Si}$), the compound with protons and carbons more highly shielded than those of most known chemical compounds, is used to calibrate the scale. A drop of TMS is added to all NMR solutions and the absorption peak of this compound, located rightmost of all other peaks in spectrum, is referred as 0 ppm.

2.4.2. Coupling constant

The multiplicity of most peaks in NMR spectra is caused by phenomena known as spin coupling. The magnetic field of a given nucleus experiences the influence of magnetic fields of neighboring nuclei, through interaction with bonding electrons. For example, a proton has two possible spin orientation, thus the magnetic field of neighboring proton will endure two different values, therefore NMR peak of that proton will be splitted by two peaks. More generally, n protons split the peak of the given proton by $(n+1)$ peaks. Since this type of interaction is possible only for nuclei connected by three or less covalent bonds, the spin coupling is a very useful tool for

determining the chemical structure of the molecule. The gap between peaks of split signal is called the coupling constant and measured in Hz. All protons, coupled to each other, demonstrate exactly the same values of coupling constants.

2.4.3. One-dimensional (1D) and two-dimensional (2D) NMR experiments

The one-dimensional, or single-pulse, NMR experiments were carried out at the initial stages, yielding the basic information about chemical shifts and coupling constants of the molecule. In 1D NMR, the usual scheme of experiment is:

Preparation → Pulse → Detection

During the preparation time, the system under the study undergoes initial pulses, for example, 90° pulse. After the pulse, each spin precesses with each own frequency, inducing the signal at the receiver coil. The signal is recorded during the detection time. Usually the experiment is repeated several times in order to increase the signal-to-noise ratio. Then the acquired amplitude *versus* time dependence is Fourier-transformed to more convenient amplitude *versus* frequency domain, so that the chemical shifts and coupling constants can be extracted.

There are some disadvantages of 1D NMR, such as difficulties in resolving the spectra of molecules, assigning the spectra etc., which can be overcome by using more advanced two-dimensional NMR methods. The basic 2D experiment starts with one, or several pulses, followed by evolution and mixing time, and detection:

Preparation → Pulse → Evolution (t_1) → Mixing (t_m) → Detection (t_2)

In the evolution time, the spin system evolves, depending on specific for every coherence factors, such as the characteristic frequency of the coherence and its coupling with other nuclei. The duration of evolution time is increased stepwise in series of consecutive experiments in order to extract additional information about the spin system, thus the second time scale is created. In some 2D experiments, other pulses can be applied during the mixing time in order to make different coherences correlate to each other. The 2D NMR technique allows users to resolve the spectra of large and complex molecules, determine their configurations and conformations.

The following NMR experiments were performed during current study:

1. **COSY** (correlation spectroscopy) experiment, which helps in determining which nuclei are connected through covalent bonds. The sequence of two 90° pulses is applied:

Preparation → $\pi/2$ → Evolution (t_1) → $\pi/2$ → Acquisition (t_2)

After the Fourier transformation we get the spectra, similar to corresponding 1D spectrum of given nucleus, on both axes. The peaks at this 2D spectrum indicate the nuclei, which are coupled to each other, allowing much simpler spectrum assigning.

2. NOESY (Nuclear Overhauser Effect spectroscopy) detects through-space connectivity between protons

Preparation $\rightarrow \pi/2 \rightarrow$ **Evolution** (t_1) $\rightarrow \pi/2 \rightarrow t_m \rightarrow \pi/2 \rightarrow$ **Acquisition** (t_2)

The correlation peaks on resulting 2D spectrum indicate which protons are close to each other in space, making this technique especially useful for the conformational studies.

3. ROESY (rotating frame modification of NOESY) allows one to overcome of some phasing problems of NOESY experiments.

Preparation $\rightarrow \pi/2 \rightarrow$ **Evolution** (t_1) \rightarrow **spin lock_y during the mixing time** \rightarrow **Acquisition** (t_2)

where spin lock designates the strong electromagnetic field, switched on at the end of evolution period t_1 during the mixing time, “locking” the spins in one direction (y) and shifting the spin frequency. Usually ROESY experiment generate a number of artifacts, particularly some TOCSY cross peaks. A modified pulse sequence called transverse-ROESY or T-ROESY may be used for suppression of these peaks (Hwang and Shaka, 1992).

4. TOCSY (total correlation spectroscopy) shows the cross peaks corresponding to all coupled nuclei within the spin system. In this experiment, magnetization is transferred over up to 5-6 bonds, making interaction between protons, separated by even 5-6 bonds, visible in form of peaks at the 2D spectrum.

Preparation $\rightarrow \pi/2 \rightarrow$ **Evolution (t_1)** \rightarrow **spin lock_x during the mixing time** \rightarrow

Acquisition (t_2)

The volume integrals of the peaks in ROESY spectra were used to determine proton-proton distances for the further SR MCM conformation studies.

1D and 2D H^1 and C^{13} spectra of tetrandrine and tetrandrine- Ca^{2+}

complexes in chloroform and TFE were acquired at room temperature of $23 \pm 1^\circ C$, using Bruker AM-500 spectrometer (500 MHz frequency). The concentration of tetrandrine was 20 mg ml^{-1} (32mM) in chloroform, 5 mg ml^{-1} (8mM) in TFE. During the titration experiments with Ca^{2+} in TFE the starting concentration of tetrandrine was chosen to be 1 mg ml^{-1} (1.6 mM), in order to achieve required ratios of $[\text{tetrandrine}] / [Ca^{2+}]$ by additions of required portions of $Ca(ClO_4)_2$ solution in TFE. The number of scans was varied from 4 to 96, depending on noise factor of given spectrum. The mixing time in NOESY experiments was $0.5 \mu s$ and $0.75 \mu s$, in ROESY experiments the mixing time usually was 0.8 ms.

Chapter 3. Results

3.1. Initial test models, based on alternative alignments

3.1.1. Test Models I and II

The first step in every homology modeling study is multiple sequence alignment of protein under investigation with template protein. In our project, two alternative alignments of S6 TM segment were studied. Initially we performed the multiple sequence alignment automatically, using *MULTALIN* Internet server (Corpet, 1987). Resulting alignments of S5, S6 TM segments and P-loops are shown in Table 3.1. An additional criterion for alignment was the comparing of our Ca^{2+} alignment with sequence alignment of Na^+ channel and KcsA. Ca^{2+} and Na^+ channels share high sequence identity. Mutational experiments have shown that local anesthetic drugs (LA), the ligands of Na^+ channel, interact with residues, located in positions 9, 12-13, and 17 of S6s (Table 3.1) (Ragsdale et al., 1994). There are a number of LCC residues, mutations of which have affected the binding of DHPs to LCC (hereafter called DHP-sensing residues). Several such DHP-sensing residues of S6 segment of LCC were found in the positions 9, 12-13 and 17, analogously to LA-sensing residues of Na. In a model of Na^+ channel, proposed by Lipkind and Fozzard (2000), such LA -sensing residues and DHP-sensing residues of LCC were aligned with pore-facing residues of

KcsA. Based on this alignment, which matched the automatic alignment performed by *MULTALIN* server, we have built Test Model I. The model was MC-minimized, as described in *Methods*, with pin constraints keeping the general topology of KcsA during the energy minimization.

Table 3.1. Aligned sequences^{a,b} of KcsA, L-type Ca²⁺ channel and Na⁺ channel.

Channel	Name ^d	Segment ^e	Sequence	
K ⁺	CIK1_DROME	S5	390	1 10 20 KASMFELGLLIFFLFIVVLFSSAVYFAE
K ⁺	KcsA	M1	23	ALHWRAAGAATVLLVIVLLAGSYLAVLAE
Ca ²⁺	CCAC_RABIT	IS5	290	IKAMVPLLHIALLVLFVIIYAIIGLELFL
		IIS5	673	LNSVRSIASLLLLLFLFIIIFSLGMLQFL
		IIIS5	1051	FVAIRTIGNIVIVTTLLOFMFACIGVQLF
		IVS5	1382	IKSFQALPYVALLIVMLFFIYAVIGMQVF
K ⁺	CIK1_DROME	P	426	33 40 50 FKSIPDAFWWAVVTMTTVGYGDMTPVG
K ⁺	KcsA	P	59	LITYPRALWWSVETATTVGYGDLYPVT
Ca ²⁺	CCAC_RABIT	IP	376	FDNFAFAMLTVFOCITMEGWTDLVLYWM
		IIP	719	FDNFQSLTTFVFOILTGEDWNSVMYDG
		IIIP	1128	FDNVLAAMMALFTVSTFEGWPELLYRS
		IVP	1429	FQTFQAVLLLLFRCATGEAWQDIMLAC
Na ⁺	CIN1_RAT	IP	365	FDTFSWAFSLSLFRLMTQDFWENLYQLT
		IIP	934	MNDEFHFSFLIVFRVLCGEWIETMWDCM
		IIIP	1415	FDNVGFGYLSLLOVATFKGWMDIMYAA
		IVP	1707	FETFGNSMICLFOITTSAGWDGLLAPI
K ⁺	CIK4_DROME	S6	455	1 10 * 20 GKIVGSLCAIAGVLTIALPVPVIVSNFN
K ⁺	KcsA ^f	M2	88	GRCVAVVVMVAGITSFGLVTAALATWFFV
Ca ²⁺	CCAC_RABIT	IS6	411	PWYFVSLVIFGSFFVLNLVGLVLSGEF
		IIS6	759	VCIYFIILFICGNYILLNVFLAIAVDNL
		IIIS6	1172	ISIFFIIYIIIIAFFMMNIFVGFVIVTF
		IVS6	1482	AVFYFISFYMLCAFLIINLFFVAVIMDNF
Na ⁺	CIN2_RAT	IS6	401	YMIFFVLVIFLGSFYLLINLILAVVAMAY
	CIN2_RAT	IIIS6	1449	MYLYFVIFIIIFGSFFTLNLFIVIIDNF
	CIN2_RAT	IVS6	1752	GIFFFVSYIIISFLVVVNMYYIAVILENF

Table 3.2. Alignment of M2_KcsA with S6s of LCC (Huber et al., 2000) used in Test Model II

KcsA	M2	1 10 * 20 GRCVAVVVMVAGITSFGLVTAALATWFFV
CCAC_RABIT	IS6	WYFVSLVIFGSFFVLNLVGLVLSGEF
	IIS6	CIYFIILFICGNYILLNVFLAIAVDNL
	IIIS6	SIFFIYIIIIIAFFMMNIFVGFVIVTF
	IVS6	VFYFISFYMLCAFLIINLFFVAVIMDNF

^a The alignment of S6s of Na⁺ channel with M2_KcsA is proposed by Lipkind and Fozzard (2000). S5s are aligned with M1_KcsA as proposed by Huber et al. (2000).

^b The coloring scheme, suggested by Zhorov et al. (2001) is used in this table. **Y,F,W**, designate aromatic residues; **N,Q,E,D,R,K,Y,H,W** are large residues with H-bonding groups; **L,I,V,M**, are large hydrophobic residues; **GSAT** - small residues; **P**- prolines. Conserved acidic residues in the P-loops are selected by red (**E,D**). Hydrophobic residues at S6.17 positions, the candidates for the channel gate, are pointed out by asterisks.

^c The yellow-highlighted residues (**Y**) are LA-sensing residues of Na⁺ channels or DHP-sensing residues of LCC, listed in Table 3.3.

^d Name of the protein or its index in the SWISS-PROT databank.

^e Genuine number of the first residue of the segment.

^f Pore-facing residues in KcsA are shown in bold.

Table 3.3. Effect of mutations in the cardiac L-type Ca²⁺ channel on binding of DHPs

WT residue	Mutant residue	Affinity decrease ^a
Thr ^{III S5.16}	Tyr	> 1000 ^b
	Ala	~ 1 ^c
Gln ^{III S5.20}	Met	29.4 ^b
Tyr ^{III S6.8}	Ala	5.2 ^{d,g} , 29.1 ^{d,h} , 25 ^e
	Phe	12 ^f
Ile ^{III S6.9}	Ala	6.2 ^e
Ile ^{III S6.12}	Ala	17 ^e , 31 ^{d,g} , 5.1 ^{d,h}
	Phe	7.9 ^{d,g} , 1.5 ^{d,h}
Met ^{III S6.16}	Ala	3.5 ^e
Met ^{III S6.17}	Ala	9.6 ^e
Tyr ^{IV S6.9}	Ile	5.7 ^{d,g} , 21 ^{d,h}
	Ala	2.9 ^e
	Phe	3.5 ^f
Met ^{IV S6.10}	Ala	1.6 ^e
Ile ^{IV S6.16}	Met	3.8 ^f
Ile ^{IV S6.17}	Ala	2.7 ^e
Asn ^{IV S6.18}	Ala	9 ^e

^a (IC₅₀ or EC₅₀ in mutant)/(IC₅₀ or EC₅₀ in WT). Unless indicated, the ligand is antagonist PN200-100.

^b He et al., 1997.

^c Huber et al., 2000.

^d Bodi et al., 1997; the holding potential of -80 mV.

^e Peterson et al., 1997.

^f Peterson et al., 1996.

^g Antagonist R-202-791

^h Agonist S-202-791

An alternative alignment of S6 segments was proposed by Huber et al, (2000), who put the DHP-sensing residues in positions, where they face the III-IV interface (Table 3.2). Although different from Na⁺ alignment with KcsA, this alignment still required a thorough study in order to test possible binding sites of DHPs. The Test Model II was built basing on that alignment of S6s, MC-minimized in the same way as Test Model I. Resulting lowest-energy conformation was used for further docking experiments, described below.

The main features of KcsA were preserved in both Test Models. The S5 and S6 TM segments of both models form an inverted teepee structure with the water-filled cavity inside the pore (hereafter called “the water lake”). On the extracellular side of the channel the water lake is bordered by the P-loops composing the selectivity filter. The lake bottom is formed by S6 segments crossing with each other. The main difference between the structures of the models is that in the Test Model I the side chains of most DHP-sensing residues face the pore, while in Test Model II most of the DHP-sensing residues are oriented toward the III/IV interface of the channel. Several DHP-sensing residues of Test Model II, such as Ile^{IVS6.16} and Asn^{IVS6.17} (see Fig.3.3 C), face the pore of the channel. In order to simulate the interaction of DHP-sensing residues with the ligand, we performed the docking of nifedipine into both Test Models.

3.1.2. Docking of DHP into both test models

In biologically active conformation, DHPs have the elongated shape, approximately inscribing into the parallelogram of $8.8 \times 11.2 \times 13.8 \text{ \AA}$ (Fig. 3.1) (Goldmann and Stoltefuss, 1991, Zhorov and Ananthanarayanan, 1996).

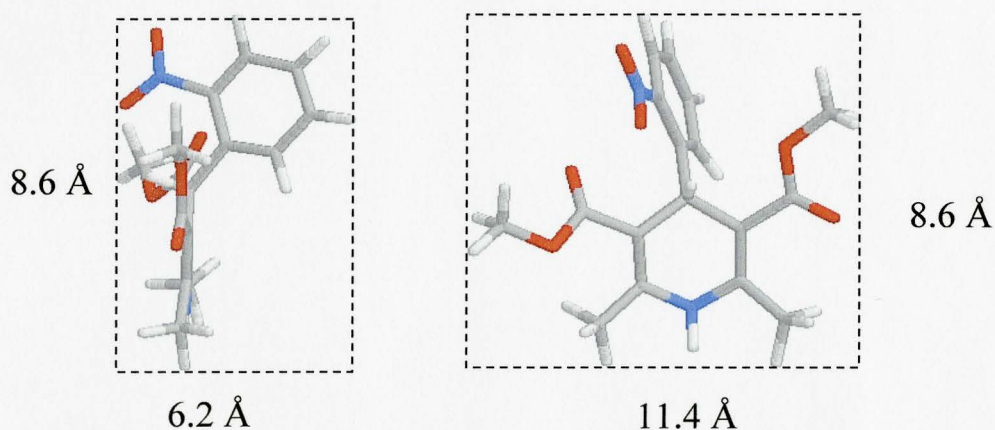


Fig.3.1. Dimensions of biologically active conformation of nifedipine. Taking into account van der Waals radii of hydrogen (1.2 \AA) and oxygen (1.4), the minimal-profile rectangles of nifedipine projections are $8.8 \times 11.2 \text{ \AA}$, and $11.2 \times 13.8 \text{ \AA}$ respectively.

If we consider different possible orientations of the drug inside the water-lake cavity of LCC model, shown on Figure 3.2, we see that only when the long axis of the drug is aligned with the pore axis, can the drug fit the pore optimally (Fig 3.2 C, D). When the drug's long axis is oriented approximately perpendicular to the pore axis, the bulky substituent groups on "starboard" or "portside" of DHP (see Fig.1.9)

prevent it from going deeper into the pore and interact with DHP-sensing residues (Fig 3.2 A, B, E). Thus, both port-side-down and starboard-down orientations of DHP inside the pore should be considered in following docking experiments.

We performed the docking of DHP drug nifedipine into both test models. The drug was initially oriented portside- down; the starboard-down orientation is studied further, in LCC model with Ca^{2+} (See section 3.4.1). For both test models, two possible DHP binding sites were explored. First, nifedipine was docked inside the pore, with flat-bottom constraints imposing the initial contacts of ligand's active groups with some DHP-sensing residues. The NH-group of nifedipine, the major element of its pharmacophore, which forms hydrogen bond with the receptor (Goldmann and Stoltefuss, 1991), was oriented towards repeats III and IV, containing DHP-sensing residues. In the second set of experiments, the interface III/IV was tested as probable DHP-binding site. Nifedipine was placed between IIIS5, IIIS6 and IVS6 segments and flat-bottom constraints imposed ligand interaction within the receptor.

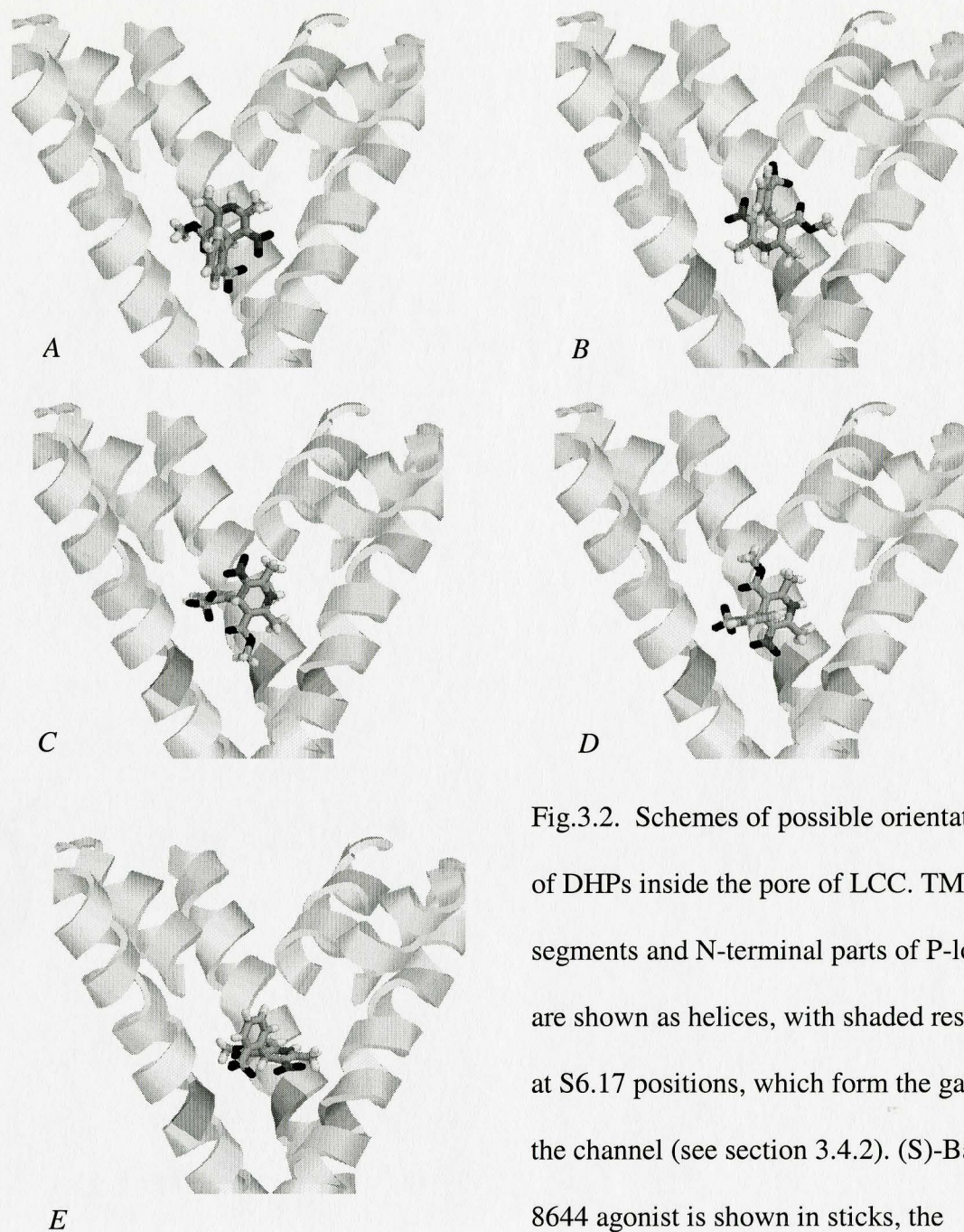


Fig.3.2. Schemes of possible orientations of DHPs inside the pore of LCC. TM segments and N-terminal parts of P-loops are shown as helices, with shaded residues at S6.17 positions, which form the gate of the channel (see section 3.4.2). (S)-Bay K 8644 agonist is shown in sticks, the

hydrogen atoms are white; carbons are light gray. Oxygens, nitrogens and fluorines are shown in black. The boat-like agonist approaches the S6 crossing by the bow (*A*), stern (*B*), starboard (*C*), portside (*D*) and bottom (*E*).

The nifedipine docking to both binding sites was performed in three steps to gradually eliminate some bad contacts, while keeping the drug inside the receptor (see *Methods*). Resulting four lowest-energy conformations are shown in Figure 3.3, their energetic characteristics are listed in Table 3.4.

Table 3.4. Docking of nifedipine into the test models.

Model	Ligand position	DHP-sensing residues within 5 Å from the ligand	Ligand-receptor energy, kcal/mol
I	Interface III/IV	Thr ^{IIIS5.14} , Ile ^{IIIS6.9} , Ile ^{IIIS6.12} , Tyr ^{IVS6.9} , Met ^{IVS6.10} , Ile ^{IVS6.17}	-18.0
I	Central Pore	Tyr ^{IIIS6.8} , Ile ^{IIIS6.9} , Ile ^{IIIS6.12} , Met ^{IIIS6.17} , Tyr ^{IVS6.9} , Ile ^{IVS6.16} , Ile ^{IVS6.17}	-38.7
II	Interface III/IV ^a	Asn ^{IIIS5.18} , Met ^{IIIS6.17} , Tyr ^{IVS6.9} , Met ^{IVS6.10} , Ile ^{IVS6.17}	-31.4
II	Central pore	Met ^{IVS6.9} , Met ^{IIIS6.17}	-27.0

^aMost of DHP-sensing residues in segment IIIS6 face lipids and cannot approach the ligand

Among the lowest-energy conformations, the best one corresponded to the Test Model I with pore-bound nifedipine (Fig 3.3 A). In this conformation, the ligand interacts with seven DHP-sensing residues (Table 3.4). Tyrosine residues of repeats III and IV, which were shown to greatly affect DHP binding (Table 3.3), are within the H-bond-forming distance of NH-group of nifedipine. Sidechains of

hydrophobic conserved residues Ile^{IIIS6.9}, Ile^{IIIS6.12}, Met^{IIIS6.17}, Ile^{IVS6.16}, and Ile^{IVS6.17} are close to methyl groups of ligand, indicating the possibility of hydrophobic interactions. Since we did all the calculations in vacuum, the quantitative contribution of these hydrophobic interactions, which could lower the energy of this model even further, was not included into the final energy.

The docking of nifedipine into III/IV interface of Test Model I (Fig 3.3 *B*) yielded a low-energy conformation with poor ligand-receptor complementarity, which was indicated by increase in energy of ligand-receptor interaction by 21 kcal/mol (Table 3.4). Among conserved tyrosine residues, only Tyr^{IVS6.9} was found in close proximity to the ligand, although several contacts were formed between methoxy group of the ligand and conserved hydrophobic residues of IVS6 TM segment. NH-group of nifedipine, protruding in the interface between IIIS5 and IVS6, was initially constrained to Thr^{IIIS5.14} and Asn^{IIIS5.18}. However, in consecutive unconstrained MCM trajectories the ligand has moved in order to find an optimal position inside III/IV interface, losing contacts with Thr^{IIIS5.14} and Asn^{IIIS5.18}. No hydrogen bonds were formed between NH-group of ligand and receptor.

MC-minimized Test Model II with nifedipine bound inside the pore (Fig 3.3 *C*) has the energy of ligand-receptor interaction higher than that of Test Model I by 12 kcal/mol (Table 3.4). In this conformation, ligand forms only two contacts with DHP-sensing residues, Met^{IVS6.9} and Met^{IIIS6.16}. Both conserved tyrosines Tyr^{IIIS6.8} and

Tyr^{IVS6.9} do not face the pore, eliminating the possibility of any contacts with the ligand. The movement of the ligand to III/V interface of Test Model II resulted in low-energy conformation (Fig 3.3 D) with ligand-receptor energy only 7 kcal/mol higher than the lowest one, the energy of Test Model I with ligand bound inside the pore. Favorable contacts were formed with four DHP-sensing residues, Met^{IIIS6.17}, Tyr^{IVS6.9}, Met^{IVS6.10}, and Ile^{IVS6.17}. However while Tyr^{IVS6.9} can form the hydrogen bond with the oxygen of methoxy group of nifedipine, the second conserved tyrosine Tyr^{IIIS6.8} faces the lipids and does not interact with ligand. In the final lowest-energy conformation, NH group of the ligand, initially constrained to Thr^{IIIS5.14} and Asn^{IIIS5.18}, appears too far from these residues to form any beneficial hydrogen bonds.

Although the Test Model I with nifedipine bound inside the pore demonstrated the best energy of ligand-receptor interaction, this energy criterion alone is not sufficient to exclude the other possible DHP binding sites from consideration. However, only in that conformation the ligand formed most advantageous contacts with conserved hydrophobic DHP-sensing residues, along with hydrogen bonds with important tyrosine residues. All these facts taken together allowed us to choose Test Model I and “inside-pore” DHP binding mode for further modeling experiments.

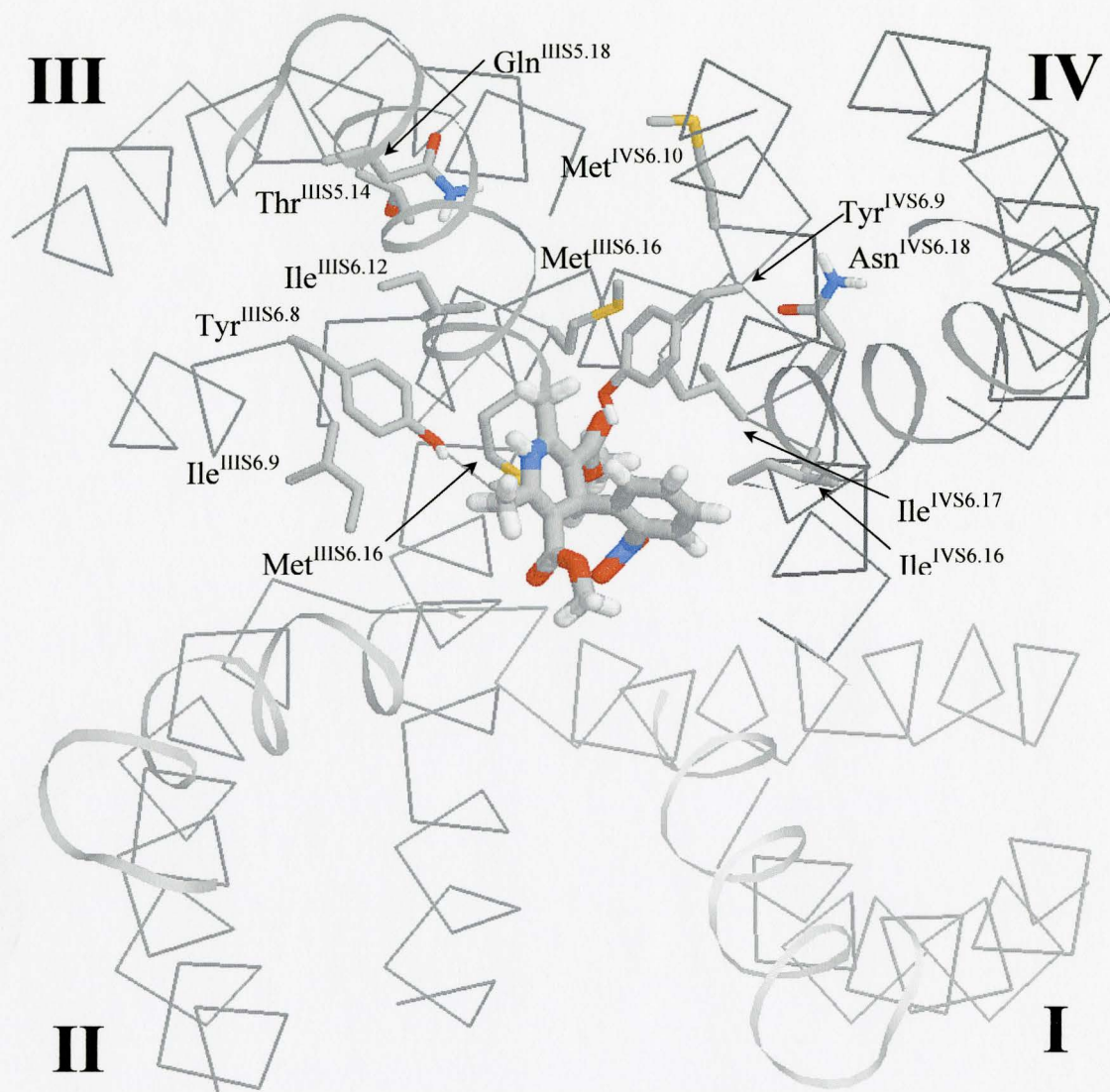


Fig. 3.3 *A, top view*. The visualization of the lowest-energy conformation of nifedipine bound inside the pore of Test Model I. TM segments are shown by C $^{\alpha}$ tracing, P-loops are presented as ribbons. The darkness of all segments increases with repeat number. Nifedipine and the side chains of DHP-sensing residues are shown in thin sticks, with red oxygens and blue nitrogens.

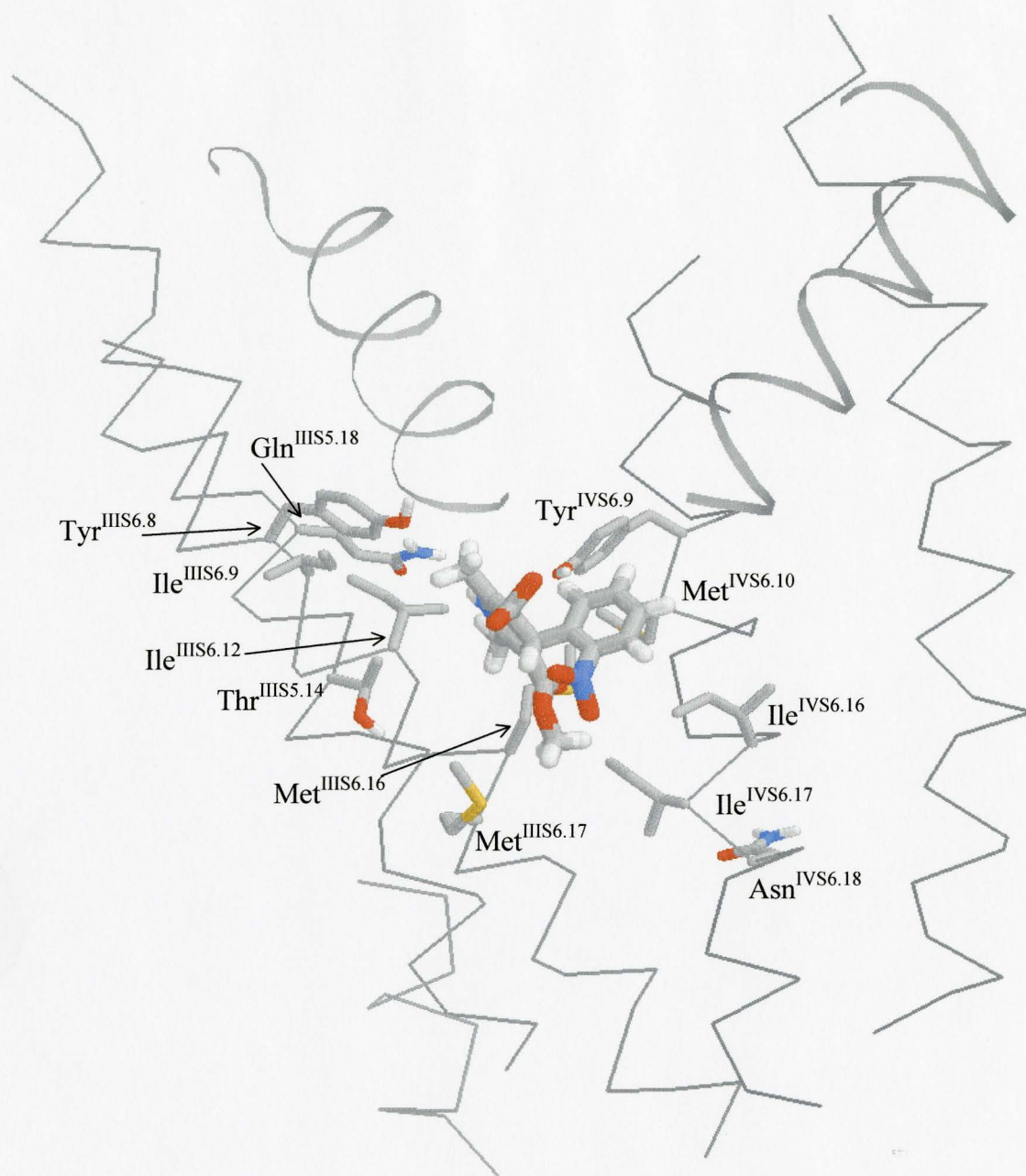


Fig. 3.3 *A*, side view of nifedipine bound inside the pore of Test Model I. *SLAB* command of *RASMOL* program is used to remove most parts of repeats I and II for clarity. (See Fig 3.3 *A top view* for description of the ligand and channel presentation).

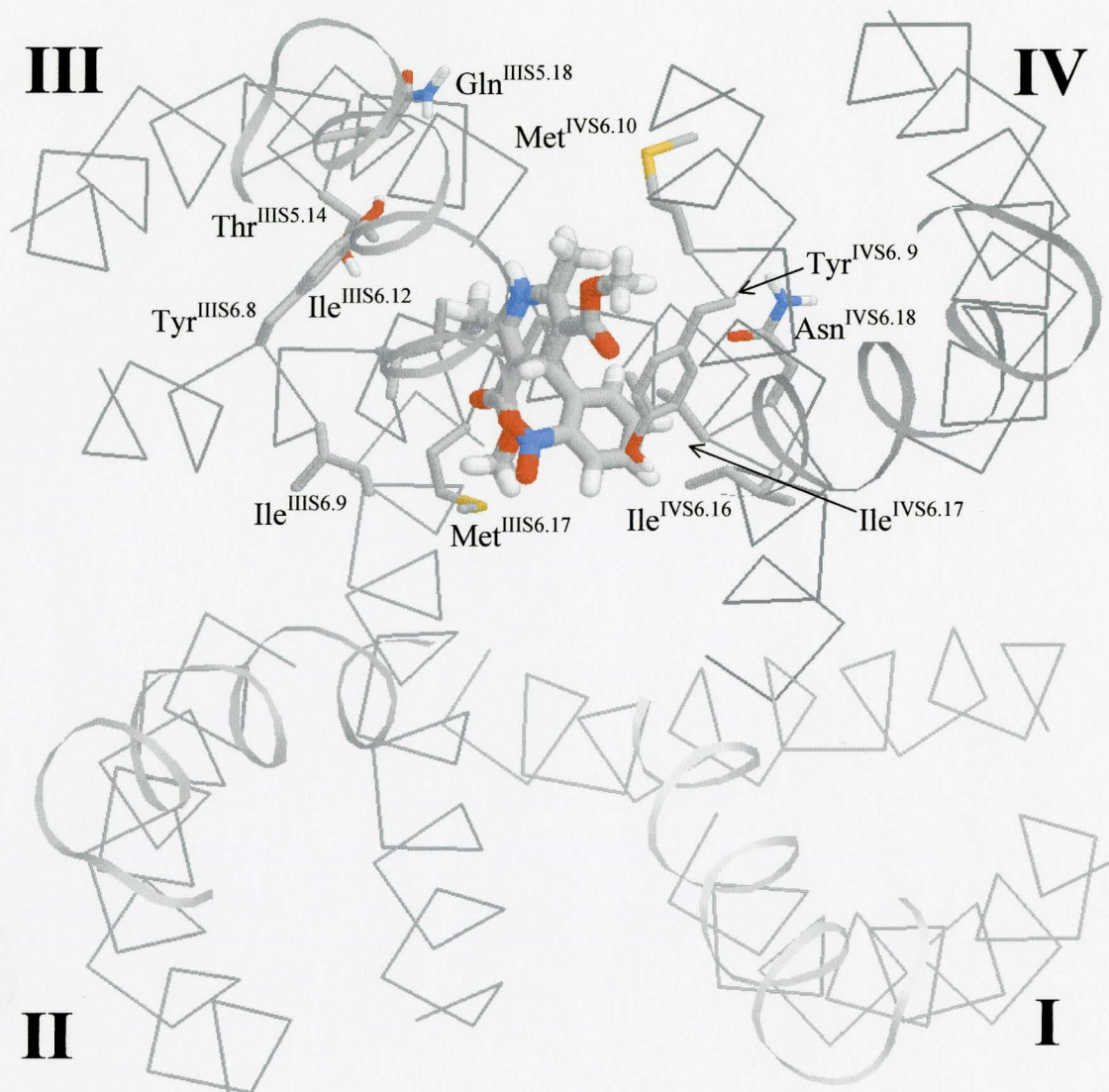


Fig. 3.3 B, *top view* . The ligand bound in the interface III/V of Test Model I. (See Fig 3.3 A *top view* for description of the ligand and channel presentation).

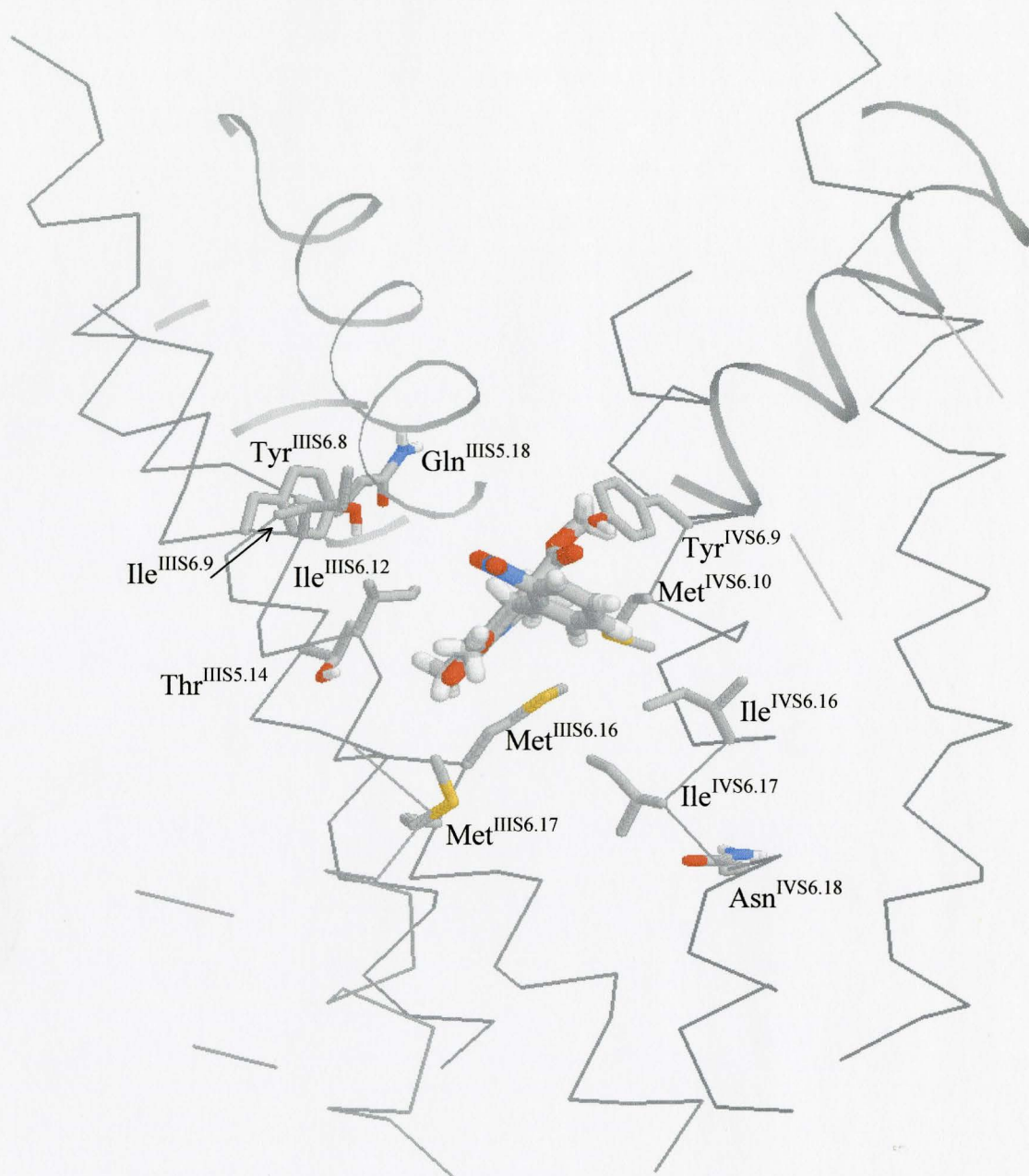


Fig. 3.3 *B, side view* .Nifedipine bound in the interface III/V of Test Model I. The parts of repeat I and II are removed by SLAB command of RASMOL for clarity. (See Fig 3.3 *A top view* for description of the ligand and channel presentation).

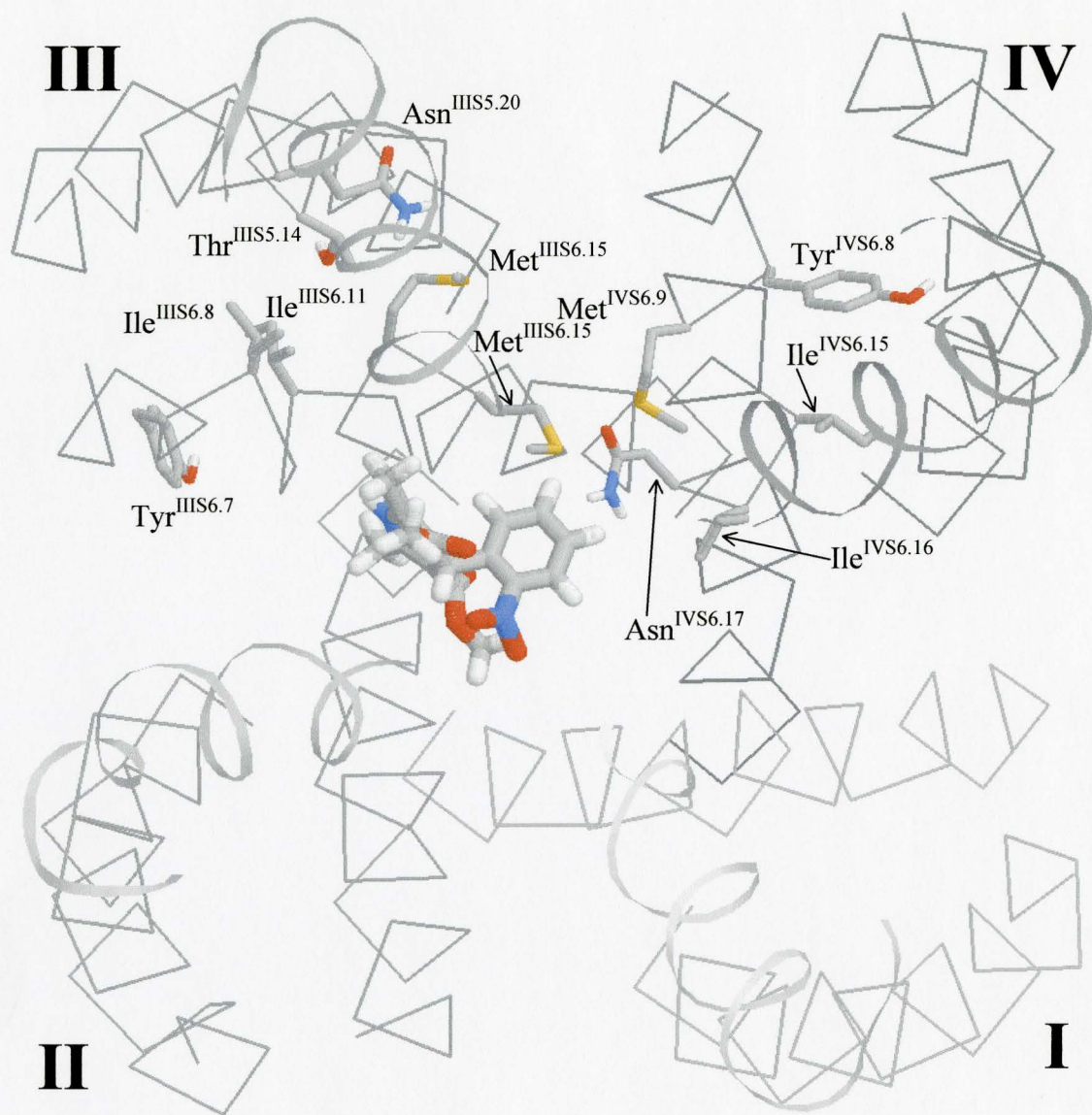


Fig. 3.3 C, *top view*. Nifedipine bound inside the pore of Test Model II. (See Fig 3.3 A *top view* for description of the ligand and channel presentation).

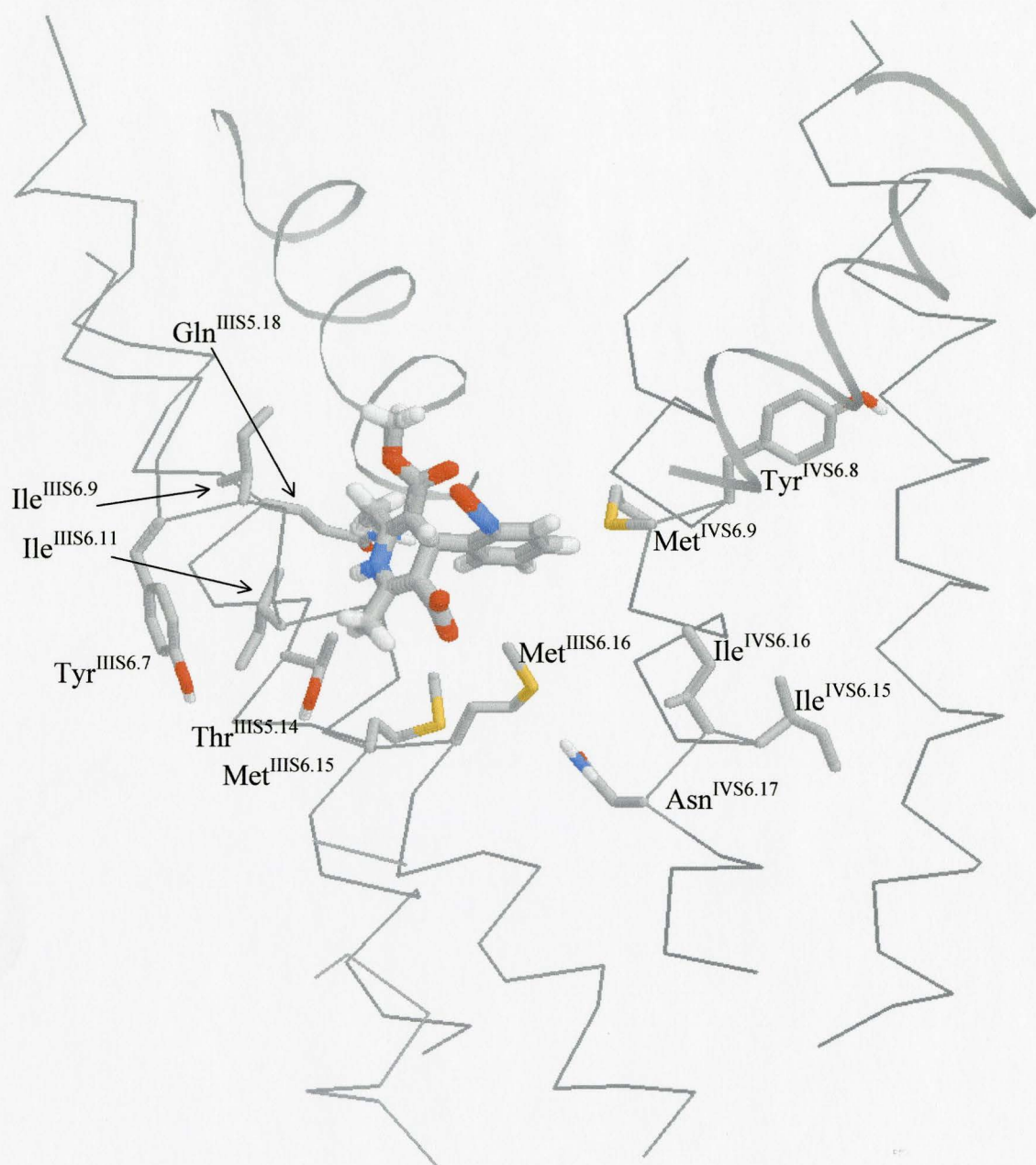


Fig. 3.3 C, *side view* of the ligand inside the pore of Test Model II. Parts of repeat I and II are removed as described before. (See Fig 3.3 A *top view* for description of the ligand and channel presentation).

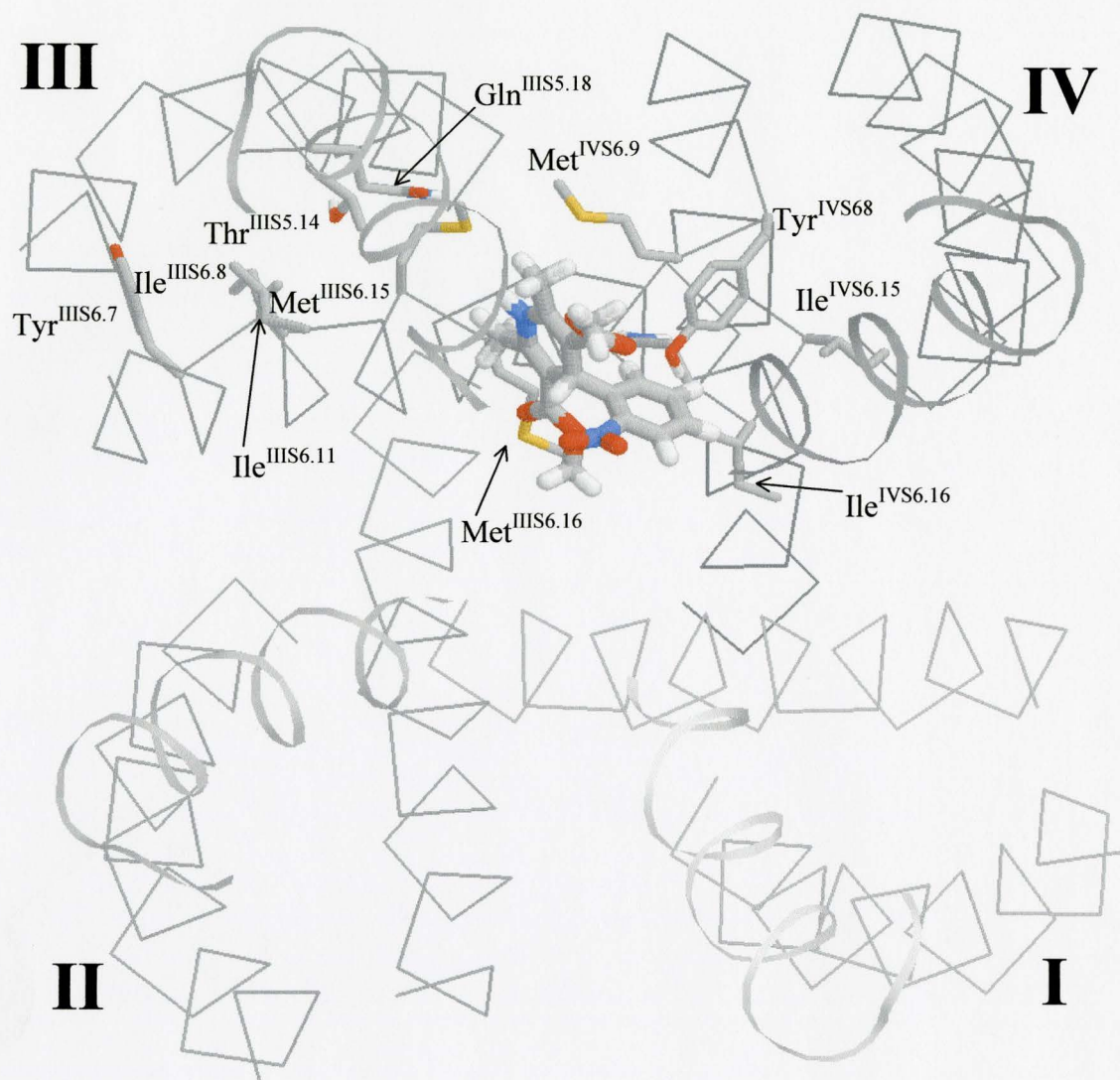


Fig. 3 D, top view . The ligand in the III/IV interface of Test Model II. (See Fig 3.3 A top view for description of the ligand and channel presentation).

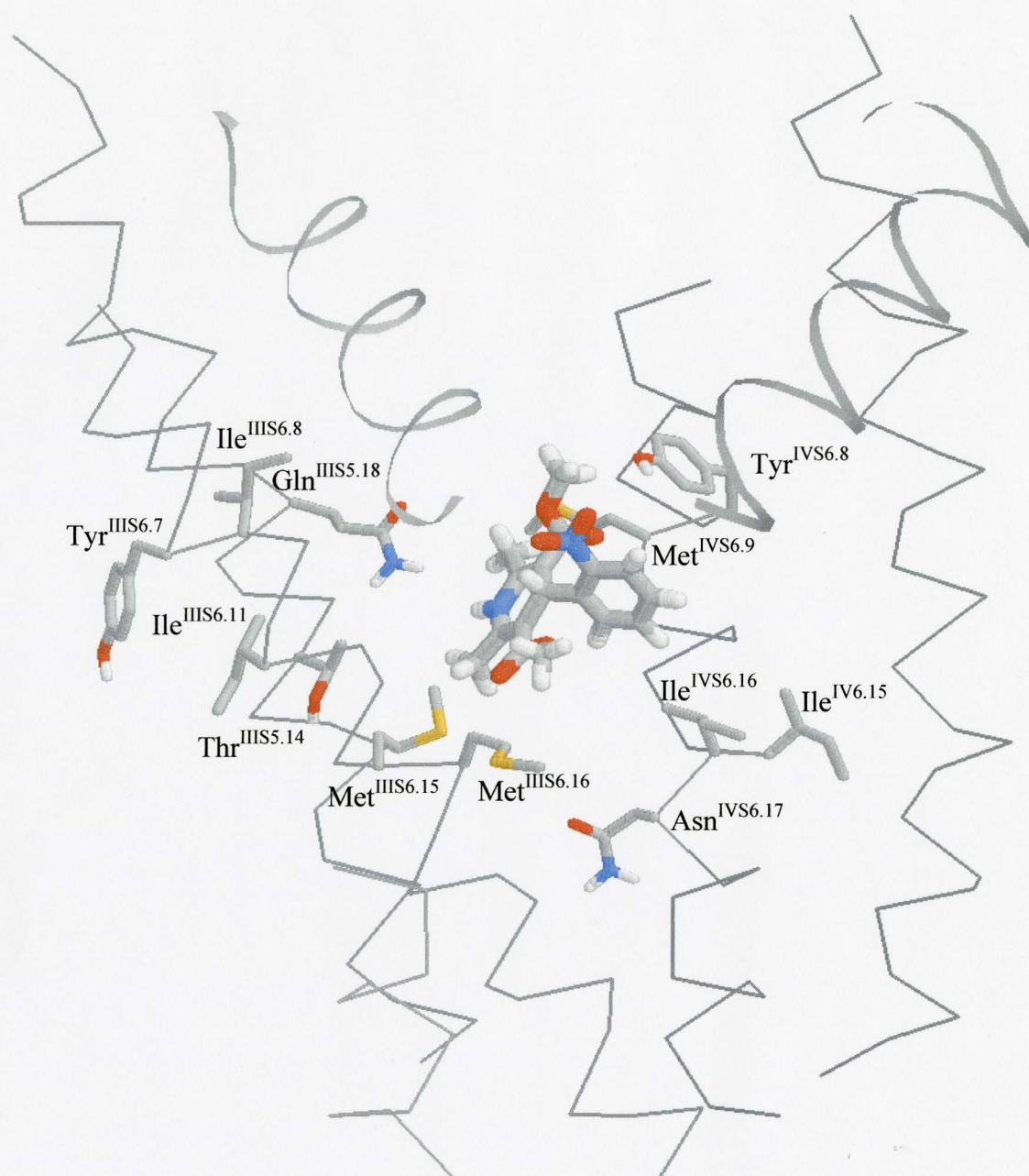


Fig. 3.3 D, *side view*. Nifedipine in the III/IV interface of Test Model II. (See Fig 3.3 A *top view* for description of the ligand and channel presentation).

3.2. Conformational studies of tetrandrine

While we can use the KcsA template for the modeling of alpha-helical TM segments of LCC, the modeling of selectivity filter of the channel, formed by flexible membrane-diving P-loops, is more complicated task, requiring additional data. The folding of P-loops is expected to be different in K^+ and Ca^{2+} channels for the following reasons. K^+ channels discriminate between incoming ions, based on their relative size. Thus the K^+ selectivity filter is formed by several rings of backbone carbonyl oxygens, and its diameter matches the size of K^+ ions. This mechanism cannot be applied for Ca^{2+} and Na^+ ions, since they have similar diameter. It was shown experimentally that the selectivity in Ca^{2+} channel is realized at the level of P.50 conserved glutamates, whose side chains are directly interact with permeating ions (Kim et al., 1993, Yang et al., 1993). The second ring of conserved acidic residues was located downstream, at the level of P.54 (and IIP.51) (Table 3.1). In KcsA these residues form the salt bridges with Arg^{S6.2}s, which are highly conserved among potassium channels. In LCC, the residues at positions S6.2 are non-ionizable and, therefore, cannot form salt bridges with P.54. The sidechains of these upper-ring residues may face the pore and interact with Ca^{2+} ions. In addition, mutation of Asp^{IVP54} to lysine has decreased the Ca^{2+} current and distorted the Ca^{2+} block of Li^{2+} current (Bahinski et al., 1997). Thus, the selectivity- filter region of LCC may comprise not

only the lower ring of P.50 glutamates, but also upper ring of Asp^{IP54}, Asp^{IIP51}, Glu^{IIIP54} and Asp^{IVP54}.

The exposure of these uncompensated negatively charged residues into the low-dielectric region of protein would result in improbable high energy of the channel. Therefore, these residues should be neutralized by counterions. In the absence of neighboring basic residues in this region of LCC, the obvious choice for the counterions is four Ca²⁺ ions, which were added to all models of selectivity filter.

Since homology modeling of the selectivity region based on the KcsA template is not consistent with the above rationale, we used another approach for the modeling of P-loops. Some LCC ligand may bind to the selectivity filter either permanently, or on their way to the binding site located down the pore. The main idea of our approach was that we can use such relatively rigid ligands to “shape” the flexible loops around them, thus finding an approximate size and geometry of the filter. An interesting LCC blocker (S,S)-(+)- tetrandrine, which competes with diltiazem for the binding site in the selectivity filter region of LCC (King et al. 1989), was used for the purpose of P-loops shaping .

The semi-rigid alkaloid tetrandrine (TD), isolated from various plants, such as *Stefania tetrandra*, is traditionally used in Chinese medicine for the treatment of angina and hypertension. In addition, tetrandrine exhibits antitumor activity, which

has stimulated extensive research and a number of clinical trials (Kupchan et al., 1973). The antihypertensive effect of TD is linked to its ability to block L-type Ca^{2+} channel (Kwan et al., 1992, Wang and Lemos, 1995). The chemical structure of tetrandrine is shown at Fig 3.4. X-Ray crystallography studies yielded the 2\AA - resolution structure of tetrandrine (Gilmore et al., 1975), demonstrating that the molecule is shaped roughly as an equilateral triangle. However, this finding cannot rule out of consideration other possible conformations of tetrandrine which may exist in physiological conditions when it interacts with LCC. In order to determine all possible low-energy conformations of tetrandrine and analyze its interaction with Ca^{2+} ions, we performed a series of computational and spectroscopic studies, described below.

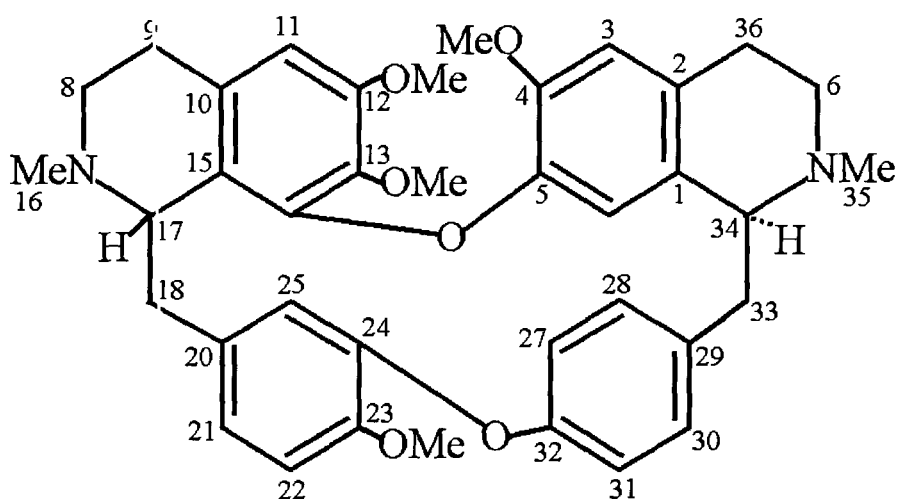


Fig. 3.4. Structural formula of (S,S) –(+)- tetrandrine

3.2.1 Computational analysis of tetrandrine

Systematic conformational search for the MEC of tetrandrine (TD) was performed from the starting points, using the method of Go and Sheraga (1970), which was shown to be very effective for the studies of macrocyclic alkaloids (Zhorov, 1993, Zhorov and Brovtyna, 1993). The main cycle of tetrandrine consists of 18 bonds and its conformation may be described by 12 independent torsions. Since this molecule has several rigid aromatic cycles, eight of these torsions would always have the definite value of either 0° , or 180° . Thus, the 18-membered cycle of tetrandrine can be substituted by a virtual 9-membered ring, shown at Fig.3.5. The bonds O4-C32 and C29-C33 of main cycle of TD are in para position of the phenyl ring. Therefore, two torsions corresponding to this aromatic ring can be substituted by one torsion, which designates the rotation of phenyl ring around the O4-C33 line.

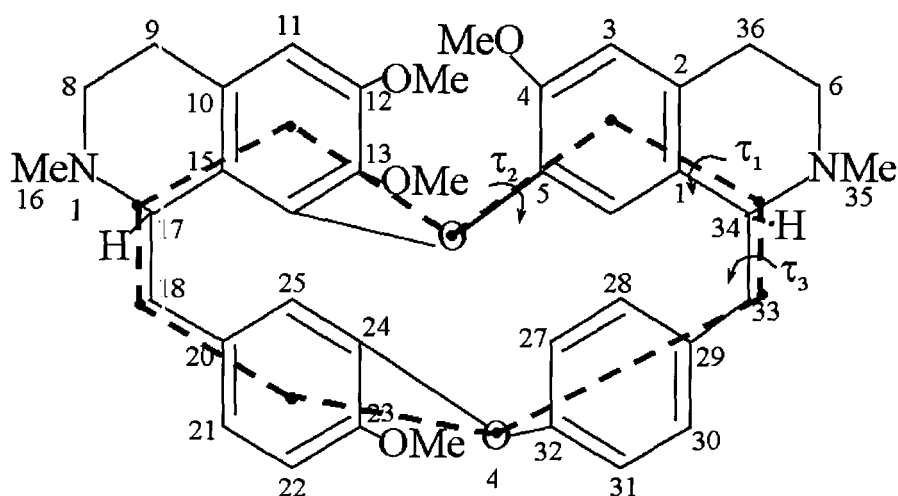


Fig.3.5. The 9-membered virtual cycle, a model for the 18-membered cycle of TD.

During the search of starting loop-closing torsions, the values of three remaining independent torsions τ_1 , τ_2 , τ_3 (Fig.3.5) were varied from 0° to 360° with the step of 30° , which gave us a three-dimensional grid with 3^{12} knots. The method of Go and Sheraga (1970) was applied to each of these knots. This procedure, realized in *ZMM* package, calculates the sets of torsions necessary for exact loop closure and local conformational deformation in cyclic molecules. In this method, the systematic sampling of any three of nine torsions allows us to determine all possible conformations in which the macrocycle is closed. Among acquired sets of torsions, we selected only those having the absolute value of torsions C2-C1-C34-N and N1-C17-C15-C10 less than 60° . This condition is necessary for rough closure of tetrahydroisoquinoline cycles. Thus, we acquired 244 starting sets of torsions, allowing the closure of all cycles of TD molecule.

These starting conformations underwent two-stage energy minimization. At the first stage, we did not take into the account electrostatic interactions; aromatic rings and bond angles were kept rigid. That allowed us to increase the speed of convergence of trajectories. MECs found at this step were then used as starting points for energy minimizations of the complete TD model. Forty six resulting MECs have the energy less than 25 kcal/mol; the energy of 10 lowest-energy conformations is listed in Table 3.5.

Table 3.5. The energy and main torsion angles of the lowest-energy MECs of tetrandrine.

Conformer				1	2	3	4	5	6	7	8	9	10
Torsion				Torsion angles, degree									
C	C1	C34	C33	-84	-81	-68	-73	-72	-93	-70	-69	-83	-46
C1	C2	C36	C6	1	0	-13	-9	-10	15	-13	-12	-2	-26
C	C5	O1	C14	-159	-153	-165	-151	-149	-174	173	-168	-151	52
C5	O1	C14	C15	-113	-118	-99	-117	-117	-98	-79	-96	-115	90
C15	C10	C8	C9	-14	-14	-14	2	0	-11	26	-10	-11	28
C10	C8	C9	N1	44	44	45	25	27	41	-5	41	39	-13
C8	C9	N1	C17	-61	-61	-63	-57	-57	-66	-44	-67	-59	-32
C14	C15	C17	C18	-69	-69	-68	-86	-84	-72	-104	-72	-73	-91
C15	C17	C18	C20	161	155	175	70	64	176	69	176	149	-61
C17	C18	C20	C25	-98	-102	-73	82	88	-68	83	-66	-102	81
C25	C24	O4	C32	35	42	-14	-86	-86	-3	-43	-17	55	14
C24	O4	C32	C27	-138	45	135	88	87	109	-123	132	-141	104
C1	C34	C33	C29	52	48	-3	52	52	47	56	1	50	-39
C1	C34	N	C6	55	54	46	50	49	56	48	48	56	27
C34	N	C6	C36	-56	-57	-63	-61	-61	-47	-62	-64	-58	-60
C3	C4	O	C37	1	5	5	6	7	-1	-8	2	19	-2
C11	C12	O2	C26	-8	0	1	-10	-9	-2	9	6	-7	-8
C12	C13	O5	C7	52	-51	-50	53	54	54	-52	-50	-49	50
C22	C23	O3	C19	110	4	110	25	-25	-29	23	26	-48	109
C4	O	C37	1H37	59	57	57	56	56	61	65	59	48	62
C23	O3	C19	1H19	67	55	66	43	73	74	-74	43	59	65
C13	O5	C7	1H7	24	95	94	25	26	25	92	94	93	24
C12	O2	C26	1H26	63	59	57	65	64	60	52	55	63	63
C34	N	C35	1H35	59	178	70	67	67	-65	70	70	38	77
C9	N1	C16	1H16	68	70	69	52	52	47	59	48	65	57
Energy, kcal/mol				4.9	6.1	7.0	7.7	7.8	8.2	8.5	8.8	10.3	10.4

Ten lowest-energy conformations can be subdivided into two subfamilies. The triangular shape of MECs 1,2,3,4,5,8,9 corresponds to the X-Ray structure, acquired by Gilmore et al.(1975), while conformers 6,7 and 10 have roughly quadrangular form (Fig.3.6). These square-shaped TD conformers, which were not detected experimentally, may also take part in biological processes blocking the ion current through LCC. In order to investigate which conformation is present in solution at physiological temperature, we performed a series of NMR spectroscopy experiments.

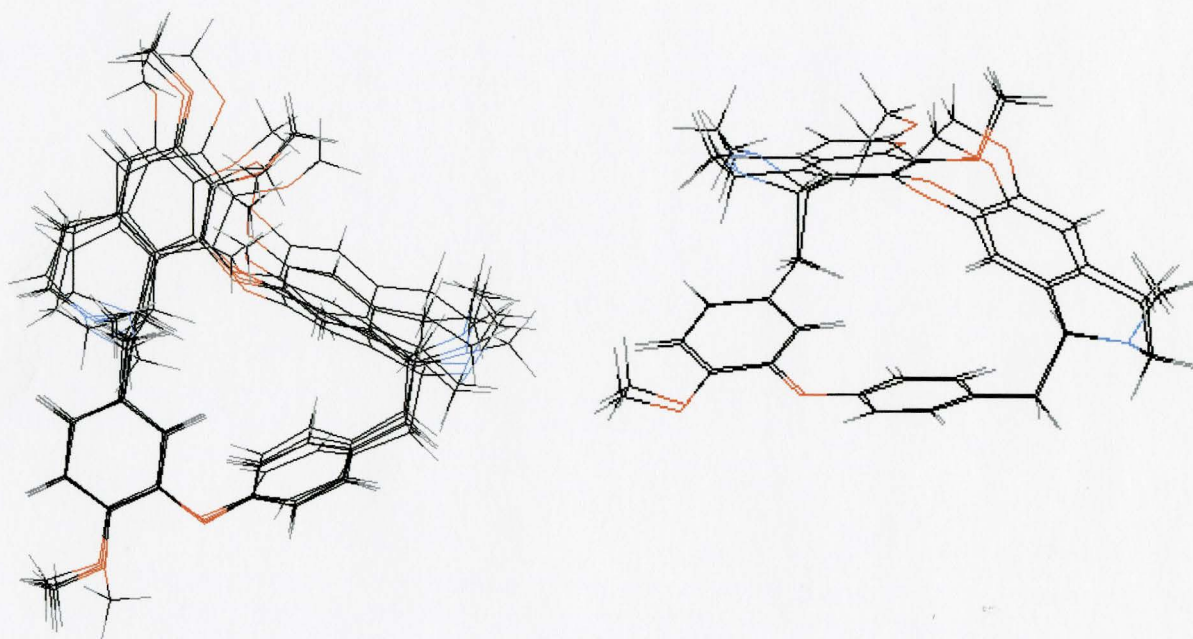


Fig. 3.6. Superposition of triangle-shaped MECs of TD (*left*) and square-shaped MECs (*right*).

3.2.2. NMR studies of the drug

Initial 1D proton spectra of tetrandrine in chloroform were recorded at room temperature of $23 \pm 1^\circ \text{C}$, as described in *Methods* (See section 3.2.2). Processing of these spectra with Gaussian multiplication helped in improving the signal-to-noise ratio (Fig 3.7). Since NMR studies on tetrandrine have already been conducted by Lin et al. (1993), we assigned 1D spectrum accordingly (Table 3.6). The difference between chemical shifts of our TD spectrum and those reported by Lin et al., is in the range of 0.1 to 0.3 ppm, The possible reason for this is that the our experiments have been conducted on more advanced 500 MHz spectrometer and are more precise.

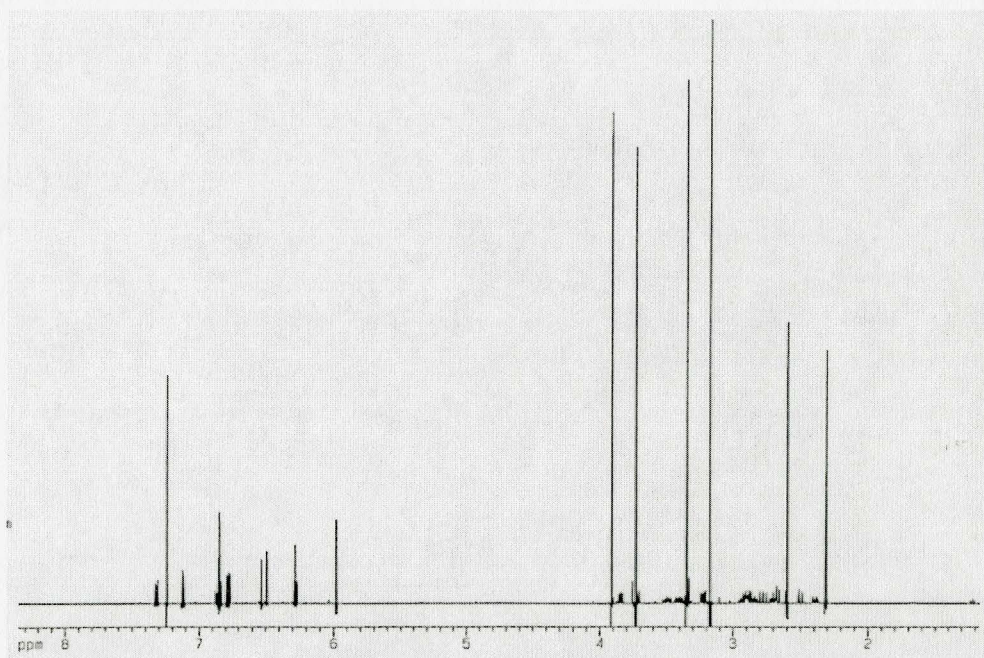


Fig.3.7. 1D proton spectrum of TD in CDCl_3 processed with Gaussian Multiplication.

Table 3.6. Chemical shifts of the protons in 1D spectrum of TD in CDCl₃

Proton	Chemical Shift, ppm	Proton	Chemical Shift, ppm
17	3.73	34	3.84
16	2.30	35	2.58
8	2.87	36	2.83
8	3.48	36	3.39
9	2.38	37	2.69
9	2.89	37	2.92
11	6.26	3	6.48
26	3.70	38	3.33
7	3.15	H	5.96
18	2.48	33	2.75
18	2.67	33	3.22
25	6.53	28	6.27
19	3.88	27	6.78
22	6.82	31	7.10
21	6.85	30	7.32

In order to determine through-space connectivities between TD protons, we acquired T-ROESY spectra of tetrandrine in CDCl₃. Sixty four scans were recorded for each of 256 increments, covering the entire area of the spectrum. The optimal spin lock time was found to be 800 ms. Negative contours of T-ROESY spectrum are shown in Fig. 3.8.

The volume integrals corresponded to intensity of each cross peak were extracted manually, using the *UNIX*-based *XWIN NMR* program. The cross peak of H30 – H31 (see Fig.3.8 B) was chosen as reference peak, because these two protons belong to the rigid aromatic ring, and the distance between them, 2.43 Å, is not affected by any

conformational changes. A relative value of 100 was assigned to intensity of this reference peak; all other intensities were recalculated correspondingly. It was not clear whether we should include only negative part of NOE intensity into our calculations, therefore two sets of data were collected. The first set corresponded to intensities of negative contours of the spectrum, and the second included intensities of both negative and positive parts of NOE cross peaks.

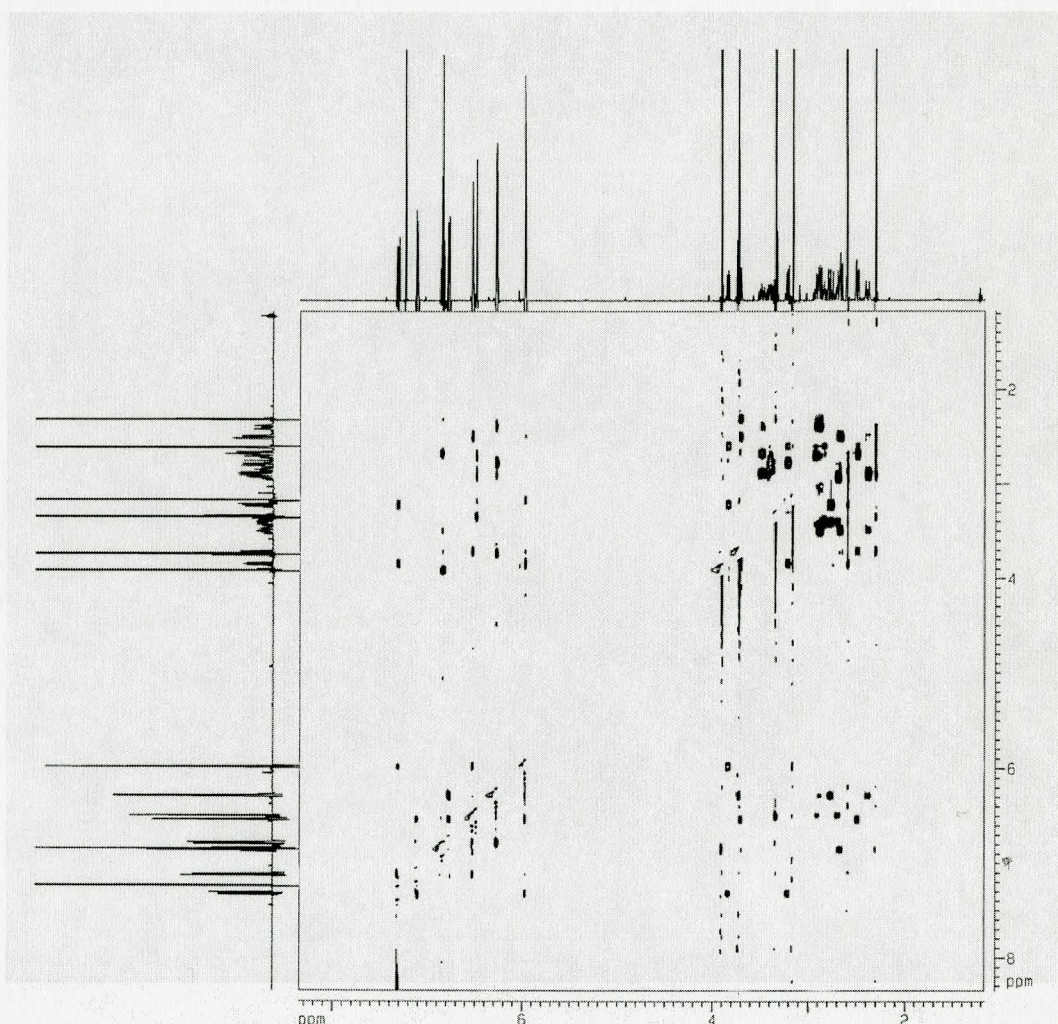


Fig.3.8 A. T-ROESY spectrum of TD in CDCl_3 , number of scans (ns) = 64, number of increments (ni) = 256, spin lock 800 ms, negative contours are shown.

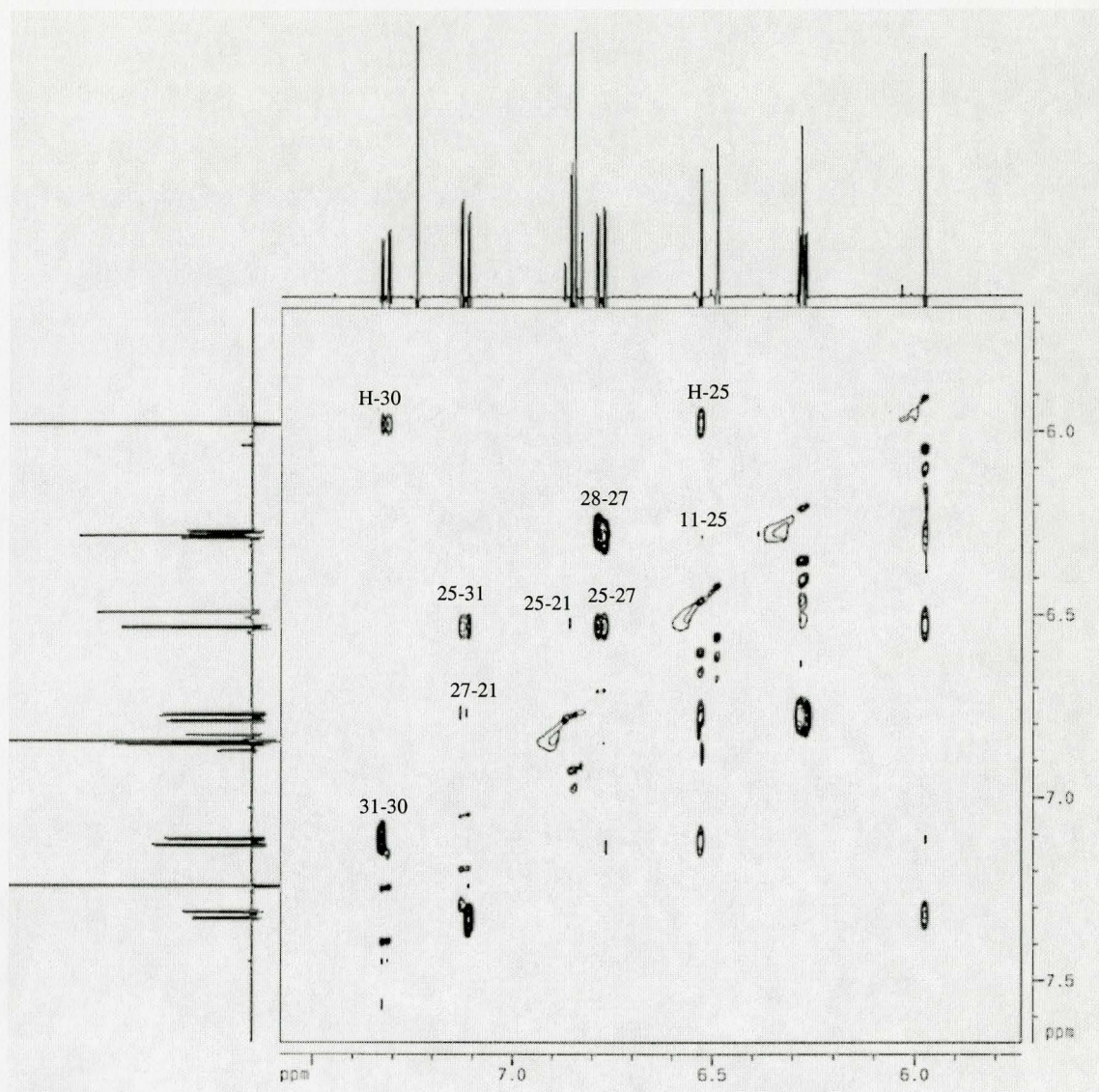


Fig.3.8 B. T-ROESY spectrum of TD in CDCl_3 . Detailed view of the left bottom corner of Fig.3.8 A.

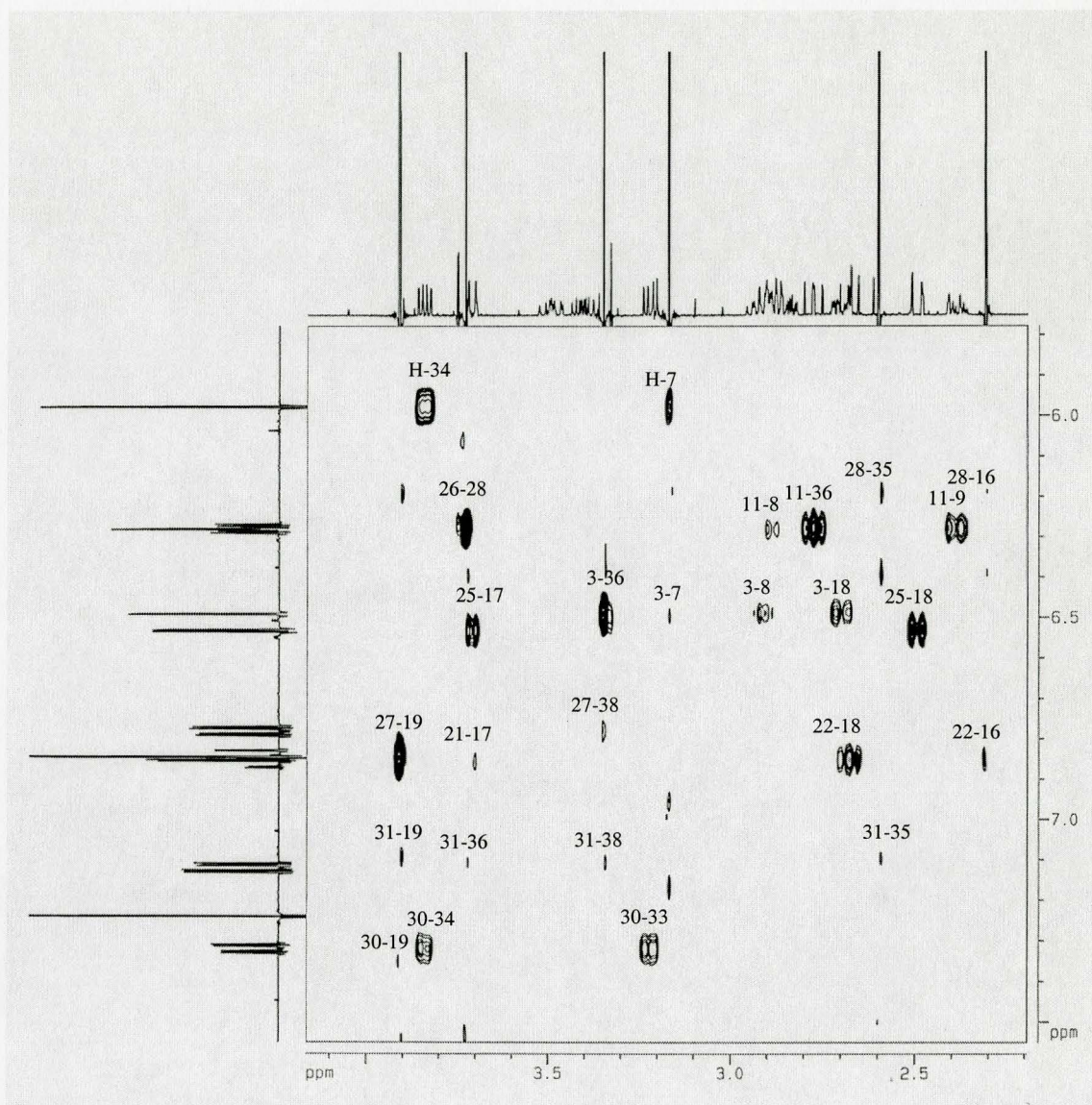


Fig. 3.8 C. T-ROESY spectrum of TD in CDCl₃. Detailed view of the right bottom corner of Fig. 3.8 A.

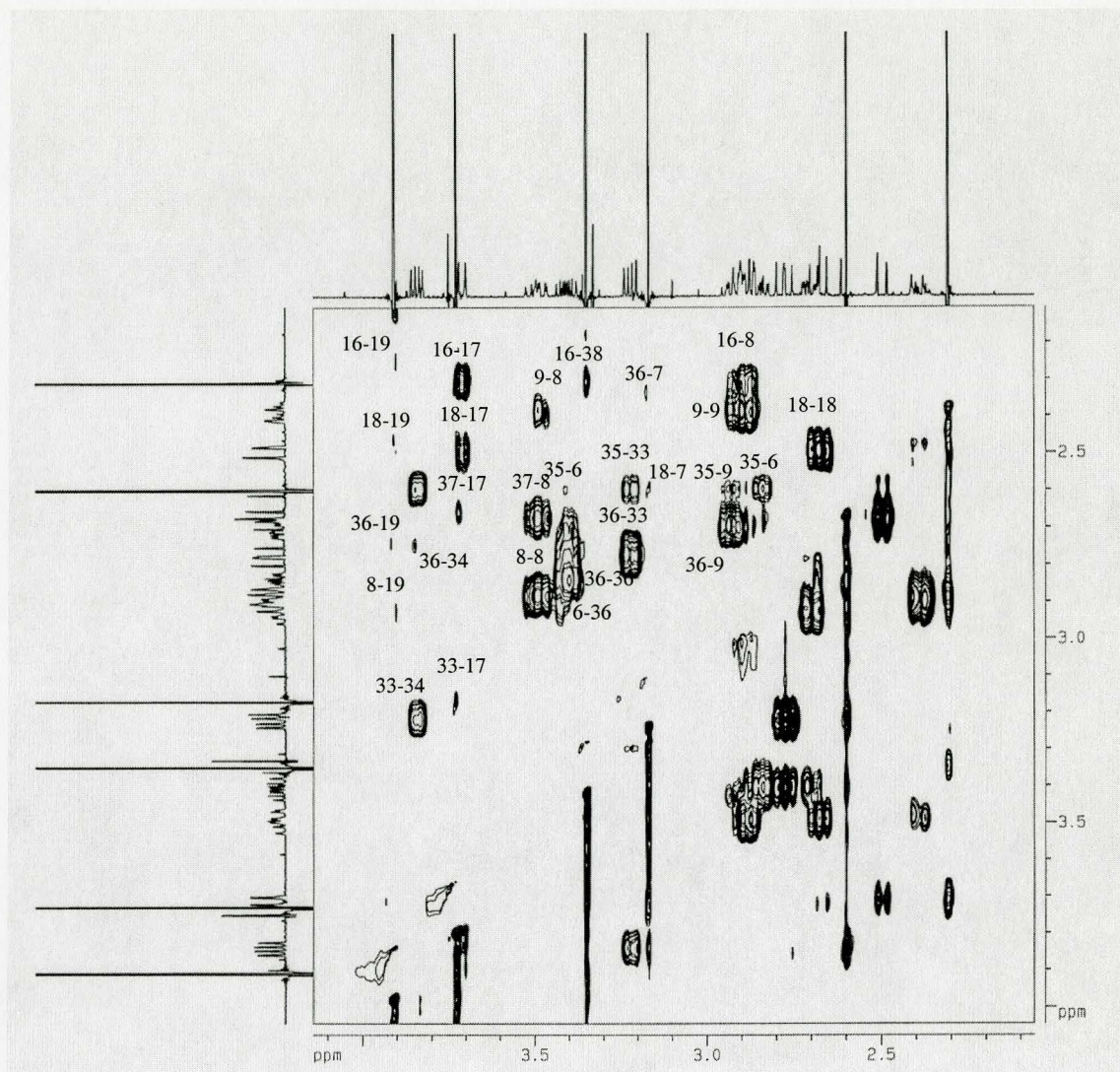


Fig.3.8 D. T-ROESY spectrum of TD in CDCl₃. Detailed view of the right top corner of Fig.3.8 A.

3.2.3. Stochastically restrained MCM search

The interproton distances in TD were calculated by *ZMM* procedure, based on known distance-intensity relationship (see *Methods*). Resulting distances, listed in Table 3.7, were then used as constraints during SR MCM search. The distances, calculated with intensities of both positive and negative parts of cross peaks, did not differ significantly from those calculated with intensities of negative parts only. Therefore only one set of distances, based on negative contours' intensities, was used for further computational studies.

Using as starting points 10 lowest-energy MECs of TD, acquired by conformational analysis described in Chapter 3.2.1, we performed SR MCM search with NOE constraints. Majority of the constraints appeared to match every MEC or most of the MECs belonging to both triangular and quadrangular family. More interestingly, some of the constraints were matched only by triangular MECs, and some only by quadrangular MECs (Table 3.7). Constraints 2H33-H17, H11-H25, H8-H25, matching quadrangular conformations of TD, are of especial interest for us. They are long-range constraints; these protons are located at opposite sides of main TD cycle. The satisfaction of these constraints only in square-shaped MECs indicates major differences in main cycle conformations of two TD families. Thus, we determined that both families of lowest-energy conformers of TD coexist in solution at room temperature, and we should perform further modeling studies with both triangular and quadrangular structures of TD.

Table 3.7. Proton-proton distance constraints, satisfied in low-energy conformations of TD.

			Low-energy conformations of tetrandrine									
			"Triangular" family							"Quadrangular" family		
Protons		NOE, Å	1	2	3	4	5	8	9	6	7	10
3H16	1H8	3.2		+	+	+	+	+	+			
1H16	3H19	4.1		+								
2H16	H28	5.0					+					
2H18	1H7	4.3					+	+				
1H19	H27	4.1			+	+			+	+		
2H35	1H6	3.7	+		+					+		
1H18	H22	3.7		+	+		+			+		
H30	H3	4.2	+		+	+			+	+		
H25	H31	3.7	+	+	+		+	+	+			
H34	H	4.3								+	+	+
2H33	H17	4.5								+		
2H8	1H19	4.3									+	+
2H8	H11	4.1									+	
H11	H25	4.5								+		+
2H8	H25	3.9									+	+
2H16	H17	3.2				+			+		+	+
1H16	H22	4.3	+	+	+				+	+		+
3H35	1H33	3.5	+	+	+	+	+	+	+	+		+
3H35	H34	4.3	+	+	+	+	+	+	+	+		+
3H35	H28	4.9	+	+	+	+	+	+		+		+
2H33	H30	3.3	+	+	+	+	+		+		+	+
1H36	H3	3.6	+	+		+	+	+	+	+	+	+
2H7	H	3.8	+	+	+	+	+	+	+		+	+
2H7	H3	4.3	+	+	+	+			+		+	
1H33	H34	4.3				+		+		+	+	+
H17	H21	4.1	+	+	+	+	+	+	+	+		+
H	H30	3.8	+	+	+	+	+	+	+		+	+
H25	H27	3.8	+	+	+		+	+	+	+	+	+
Satisfied			23	24	25	23	23	24	26	19	21	25

Note: several constraints that were satisfied in all conformers or those that were not satisfied in any MEC are not shown.

3.2.4. NMR of Ca^{2+} - bound tetrandrine in TFE

Studies of some LCC drugs have indicated the formation of ligand- Ca^{2+} ions complexes in nonpolar milieu (Belciug and Ananthanarayanan, 1994, Ananthanarayanan et al., 1993, Tetreault and Ananthanarayanan, 1993). If tetrandrine also interacts with Ca^{2+} ions, the conformational changes occurring upon such interaction should be observable by NMR spectroscopy. This technique has already been used to investigate the conformational changes, which occur in several peptides upon their interaction with cations (Ananthanarayanan et al., 1997, Qi et al., 2000). In the present TD studies, we expected to detect the conformational changes caused by the drug interaction with Ca^{2+} ions in TFE by tracking the changes in chemical shifts of TD protons.

Since all previous NMR spectra of TD were acquired in chloroform solution, we started the NMR studies of TD in TFE with acquisition and assigning of its 1D spectra. The first 1D spectrum, processed with Gaussian multiplication, was obtained at room temperature of $23 \pm 1^\circ\text{C}$. TD concentration of 5 mg/ml (8mM) was found to be optimal for obtaining well-resolved spectra. The spectrum assignment was performed by extracting all coupling constants and chemical shifts. Additional information about proton-proton connectivities was obtained from 1D TOCSY and COSY spectra of TD. The latter is acquired with 256 increments, 2 scans per every increment.

For the titration studies with Ca^{2+} , four 1D spectra were obtained starting with the 1D spectra of TD in TFE. Then aliquots of 10 μl of the stock $\text{Ca}(\text{ClO}_4)_2$ solution in TFE (0.8 M) were added in order to get 1:1, 2:1 and 3:1 ratios of Ca^{2+} to TD (Fig.3.9). Significant changes in chemical shifts (Fig.3.10) and coupling constants were observed at 1:1 ratio. The saturation of chemical-shift changes at about 1:1 – 2:1 ratios indicates formation of Ca^{2+} - drug complex in TFE (Fig.3.10 A)

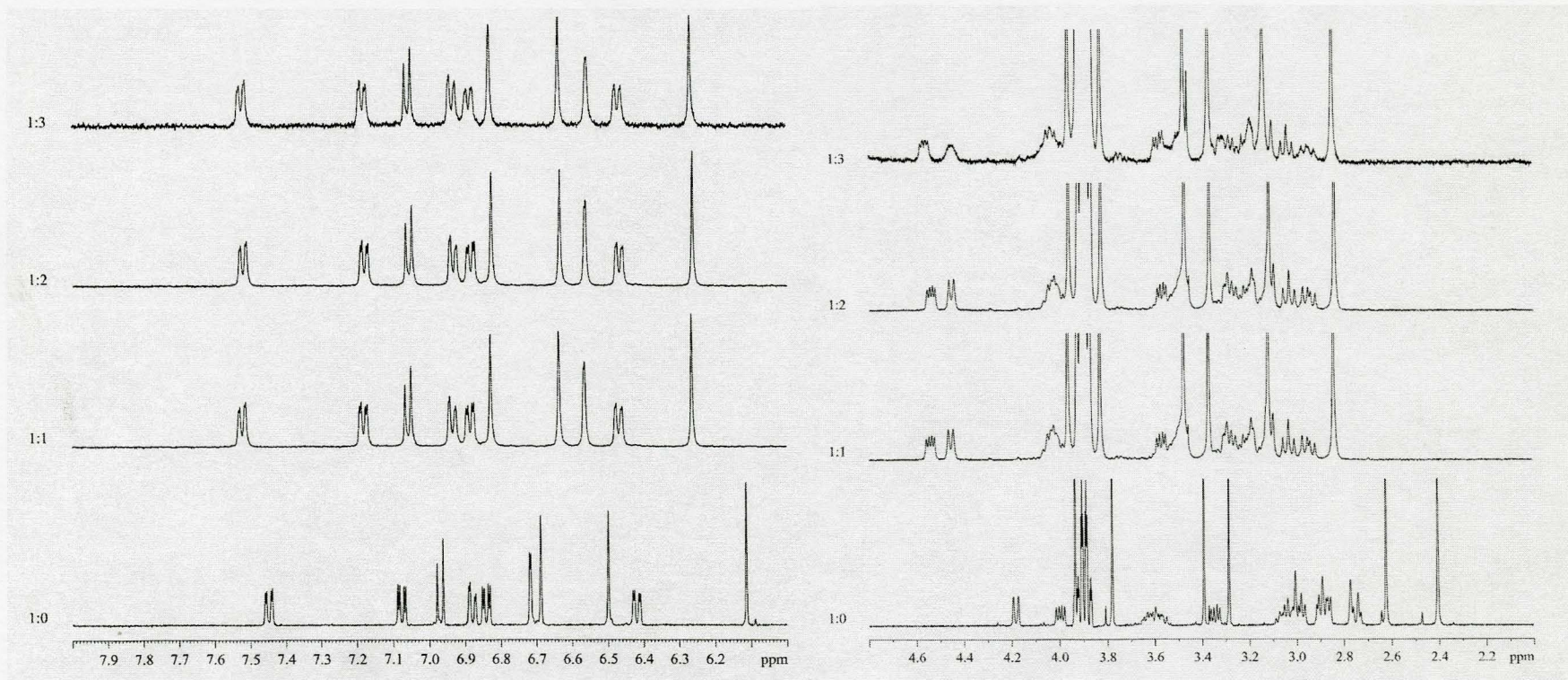


Fig. 3.9. 1D ¹H-NMR spectra (processed with Gaussian Multiplication) of TD in TFE (5 mg/ml) without Ca²⁺ and after addition of 1:1 molar ratio of Ca²⁺.

Table 3.8. Chemical shifts of protons of 1D spectrum of TD in TFE.

Proton	Chemical Shift (ppm) of TD	Chemical Shift (ppm) of 1:1 TD : Ca²⁺
17	4.25	4.50
16	2.62	3.14
8	3.05	3.51
9	3.51	3.95
11	6.50	6.64
26	3.79	3.83
7	3.30	3.39
18	2.90	3.48
25	6.72	6.59
19	4.02	4.05
22	6.91	7.07
21	6.92	7.08
34	3.80	4.35
35	2.40	2.85
36	2.65	3.15
37	3.38	3.58
3	6.70	6.83
38	3.40	3.41
H	6.11	6.27
33	2.85	3.09
28	6.42	6.48
27	6.84	6.90
31	7.08	7.18
30	7.45	7.50

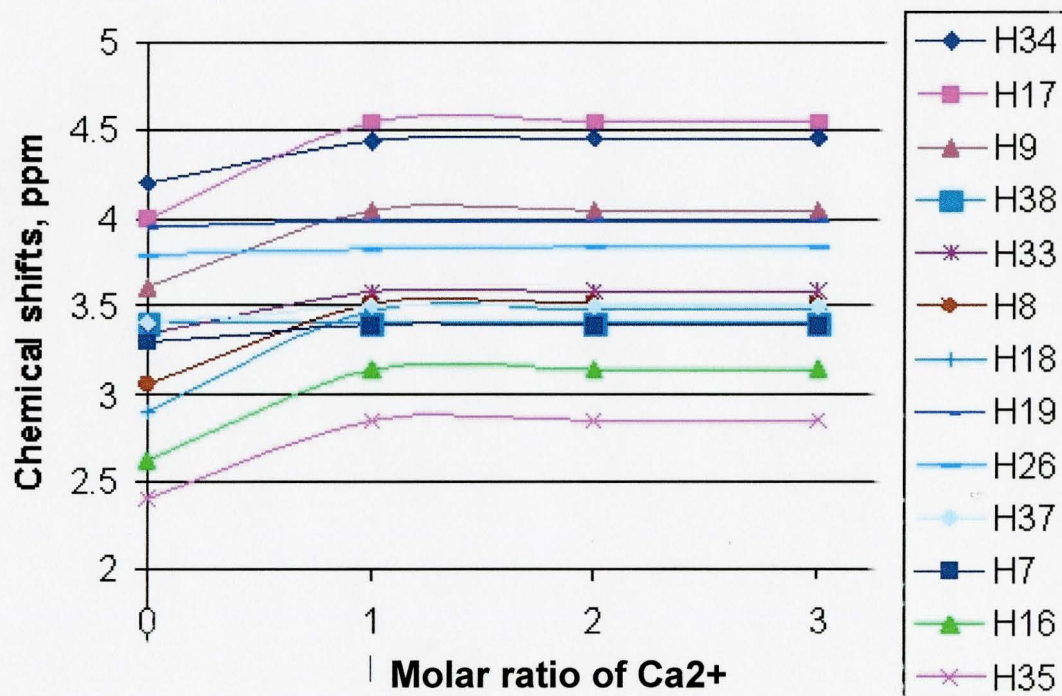
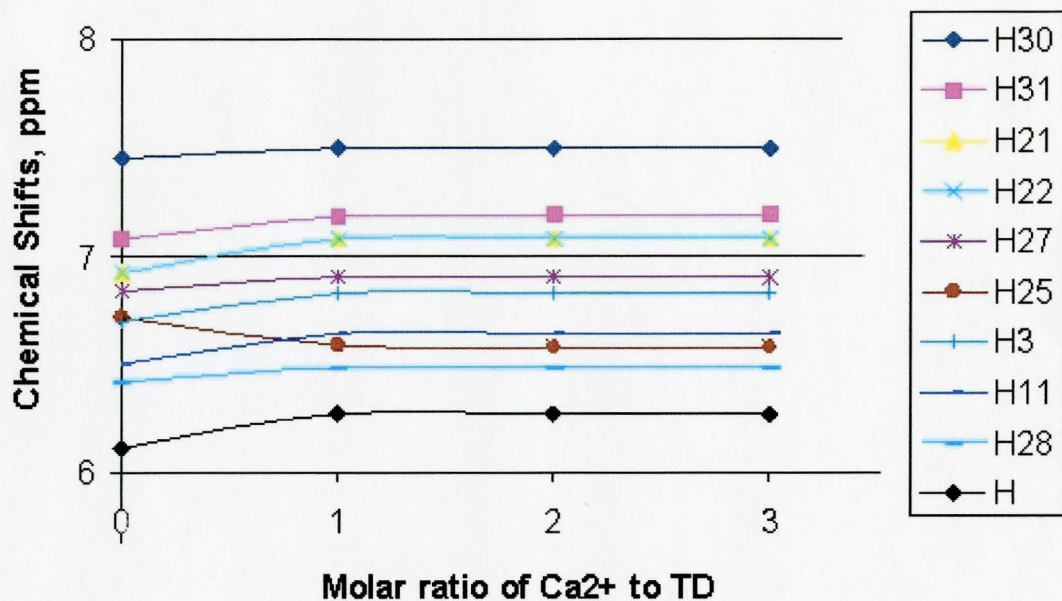


Fig. 3.10 A. Changes in chemical shifts of 1D proton spectra of TD in TFE after addition of Ca²⁺

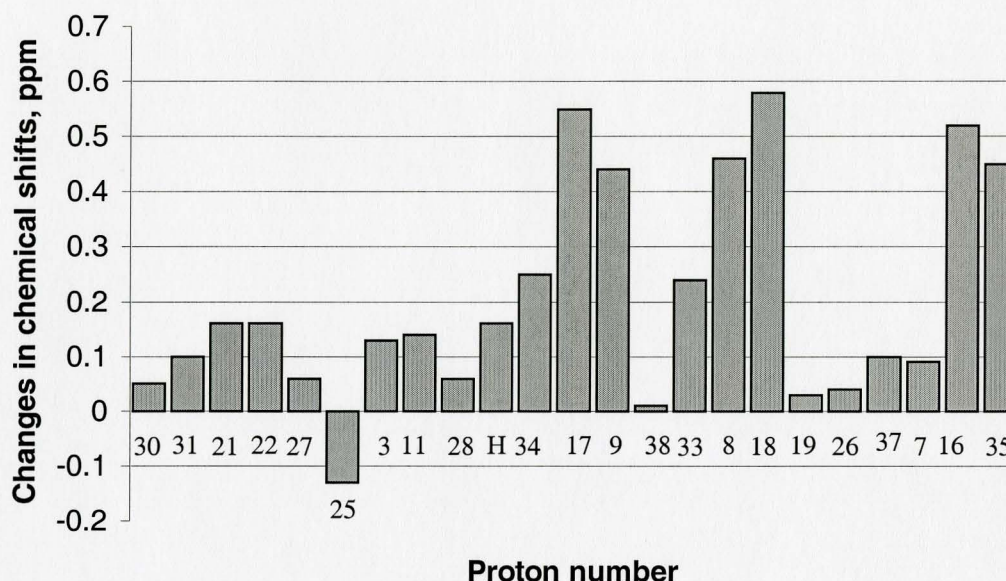


Fig. 3.10 *B*. Changes in chemical shifts of 1D proton spectra of TD in TFE after addition of one molar equivalent of Ca^{2+}

It is likely that the addition of Ca^{2+} ions to TD solution stabilizes either one of TD lowest-energy conformations, or both of them. In order to find which TD conformation corresponds to the spectra of Ca^{2+} -bound TD, we extracted volume integrals of T-ROESY spectra of TD with Ca^{2+} (1:1 molar ratio) (Fig. 3.11), similar to what we did for TD alone. The proton-proton distances, calculated according to known formula of distance dependence on peak intensity (see *Methods*), were then used as constraints during SR MCM search. At this search, 10 starting low-energy TD conformations were used to determine which NOE constraints would match them. The resulting list of matched NOEs is shown in Table 3.9. Most of them, as in the case of TD without Ca^{2+} , matched both families of TD MECs. However, constraints H30-H34,

H30-H21, H25-H17, H28-1H33 matched only conformers belonging to triangle-families, while none of these NOEs matched the quadrangular family only. Thus, only conformers of triangle family can be observed after TD interaction with Ca^{2+} . In the other words, addition of one molar equivalent of Ca^{2+} to one molar equivalent of TD stabilizes the triangular conformation of the drug.

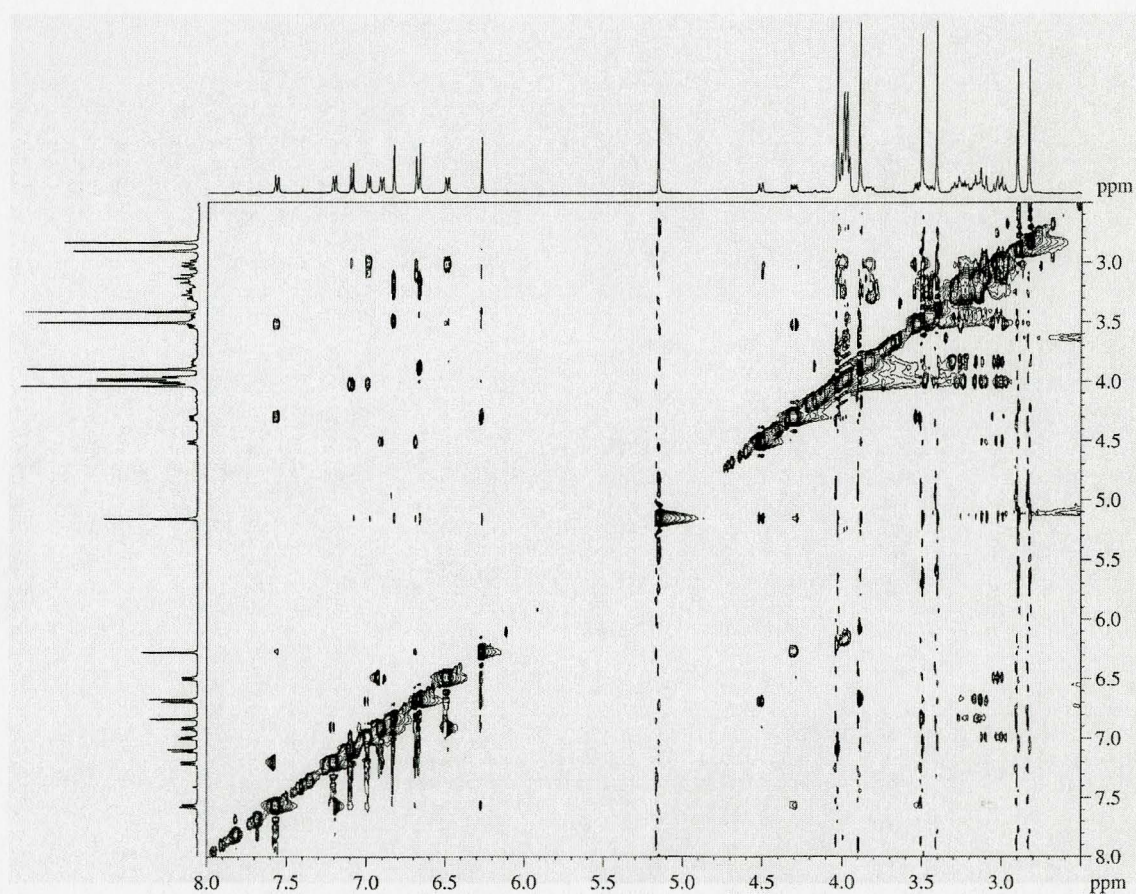


Fig.3.11 A. NOESY spectrum of TD + Ca^{2+} (1:1) in TFE.(with Watergate Suppression).

Mixing time : 0.5 s, ns= 96, ni = 256.

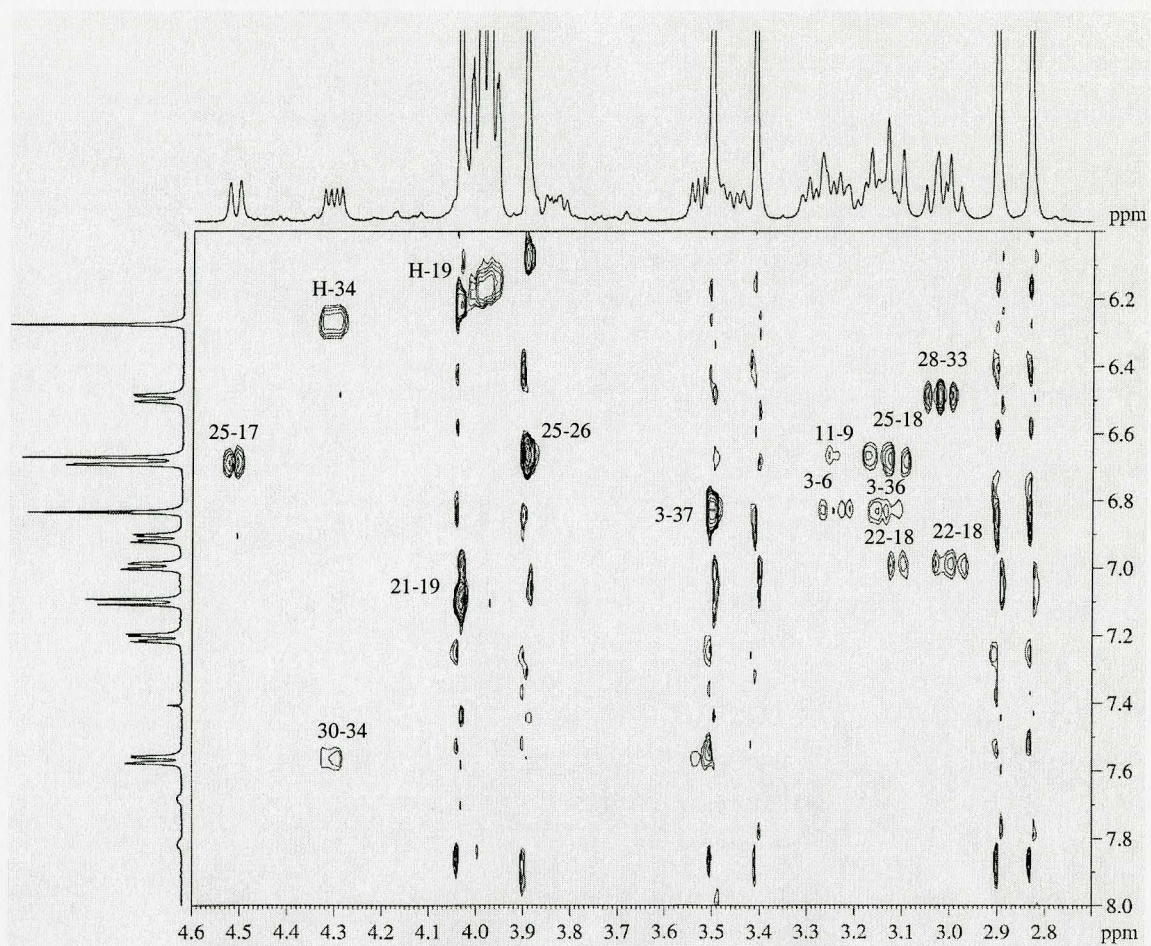


Fig.3.11 B. Detailed view of the bottom right corner of Fig.3.16 A.

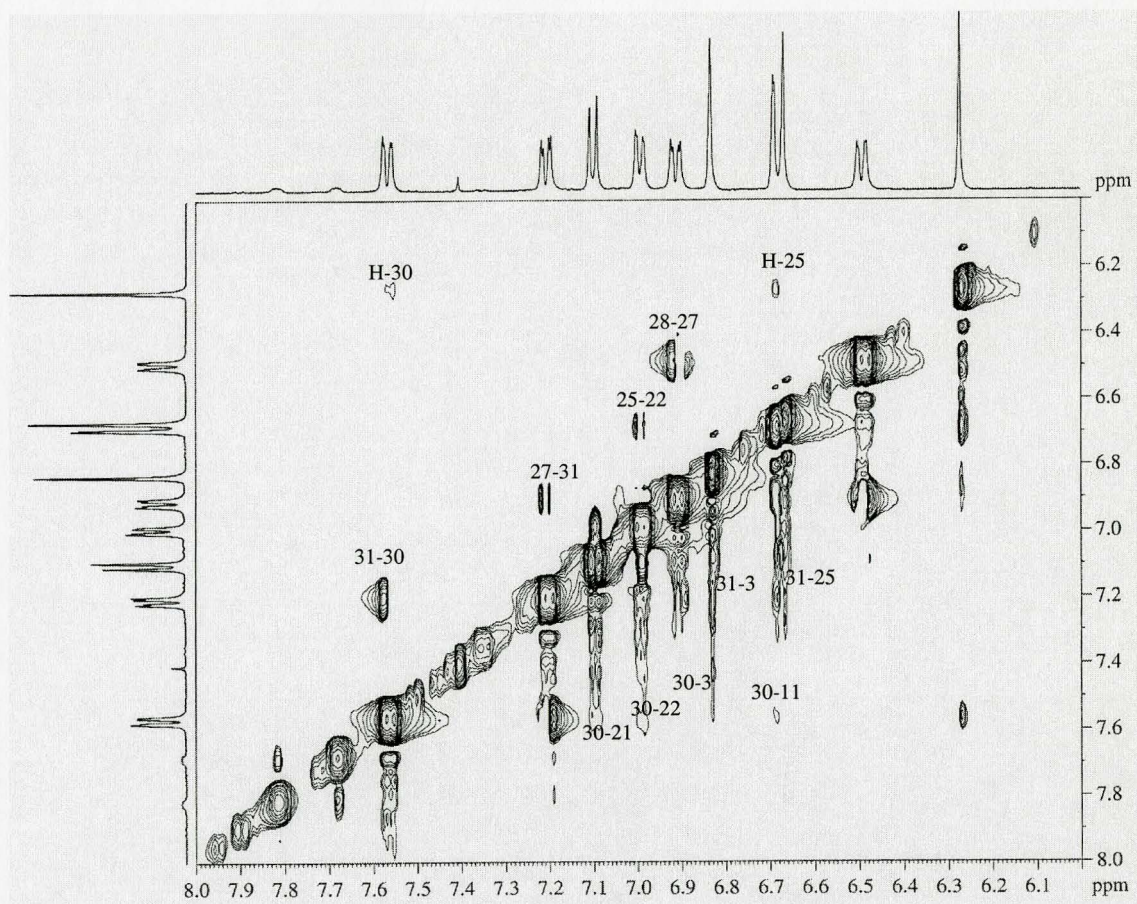


Fig.3.11 C. Detailed view of the bottom left corner of Fig.3.16 A. Note the reference peak of H31-H30 protons.

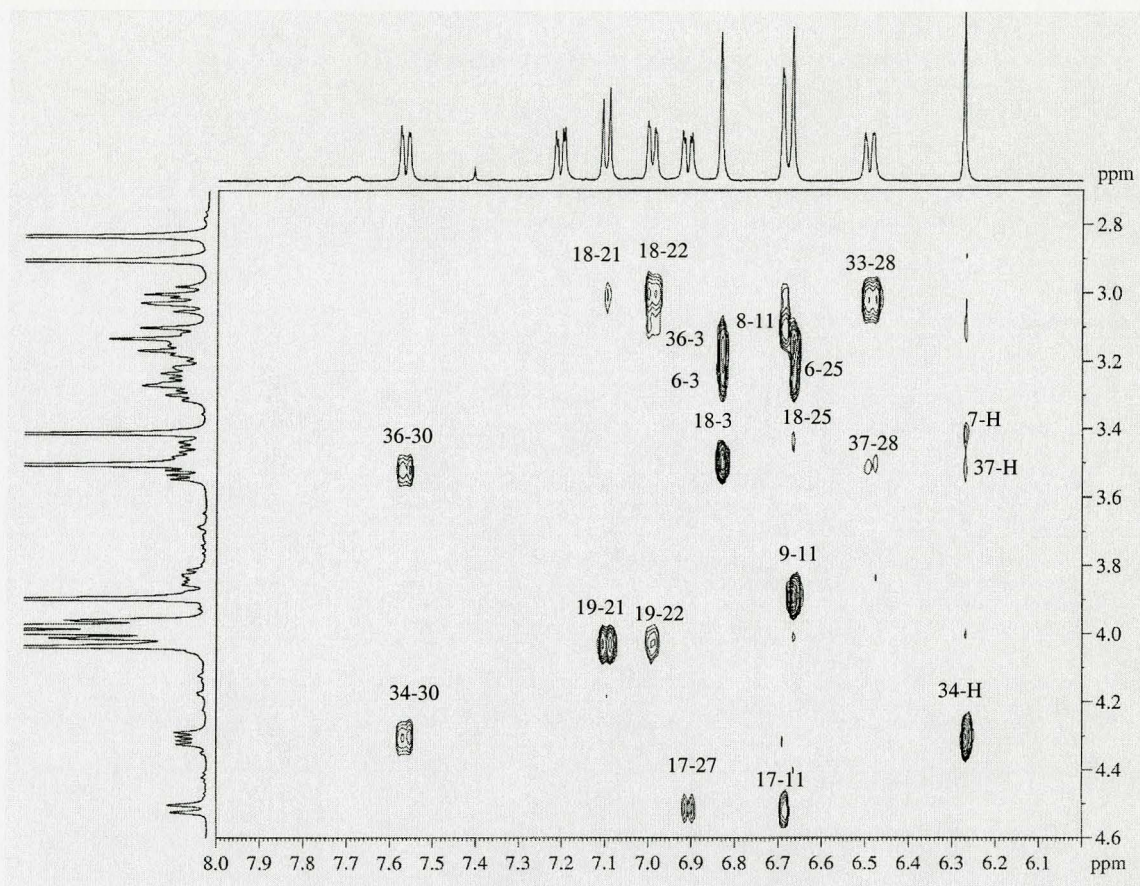


Fig.3.11 D. Detailed view of the top left corner of Fig.3.16 A..

Table 3.9. Proton-proton distance constraints derived from the spectra of TD with Ca^{2+} satisfying the low-energy conformations of TD.

		NOE, Å	Low-energy conformations of tetrandrine									
			"Triangular" family						"Quadrangular" family			
Protons			1	2	3	4	5	8	9	6	7	10
H30	H34	2.8		+			+					
H30	H21	9.3		+			+					
H25	H17	3.0	+	+	+	+	+	+	+			
H28	2H33	2.5		+			+	+				
1H37	H28	5.5	+	+	+	+		+	+			+
1H6	H25	7.2		+	+	+	+	+	+		+	+
1H7	H	5.6	+	+			+	+		+		
1H37	H	6.2	+	+	+		+	+	+	+	+	+
H30	H	3.3	+	+	+	+	+		+	+		+
H25	H	3.1	+	+	+		+	+	+	+	+	+
H25	1H18	2.6	+	+	+	+	+			+	+	+
H25	H31	2.3	+	+	+	+	+	+	+		+	+
H	H25	2.7	+	+	+		+	+	+		+	+
Satisfied			34	38	35	31	17	34	3	31	32	33

Note: several constraints that were satisfied in all conformers or those that were not satisfied in any MEC are not shown.

3.2.5. The modeling of TD interaction with Ca^{2+}

In order to model the possible Ca^{2+} - TD interaction, we MC-minimized one of the lowest-energy MECs of tetrandrine with Ca^{2+} ion, constrained to different nucleophilic atoms of TD. In the lowest-energy conformation obtained, the ion interacts with O, O1 and O4 oxygens of TD (Fig 3.12). Interestingly, most of the protons whose chemical shifts were affected by binding of Ca^{2+} appeared close to the ion, some of them form favorable van der Waals contacts with Ca^{2+} (Fig 3.12 *B, C, D*). H16 and H35 of NH_3 groups and H8, H9 of tetrahydroisoquinoline cycle, which were greatly affected by Ca^{2+} binding (see Fig 3.10), do not directly interact with the ion in our model. The deprotonated nitrogens of TD have the potential to interact with positively charged Ca^{2+} ion. Thus we suggest that, in some cases, Ca^{2+} can bind to one of these nitrogens. This could explain the changes in the corresponding chemical shifts.

If we compare the structure of triangular-and quadrangular-shaped TD, the main observable difference is that the upper part of triangular conformation, formed by methoxy groups oxygens, “bends over” (Fig.3.13 *B*). As we have shown before, the Ca^{2+} ion binds to the drug, interacting with several atoms of the inner ring of TD and “filling” the suitable opening in the center of TD (Fig.3.12 *A*). This favorable interaction prevents the conformational changes of TD, which could result in transition from triangular to quadrangular structure, thus stabilizing the triangular conformation of TD in solution.

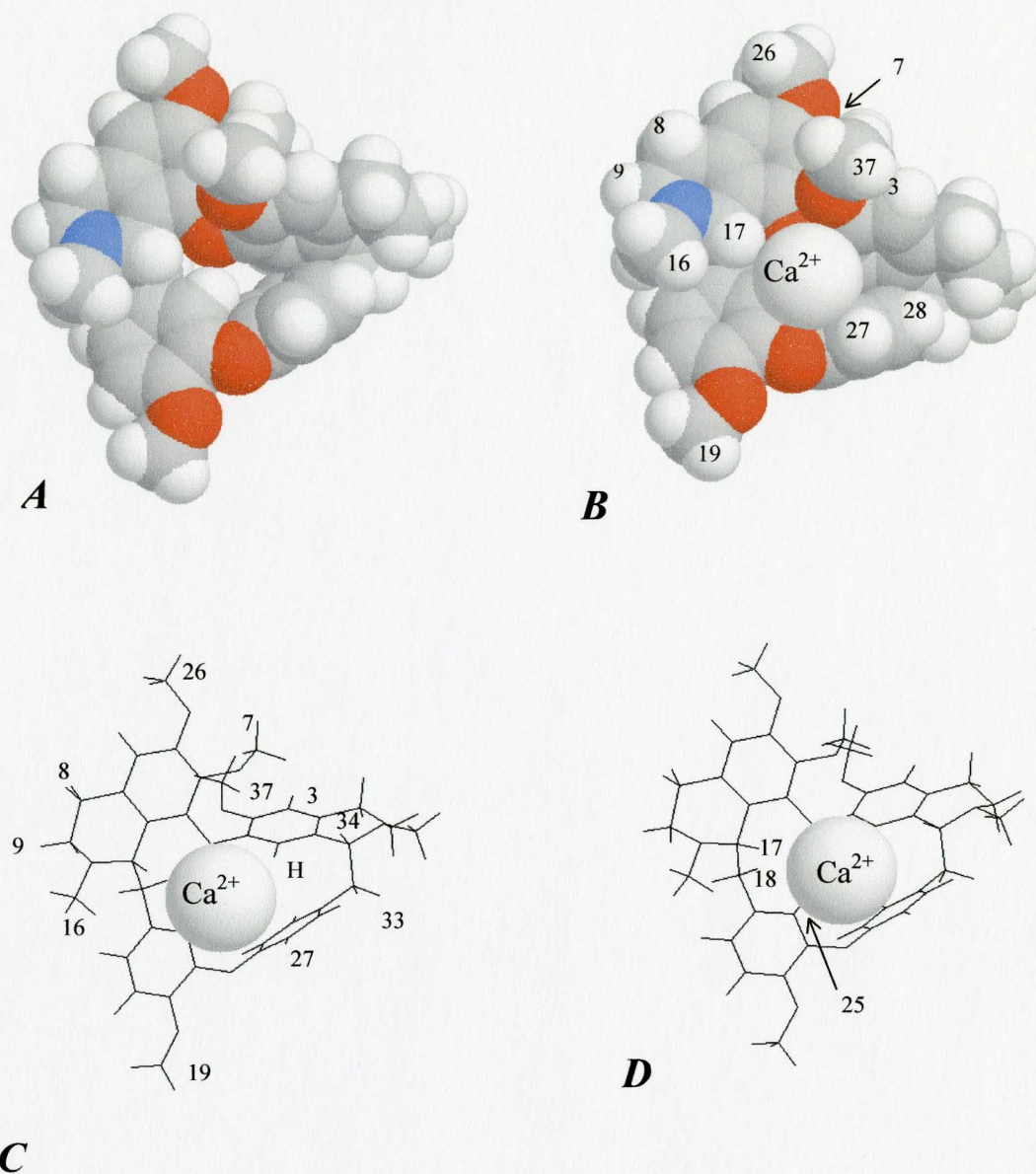


Fig.3.12. The lowest-energy triangular conformation of Ca^{2+} - bound TD. The cation is shown as sphere. *A* – low-energy MEC of TD without Ca^{2+} . *B* – spacefilled model of TD with bound Ca^{2+} ; the protons of TD whose chemical shifts were affected upon Ca^{2+} binding are shown by their numbers. *C*, *D* – two wireframe models of the conformation in *B*, showing clearer view of the main TD ring.

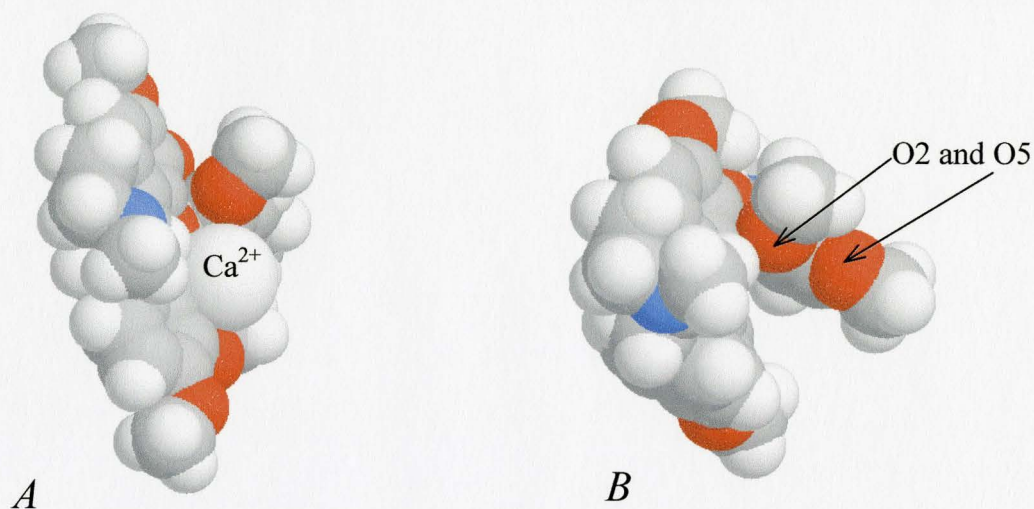


Fig. 3.13. *A* – side view of spacefilled model of the lowest-energy triangular conformation of TD + Ca²⁺, analogous to that shown in Fig.3.12 *B*. *B* – side view of spacefilled model of square conformation of TD. The binding of Ca²⁺ ion prevents the “bending” of the upper part of the molecule and consecutive transition from the triangular to quadrangular conformation, thus stabilizing the former in solution.

3.2.6. Tetrandrine docking into the model

In order to study the TD binding to the channel, the model of LCC selectivity filter was constructed. The model consists of P-loops, which form the filter, and the upper part of S6 segments. While S5 TM segments are too far from the region of selectivity filter to affect the drug binding, the S6 segments embrace P-loops and, therefore, are needed to be included into the model. The S6.1 – S6.9 and P33-P47, and P56-P59 residues were constrained to positions of corresponding atoms of the KcsA

template, using the alignment of Test Model I. P48-P55 residues were kept unconstrained to allow the movement of the loops and their adjustment to shape and size of bound TD.

As discussed earlier, the addition of four Ca^{2+} ions is necessary to neutralize eight acidic residues that form the selectivity filter of LCC. Each Ca^{2+} ion is chelated by two acidic residues, located on the same level of the pore (Zhorov and Ananthanarayanan, 1996). Thus, four possible chelating modes are possible. As the triangular conformation of TD is shown by NMR data to be more preferable in the presence of Ca^{2+} ions, we performed the docking of this conformation to the model of selectivity filter. Four Ca^{2+} - binding sites of TD molecule formed by its nucleophilic atoms allow the drug to interact simultaneously with four cations. The latter are chelated by acidic residues in the selectivity filter of the channel. Six possible orientations of TD in selectivity filter were docked into four models, which correspond to four Ca^{2+} chelating modes. The other orientations were rejected after visual inspection. Several constraints between nucleophilic atoms of TD, Ca^{2+} ions, P.50 and P.54 residues imposed the chosen TD orientations and chelation modes at the initial stages of MCM search. Resulting energy of lowest-energy conformations is shown in Table 3.10.

Table 3.10. The lowest-energy conformations of TD-Ca²⁺ complex in the selectivity filter

Model	Atoms of tetrandrine and LCC, that coordinate Ca ²⁺ ions in the selectivity filter				Energy, kCal/mol
"Triangular" conformation of tetrandrine:					
1	N, Glu ^{IP50} , Glu ^{IVP50}	O5, O2, Glu ^{IIP50} , Glu ^{IIP50}	N1, Asp ^{IP54} , Asp ^{IIP51}	O3, O4, Glu ^{IIP54} , Asp ^{IVP54}	-66.56
2	O5, O2, Glu ^{IP50} , Glu ^{IVP50}	N, Glu ^{IIP50} , Glu ^{IIP50}	O3, O4, Asp ^{IP54} , Asp ^{IIP51}	N1, Glu ^{IIP54} , Asp ^{IVP54}	-70.57
3	O5, O2, Glu ^{IP50} , Glu ^{IIP50}	N, Glu ^{IIP50} , Glu ^{IVP50}	O3, O4, Asp ^{IP54} , Asp ^{IIP51}	N1, Glu ^{IIP54} , Asp ^{IVP54}	-71.27
4	O5, O2, Glu ^{IP50} , Glu ^{IVP50}	N1, Glu ^{IIP50} , Glu ^{IIP50}	O3, O4, Asp ^{IP54} , Asp ^{IVP54}	N, Glu ^{IIP54} , Asp ^{IIP51}	-92.67
5	O5, O2, Glu ^{IP50} , Glu ^{IVP50}	N1, Glu ^{IIP50} , Glu ^{IIP50}	O3, O4, Asp ^{IP54} , Asp ^{IIP51}	N, Glu ^{IIP54} , Asp ^{IVP54}	-82.38
6	N1, Glu ^{IP50} , Glu ^{IVP50}	O5, O2, Glu ^{IIP50} , Glu ^{IIP50}	O3, O4, Asp ^{IP54} , Asp ^{IVP54}	N, Glu ^{IIP54} , Asp ^{IIP51}	-29.59
7	N1, Glu ^{IP50} , Glu ^{IVP50}	O5, O2, Glu ^{IIP50} , Glu ^{IIP50}	O3, O4, Asp ^{IP54} , Asp ^{IIP51}	N, Glu ^{IIP54} , Asp ^{IVP54}	-56.75
8	N, Glu ^{IP50} , Glu ^{IVP50}	O3, O4, Glu ^{IIP50} , Glu ^{IIP50}	N1, Asp ^{IP54} , Asp ^{IVP54}	O5, O2, Glu ^{IIP54} , Asp ^{IIP51}	-68.04
9	N, Glu ^{IP50} , Glu ^{IVP50}	O3, O4, Glu ^{IIP50} , Glu ^{IIP50}	N1, Asp ^{IP54} , Asp ^{IIP51}	O5, O2, Glu ^{IIP54} , Asp ^{IVP54}	-82.84

24 starting orientations of TD in the selectivity filter were considered: (six modes of TD binding to four Ca²⁺ ions) × (4 patterns of Ca²⁺ chelation by the eight acidic residues). 15 orientations were rejected after visual inspection or if calculations showed high ligand-receptor energy

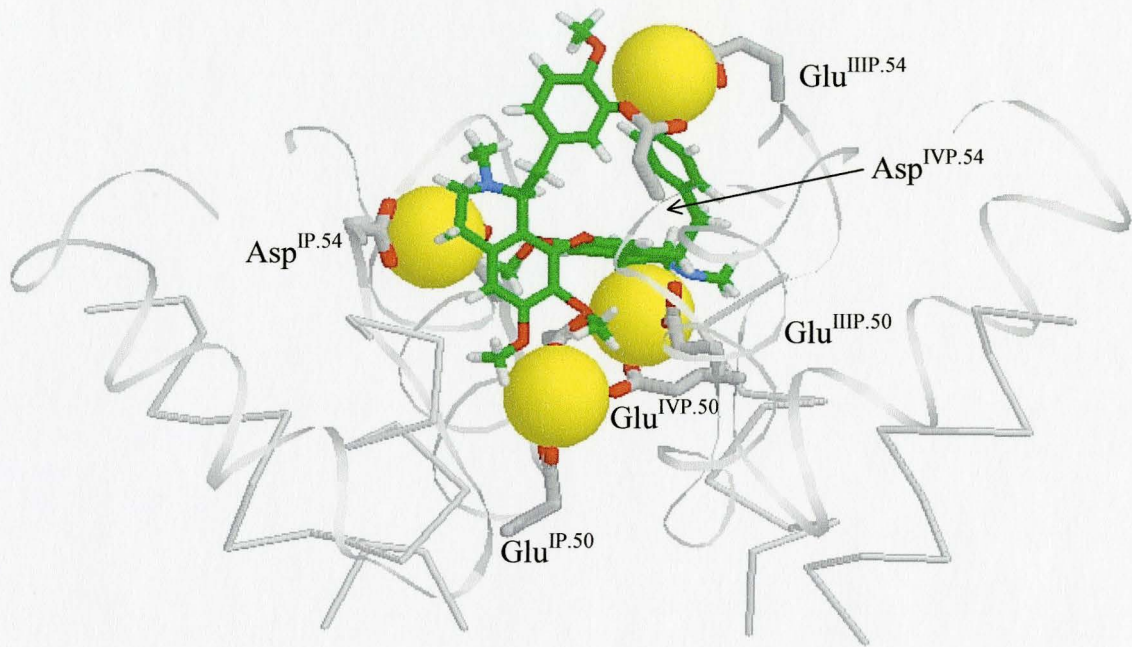


Fig. 3.14 *A* . Side view of Model 2 (See Table 3.10) of TD in the selectivity filter of LCC. S6 segments of LCC are shown as C_{α} tracing (gray), P-loops – as gray ribbons. The sidechains of conserved acidic residues are shown by sticks. Ca^{2+} ions are yellow spheres, TD molecule is shown by sticks, carbon atoms are green, oxygens are red and nitrogens are blue. Although not having the lowest-energy among 9 models, Model 2 is especially interesting because of the match of asymmetric nucleophilic atoms of TD with four Ca^{2+} ions, asymmetrically chelated by P.50-P.54 residues.

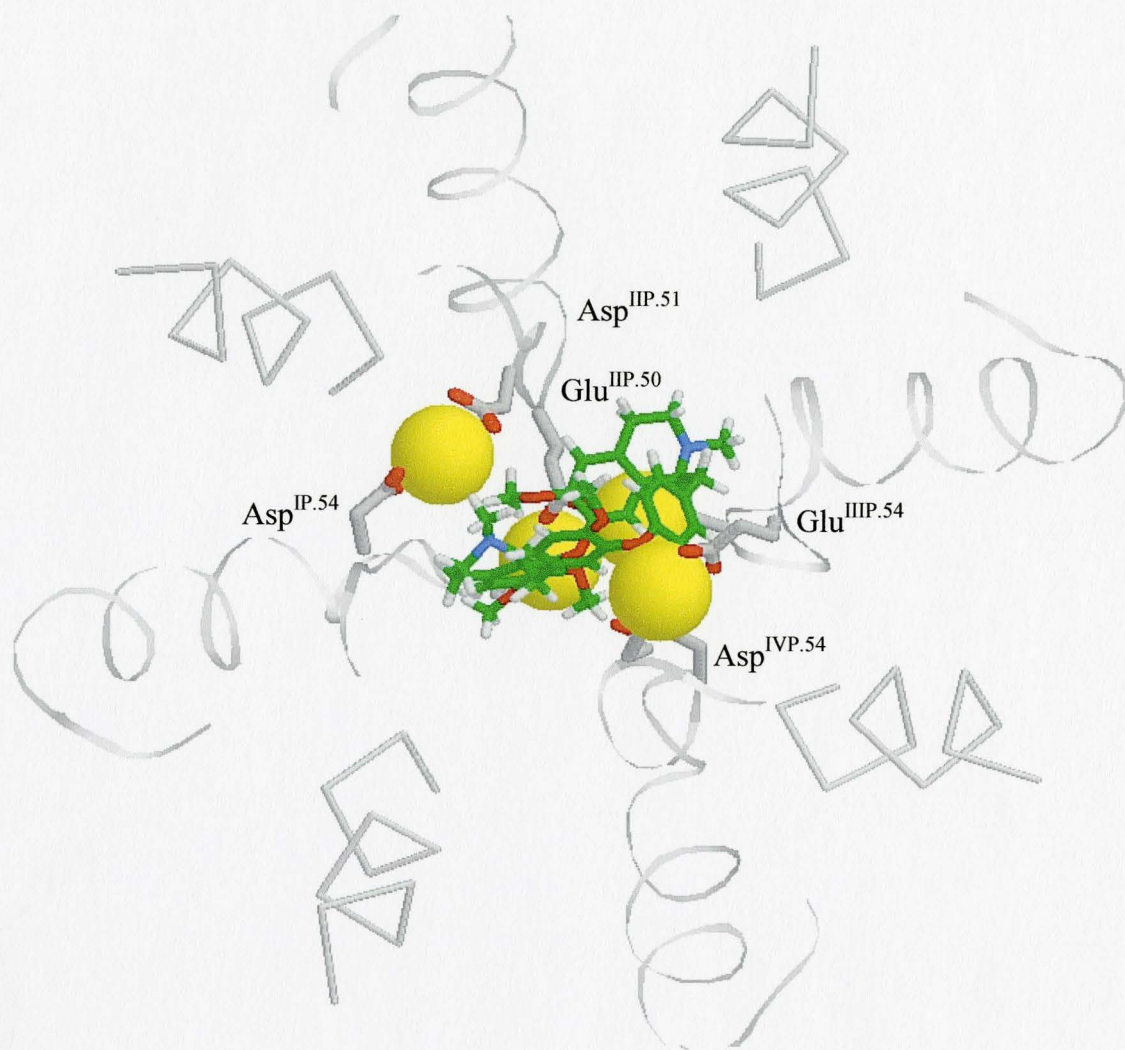


Fig. 3.14 *B*. Top view of Model 2 (Table 3.10) of TD in the selectivity filter of LCC

At this moment, the detailed modeling of selectivity filter is difficult to perform as more experimental data are required. The objective of the current study of the selectivity filter was only to determine the approximate geometry of the P-loops and positions of Ca^{2+} ions inside the pore. These are necessary for further modeling studies of DHP-binding site.

3.3. Modeling of LCC selectivity filter with bound nifedipine

As we showed in Test Model I of LCC (section 3.1.2), nifedipine forms hydrogen bonds with the conserved Tyr^{III}S6.8 and Tyr^{IV}S6.9 by its NH-group. In this case, the six oxygen atoms of nifedipine remain unbound and lacking their counterions. The hydration of these oxygens is unlikely to occur, because DHPs are lipophilic compounds. While DHPs have several acceptors of H-bonds, located on the one side of the molecule, they have only one H-bond donor, located on the opposite side. In this situation, the formation of H-bonds between the drug's oxygens and water molecules would force water to arrange in specific order near the molecule. Such reorganization of water molecules would be entropically unfavorable.

Further, the formation of hydrogen bonds between nifedipine oxygens and some residues of LCC would result in a situation where the ligand is H-bonded to opposite sides of the channel simultaneously, completely blocking ion permeation. Since some of DHPs are LCC agonists, this situation is also improbable.

One possibility for neutralizing DHP's negative charges is its interaction with positively charged Ca^{2+} ions inside the channel (Govyrin and Zhorov, 1994, Zhorov and Ananthanarayanan, 1996). The formation of this complex was predicted theoretically (Govyrin and Zhorov, 1994, and shown experimentally in nonpolar milieu (Belciug and Ananthanarayanan, 1994). Therefore the modeling studies of DHP docking inside the channel were performed in the presence of Ca^{2+} ions, interacting with negatively charged atoms of the drug.

DHPs interact with receptor when applied extracellularly, not intracellularly (Bangalore et al, 1994). They can reach their binding site either via the membrane, or via the selectivity filter. In the first pathway, DHPs that carry permanently charged groups would have to overcome high dielectric barrier of lipids. Besides, DHPs would encounter tightly packed bundle of transmembrane segments S1-S4, surrounding the pore-forming S5-S6 segments. Successful diffusing of bulky DHPs through this bundle of 16 alpha-helical segments seems less probable than permeation of DHPs through selectivity filter. If DHPs indeed access their binding site via selectivity filter, the latter should be wide enough to let them through. In order to check whether it is possible for nifedipine to fit into this transient binding site, we have built several models of the drug bound in the region of selectivity filter.

The models were constructed of the P33 - P56 residues of P-loops and S6.1 - S6.9. residues of S6 TM segments, as described earlier (see chapter 3.2.5),

similarly to the model of the selectivity filter with bound TD. The starting geometry of P-loops, acquired during the modeling studies of tetrandrine in selectivity filter, was kept by constraining of C_{α} atoms to the corresponding coordinates of Model 2 of TD-bound LCC. Residues P.49 – P52 were allowed to move in order to form the ternary complex with Ca^{2+} ions and nucleophilic atoms of nifedipine. C_{α} atoms of S6 residues were constrained by pins to corresponding coordinates of KcsA template.

Similarly to the modeling of tetrandrine in selectivity filter, we checked four possible patterns of Ca^{2+} ions, chelated by eight acidic residues of LCC (Table 3.11). We performed the docking of low-energy elongated conformation of nifedipine into these four models of selectivity filter. The long axis of the drug was oriented parallel to the pore axis, with NH-group facing the III/IV interface and nucleophilic atoms of nifedipine interacting with chelated Ca^{2+} ions. Four resulting models were MC-minimized. The ligand-receptor interaction energy of resulting lowest-energy conformations are listed in Table 3.11. The asymmetrical model of selectivity filter with chelation pattern of $Glu^{IP50} \dots Ca^{2+} \dots Glu^{IVP50}$, $Glu^{IIP50} \dots Ca^{2+} \dots Glu^{IIIP50}$, $Asp^{IP54} \dots Ca^{2+} \dots Asp^{IIP51}$, and $Glu^{IIIP54} \dots Ca^{2+} \dots Asp^{IVP54}$ demonstrated the best energy of ligand-receptor interaction (Fig 3.15). The model 2 of TD in the selectivity filter, which was found to demonstrate the best ligand-receptor complementarity, was based on the same mode of Ca^{2+} chelation. Thus, this pattern of Ca^{2+} interaction with conserved acidic residues of selectivity filter was chosen for the further modeling studies.

The acquired folding of flexible P-loops around the drugs may not be correct in every detail and obviously requires further studies. However, there are several important structural features found during the modeling, such as the pattern of Ca^{2+} chelation by acidic residues, as well as general topology of selectivity filter, allowing the accommodation of bulky LCC ligands while keeping the geometry of surrounding TM S5 and S6 segments as in template. These features are consistent with experimental data and can be used for further modeling of DHPs binding site as described below.

Table 3.11. Different modes of nifedipine interaction with Ca^{2+} ions, chelated by acidic residues of selectivity filter

Pairs of acidic residues chelating Ca^{2+} ions				Energy ^a
Glu^{IP50} , $\text{Glu}^{\text{IIP50}}$	$\text{Glu}^{\text{IIIP50}}$, $\text{Glu}^{\text{IVP50}}$	Asp^{IP54} , $\text{Asp}^{\text{IIP51}}$	$\text{Glu}^{\text{IIIP54}}$, $\text{Asp}^{\text{IVP54}}$	18.2
Glu^{IP50} , $\text{Glu}^{\text{IIP50}}$	$\text{Glu}^{\text{IIIP50}}$, $\text{Glu}^{\text{IVP50}}$	Asp^{IP54} , $\text{Asp}^{\text{IVP54}}$	$\text{Glu}^{\text{IIIP54}}$, $\text{Asp}^{\text{IIP51}}$	16.1
Glu^{IP50} , $\text{Glu}^{\text{IVP50}}$	$\text{Glu}^{\text{IIP50}}$, $\text{Glu}^{\text{IIIP50}}$	Asp^{IP54} , $\text{Asp}^{\text{IIP51}}$	$\text{Glu}^{\text{IIIP54}}$, $\text{Asp}^{\text{IVP54}}$	0
Glu^{IP50} , $\text{Glu}^{\text{IVP50}}$	$\text{Glu}^{\text{IIP50}}$, $\text{Glu}^{\text{IIIP50}}$	Asp^{IP54} , $\text{Asp}^{\text{IVP54}}$	$\text{Glu}^{\text{IIIP54}}$, $\text{Asp}^{\text{IIP51}}$	22.4

^a kcal/mol, relative to the lowest ligand-receptor energy found in the four models shown in the Table.

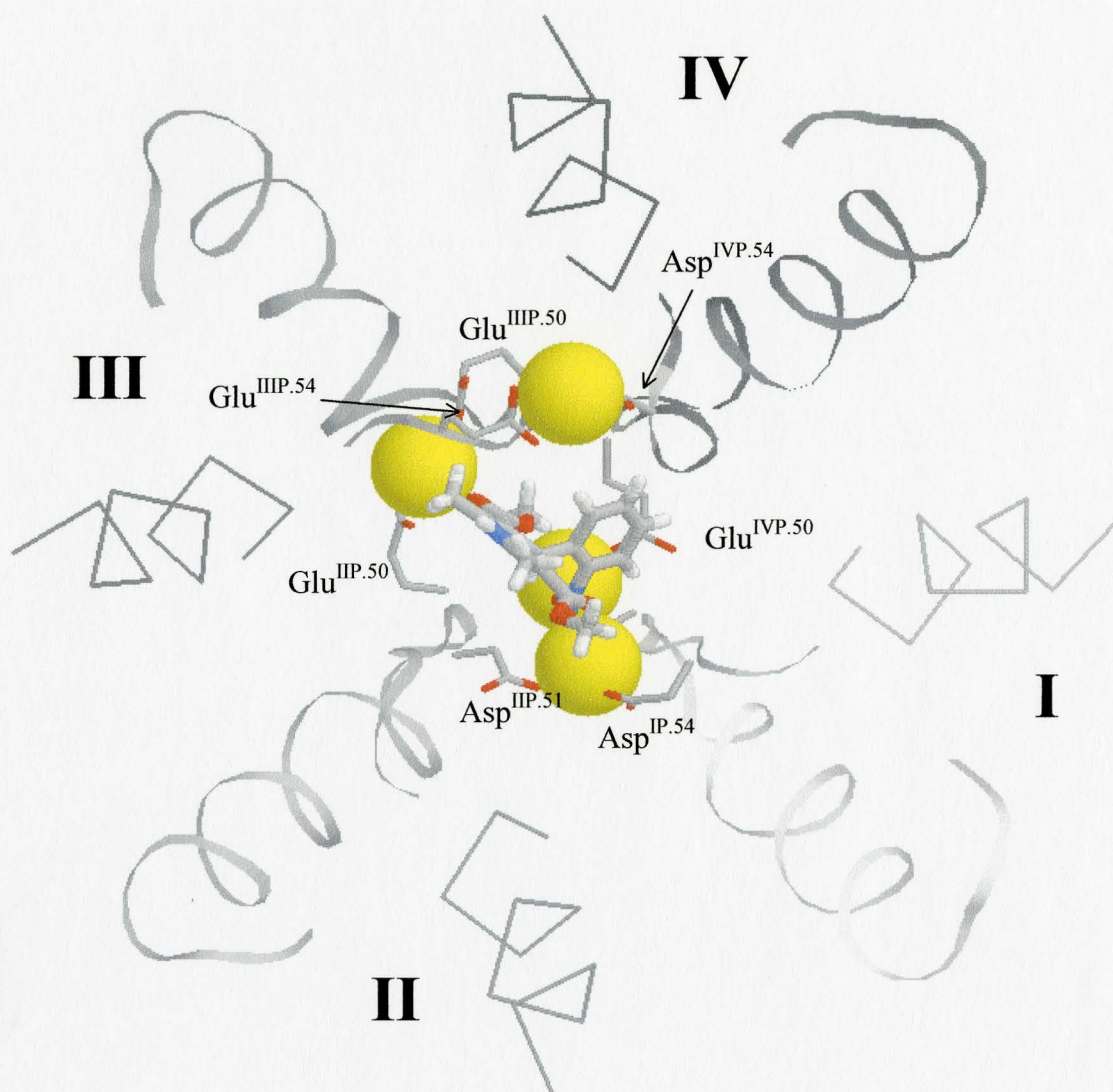


Fig.3.15 A. Top view of the lowest-energy conformation of nifedipine bound inside the selectivity filter. S6 segments and P-loops of LCC are shown by C_{α} - tracing and ribbons respectively. The yellow spheres designate Ca^{2+} ions. The drug is shown by sticks, carbons are gray, oxygens are red and nitrogens are blue.

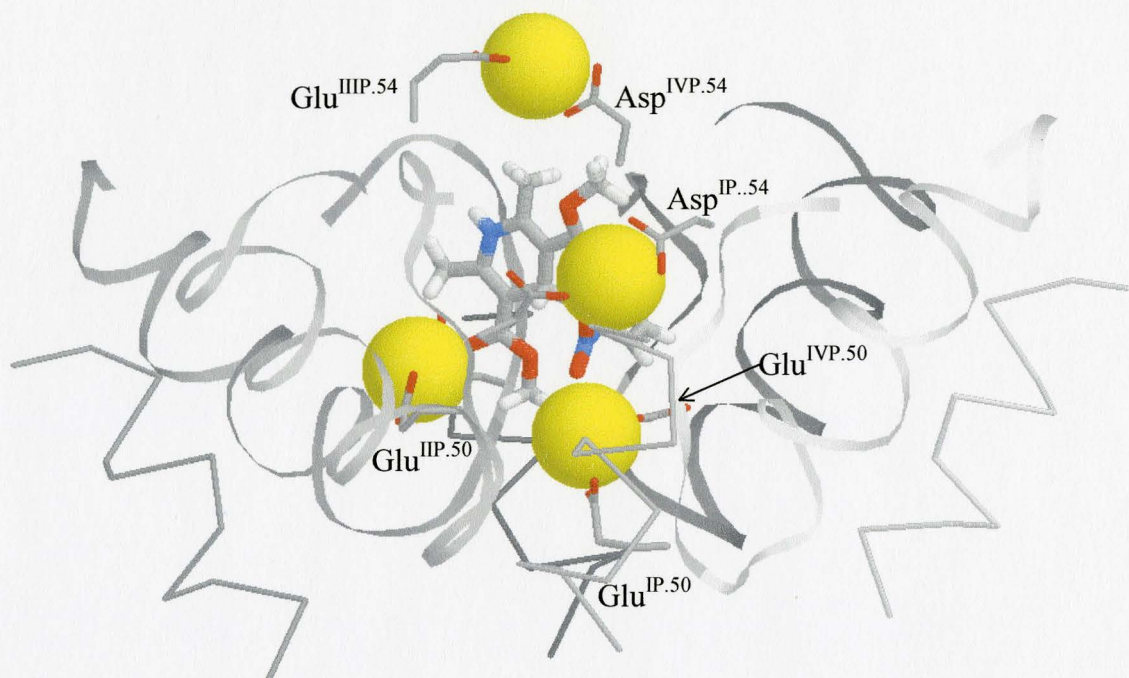


Fig.3.15 *B*. Side view of the lowest-energy conformation of nifedipine bound inside the selectivity filter (see Fig.3.15 *A* for other details).

3.4. The docking of DHP ligands into the pore of LCC

3.4.1. Different binding modes of nifedipine

As we found earlier, when DHP ligand nifedipine is bound inside the pore of LCC and its portside group points down the pore (see section 3.1.2), the ligand forms most favorable contacts with DHP-sensing residues and demonstrate the best ligand-receptor interaction energy. In order to explore further the possible binding modes of DHPs, we performed the docking of nifedipine to the binding site inside the pore of LCC.

The starting structure of the DHP receptor was based on Test Model I, with P-loops folding described in previous chapter. Four Ca^{2+} ions were added to neutralize the eight negatively charged acidic residues of selectivity filter. Initially, nifedipine was placed inside the channel pore in three different orientations. First, in portside-down binding mode, the methoxy group on the port side of the drug pointed down the pore. Then in the second model, the drug was rotated up-side down, so that the portside methoxy group pointed up. Finally, we checked another possible orientation of the ligand where the portside group also pointed down but the NH-group oriented towards interface I/II instead of towards III/IV.

These three models were MC-minimized, with gradual relaxation of ligand-receptor contacts (see *Methods*). Several constraints between DHP-sensing residues and nifedipine were imposed at initial stages of energy minimization. The energy characteristics of resulting lowest-energy conformations are shown in Table 3.12. Among these three models, the portside-down model with NH-group of nifedipine facing the I/II interface has the highest energy of ligand-receptor interaction which resulted from drug repulsion from the Ca^{2+} ion chelated to the $\text{Glu}^{\text{IP}50}$ and $\text{Glu}^{\text{IVP}50}$. The ligand weakly interacts with $\text{Tyr}^{\text{III}S6.8}$ but repulses from the other important DHP-sensing residue $\text{Tyr}^{\text{IV}S6.9}$. Only two other DHP-sensing residues form contacts with the drug in this binding mode, namely $\text{Ile}^{\text{IV}S6.17}$ and $\text{Ile}^{\text{III}S6.9}$ (Table 3.12)

In contrast, the portside-down model with drug rotated to 180° , so that the NH-group was oriented toward III/IV interface, showed the lowest ligand-receptor interaction energy. The contact distances between Ca^{2+} ions and chelating atoms of LCC and nifedipine are given in Table 3.14. All LCC residues, which have the energy of interaction with nifedipine more than 0.5 kcal/mol, are listed in the Table 3.12.. Among them, five DHP-sensing residues are shown to form favorable contacts with the drug. Conserved $\text{Tyr}^{\text{III}S6.8}$ and $\text{Tyr}^{\text{IV}S6.9}$ both formed hydrogen bonds with NH-group of nifedipine (Fig 3.16). Ca^{2+} ion, chelated by $\text{Glu}^{\text{IP}.50}$ and $\text{Glu}^{\text{IVP}.50}$, interacts with negatively charged oxygens on bowsprit of nifedipine. Methoxy group of the portside of the ligand approaches conserved $\text{Ile}^{\text{IV}S6.17}$ and $\text{Met}^{\text{III}S6.17}$, located on the bottom of “water lake” near the crossing of TM S6 segments. The ligand interaction with several residues

of repeat I and II, including highly conserved Ser^{IS6.13} and Asn^{IS6.13}, further stabilize portside-down binding mode of nifedipine.

The model of nifedipine with portside group pointed up has the energy of ligand-receptor interaction just 0.8 kcal/mol higher than the previous portside-down model. The conserved tyrosines were also found in H-bonding distance from stem NH-group. Ca²⁺ ion, chelated by Glu^{IP.50} and Glu^{IVP.50}, was also coordinated by ligand's oxygens. The corresponding distances are listed in Table 3.15. However the portside-down mode is more relevant to the experimental data for the following reasons. First, portside-up model lacks beneficial stacking interaction of DHP's aromatic ring and Tyr^{IVS6.9}, which stabilizes nifedipine in portside-down mode (see Table 3.13 for the partitioned energy of phenyl ring). Second, in portside-down mode nifedipine forms contacts with maximum number of DHP-sensing hydrophobic residues (Fig 3.16). If the calculations had been conducted with taking into account solvation effect, the contribution of the ligand's hydrophobic interaction with these residues and with aromatic ring of Tyr^{IVS6.9} would significantly lower the ligand-receptor interaction energy of portside-down model.

Table 3.12. Energy contribution (kcal/mol) of LCC residues to interaction with nifedipine. DHP-sensing residues are shown in bold. Only residues whose energy contribution exceeds 0.5 kcal/mol are listed in this table.

Ligand orientation in DHPR model					
Portside-down, NH at III/IV		Portside-down, NH at I/II		Portside-up, NH at III/IV	
Residue	Energy	Residue	Energy	Residue	Energy
Ca ²⁺ _{I-IV}	-38.1	Ca ²⁺ _{I-IV}	9.8	Ca ²⁺ _{I-IV}	-40.1
Glu ^{IP50}	3.9	Glu ^{IVP50}	-7.3	Gly ^{IIP49}	-4.6
Thr ^{IVP48}	-3.6	Glu ^{IP50}	-4.5	Glu ^{IP50}	4.2
Tyr^{IVS6.9}	-2.9	Ca ²⁺ _{II-III}	-3.2	Val ^{IIP46}	-3.8
Thr ^{IP48}	-2.2	Glu ^{IIP50}	-1.5	Ser ^{IIP47}	-2.6
Glu ^{IVP50}	-2.0	Thr ^{IIP48}	-1.0	Asn ^{IIS6.13}	-2.5
Ser ^{IS6.13}	-1.9	Gly ^{IIP49}	-1.0	Glu ^{IVP50}	2.5
Tyr^{IIS6.8}	-1.8	Thr ^{IVP48}	0.9	Thr ^{IIP48}	-2.0
Gly ^{IIP49}	-1.7	Tyr^{IIS6.8}	-0.7	Thr ^{IIP45}	-1.9
Ile^{IVS6.17}	-1.5	Val ^{IS6.16}	-0.7	Met^{IIS6.16}	-1.8
Ser ^{IIP47}	-1.4	Ile^{IIS6.9}	-0.6	Thr ^{IP48}	-1.7
Val ^{IIP46}	-1.4	Tyr^{IVS6.9}	0.6	Tyr^{IVS6.9}	-1.6
Asn ^{IIS6.13}	-1.2	Ile^{IVS6.17}	-0.6	Tyr^{IIS6.8}	-1.3
Glu ^{IIP50}	-1.1			Thr ^{IIP48}	-1.1
Val ^{IS6.9}	-1.1			Gly ^{IVP49}	-1.1
Met^{IIS6.17}	-1.1			Phe ^{IIS6.9}	-0.9
Trp ^{IP52}	-1.0			Leu ^{IIP47}	-0.7
Val ^{IS6.9}	-0.9			Val ^{IS6.9}	0.7
Phe ^{IIS6.20}	-0.9			Phe ^{IIP49}	-0.7
Ala ^{IVS6.13}	-0.8			Ile ^{IIP46}	-0.6
Ala ^{IVP47}	-0.7			Ca ²⁺ _{II-III}	0.5
Ile^{IVS6.16}	-0.6			Gln ^{IIP46}	-0.5
Thr ^{IIP45}	-0.6			Ala ^{IIS6.13}	-0.5
Phe ^{IIP49}	-0.5				
Met ^{IP49}	-0.5				
Total energy	-67.9		-14.3		-67.1

Table 3.13. Energy contributions (kcal/mol) of DHPR residues to interaction with the aromatic ring of nifedipine. DHP-sensing residues are shown in bold

Ligand orientation in DHPR model					
Portside-down, NH to III/IV		Portside-down, NH to I/II		Portside-up, NH to III/IV	
Residue	Energy	Residue	Energy	Residue	Energy
Thr ^{IVP48}	-2.1	Tyr^{IIIS6.8}	1.6	Asn ^{IIIS6.13}	-1.5
Ile^{IVS6.16}	-1.1	Gly ^{IIP49}	-1.2	Thr ^{IIP48}	-1.0
Ser ^{IS6.13}	-1.1	Tyr^{IVS6.9}	-0.7	Phe ^{IIIS6.9}	-0.8
Glu ^{IVP50}	-1.1	Ile^{IIIS6.9}	-0.6	Glu ^{IP50}	-0.7
Tyr^{IVS6.9}	-0.9	Thr ^{IIP48}	-0.5	Thr ^{IIP48}	-0.6
Ala ^{IVP47}	-0.7	Val ^{IIIP46}	-0.5	Gly ^{IIP49}	-0.6
Glu ^{IVP50}	-0.6	Glu ^{IIP50}	-0.4	Thr ^{IVP48}	0.1
Ala ^{IVS6.13}	-0.6	Ile^{IIIS6.12}	0.4	Ser ^{IS6.13}	-0.1
Gly ^{IVP49}	-0.3	Met^{IIIS6.17}	-0.4	Val ^{IS6.16}	-0.1
Ile ^{IS6.10}	-0.3	Glu ^{IVP50}	-0.2		
Thr ^{IP48}	-0.2	Ser ^{IIIP47}	-0.2		
Met ^{IP49}	-0.2	Met^{IIIS6.16}	-0.2		
Cys ^{IVS6.12}	-0.2	Ile ^{IIIS6.10}	0.1		
Phe ^{IS6.14}	-0.1	Ile ^{IIIS6.11}	-0.1		
Ile^{IVS6.17}	-0.1				
Total energy	-9.4		-3.1		-5.9

Table 3.14. Contact distances between Ca^{2+} ions and atoms of LCC and nifedipine in the portside-down binding mode (see Fig.3.16)

Atom	Ca^{2+} ion	Distance, Å
OE1.GL- .736	1	2.30
OE2.GL- .736	1	2.33
OE1.GL- .1145	1	2.31
OE2.GL- .1145	1	2.34
OO3-nifedipine	1	3.16
OE2.GL- .393	2	2.28
OE1.GL- .393	2	2.53
OE1.GL- .1446	2	2.33
OE2.GL- .1446	2	2.35
OO2 - nifedipine	2	2.32
O3-nifedipine	2	2.65
OD1.AS- .737	3	2.25
OD2.AS- .737	3	2.46
OD1.AS- .397	3	2.29
OD2.AS- .397	3	2.37
O .TRP .395	3	2.41
OD1.ASN .739	3	2.44
OD1.AS- .1450	4	2.41
OD2.AS- .1450	4	2.28
OE1.GL- .1149	4	2.31
OE2.GL- .1149	4	2.37
O .GLN .1449	4	2.32
O .TRP .1147	4	2.40

Table 3.15. Contact distances between Ca^{2+} ions and atoms of LCC and nifedipine in the portside-up binding mode (see Fig.3.17)

Atom	Ca^{2+} ion	Distance, Å
OE1.GL- . 736	1	2.31
OE2.GL- . 736	1	2.41
OE1.GL- .1145	1	2.32
OE2.GL- .1145	1	2.36
OG1.THR .1140	1	2.42
OH .TYR .1152	1	2.44
OE2.GL- . 393	2	2.24
OE1.GL- . 393	2	2.86
OE1.GL- .1446	2	2.38
OE2.GL- .1446	2	2.24
OO1 - nifedipine	2	2.35
O5-nifedipine	2	2.57
OD1.AS- . 737	3	2.42
OD2.AS- . 737	3	2.31
OD1.AS- . 397	3	2.37
OD2.AS- . 397	3	2.34
OD1.ASN . 739	3	2.37
O .TRP . 395	3	2.38
OD1.AS- .1450	4	2.41
OD2.AS- .1450	4	2.35
OE1.GL- .1149	4	2.32
OE2.GL- .1149	4	2.34
O .AS- .1450	4	2.41

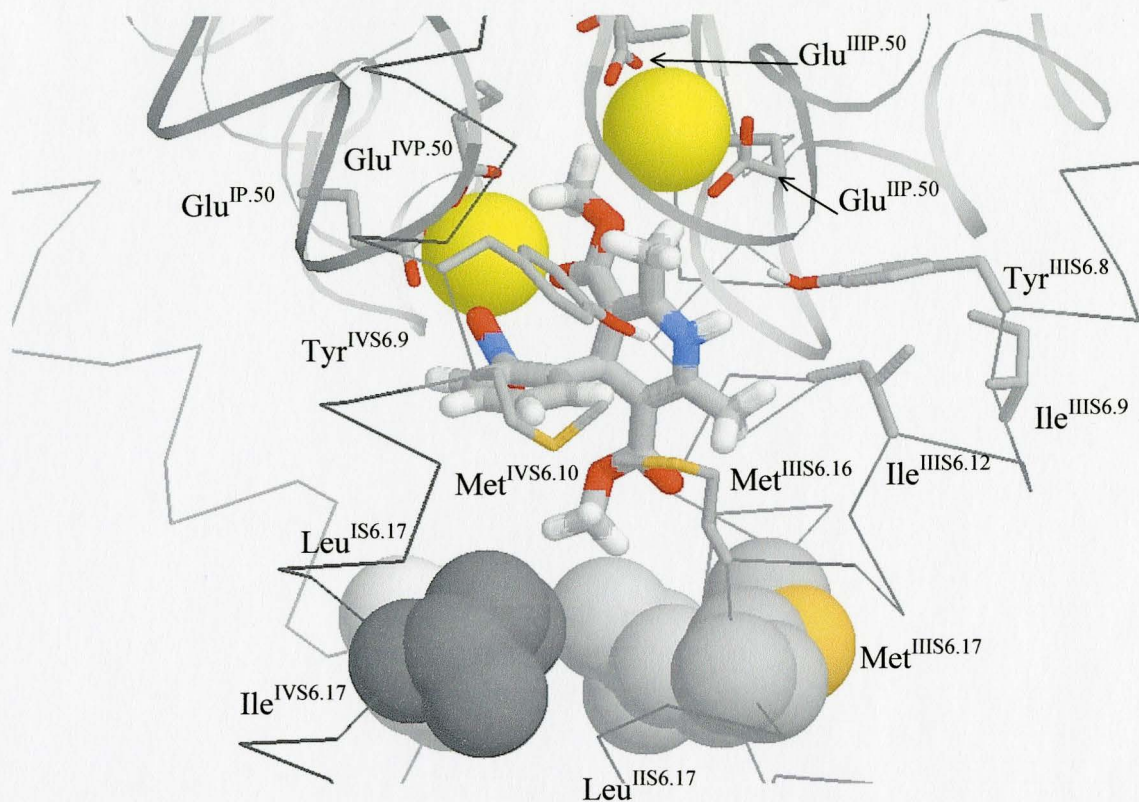


Fig.3.16. Side view of MC-minimized model of nifedipine bound in portside-down mode in the pore of LCC. S6 segments and P-loops are shown by C_{α} tracing and ribbons, respectively. Different shadows of gray designate different repeats of LCC. S5 segments are not shown for clarity. DHP-sensing residues, as well as the conserved acidic residues of selectivity filter, are shown. The ions are shown as yellow spheres. Nifedipine is presented by sticks, with gray carbon atoms, white hydrogens, red oxygens and blue nitrogens. The bracelet of hydrophobic residues near the S6 crossing is spacefilled. The ligand forms contacts with Tyr^{IIIS6.8}, Tyr^{IVS6.9} and several other DHP-sensing residues.

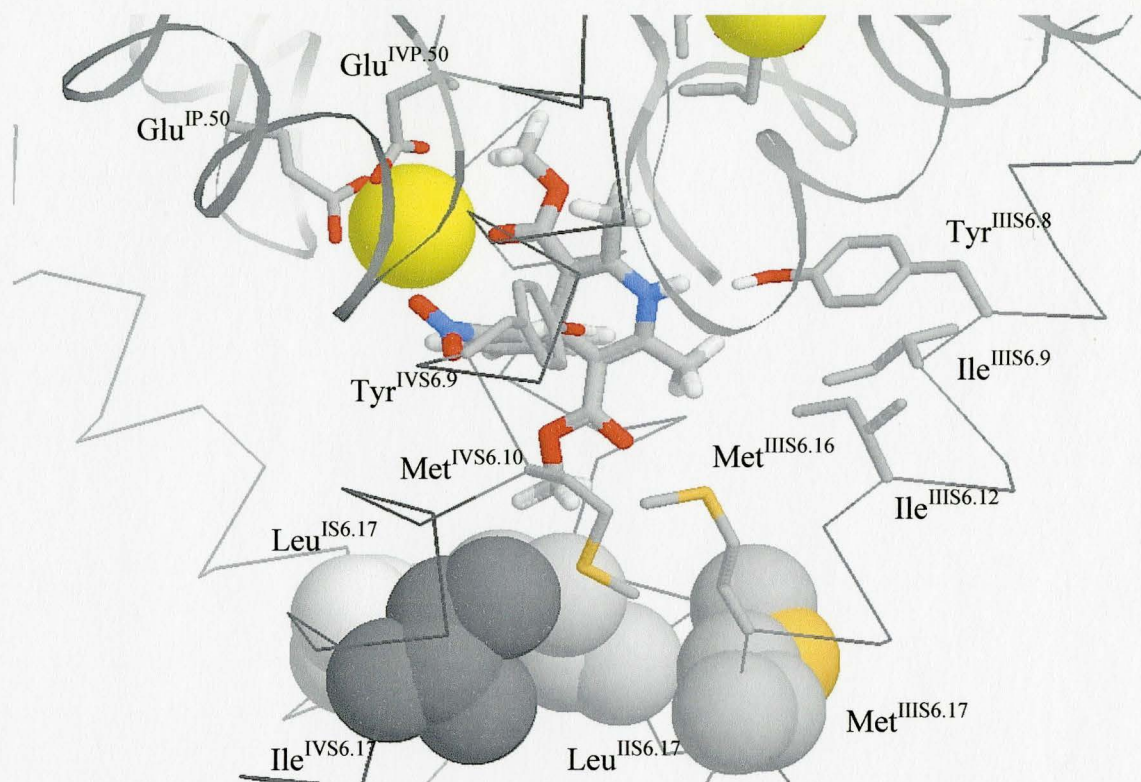


Fig.3.17. Side view of MC-minimized model of nifedipine bound in portside-up mode in the pore of LCC (see Fig.3.16 for other details).

3.4.2. Docking of (R)- and (S)-enantiomers of Bay K 8644 into the model

The (R)- and (S)-enantiomers of Bay K 8644 differ from each other only by substitute groups on portside and starboard (Fig 1.3). However, R-Bay K 8644 blocks the Ca^{2+} current and S-Bay K 8644 was found to be the LCC agonist (Wei et al., 1986). To study this paradoxical interaction of these interesting DHP ligands with LCC, we have built two models with antagonist R-Bay K 8644 and agonist S-Bay K 8644 bound inside the pore. As the starting structure, we took Test Model I. The folding of P-loops and Ca^{2+} chelation pattern were chosen as in the optimal model of nifedipine bound in the selectivity filter. Both ligands were docked into the model in portside-down mode, which was found to be the best during the previous docking experiments. Both models were MC-minimized, resulting low-energy conformations are shown on Fig. 3.18.

In the models obtained, both R- and S-Bay K 8644 interact with conserved DHP-residues and chelate Ca^{2+} ion similarly to nifedipine. While R-Bay exposes its hydrophobic group to the S6s crossing, the S-enantiomer exposes its hydrophilic group to the crossing. H-bonds with Tyr^{IVS6.9} and Tyr^{IIIS6.8} stabilize the orientation of the NH-group of the ligands towards the III/IV interface, while favorable interaction of both ligands' phenyl ring with Tyr^{IVS6.9} stabilize portside-down binding mode. The energy of R-Bay K 8644 interaction with LCC is -68.2 kcal/mol, and the energy of S-Bay K 8644 interaction with LCC is -60.1 kcal/mol. S-Bay K 8644 has its hydrophilic NO_2 -group on

the portside and the bad contacts of this group with hydrophobic residues near the crossing increases ligand-receptor energy increasing 8 kcal/mol. (Fig3.18 B).

Four hydrophobically conserved residues Leu^{IS6.17}, Leu^{IIS6.17}, Met^{IIIS6.17} and Ile^{IVS6.17}, located near the crossing at the bottom of “water lake”, form hydrophobic bracelet. This may work as a “gate” of the channel. Several experiments have been shown that in K⁺ channels the gating is realized on the level of bundle crossing (Yellen et al, 1999). Transition from the closed to the open state in K⁺ channel is associated with changes in the size of pore opening at the level of the crossing (Perozo et al., 1998). In both Na⁺ and Ca²⁺ channels, mutations of S6.17 residues affect LA and DHP binding correspondingly (Peterson et al., 1997). In our models, the antagonists nifedipine and R-Bay K 8644 expose their hydrophobic methoxy groups to the bracelet, while agonist S-Bay K 8644 approach it by hydrophilic portside group. Since antagonist and agonist properties of DHPs are determined by the substituent group on the portside, the interaction of DHP's portside group with hydrophobic bracelet modulates channel gating by changing the probability of hydrated Ca²⁺ ion permeating the hydrophobic gate. In the case of S-Bay K 8644 agonist, the presence of hydrophilic nitro group near the bracelet may facilitate the overcoming of hydrophobic barrier by hydrated ion. In order to explore other important for ion permeation structural determinants, we simulated the passage of hydrated Ca²⁺ ion through the pore with agonist S-Bay K 8644 bound inside.

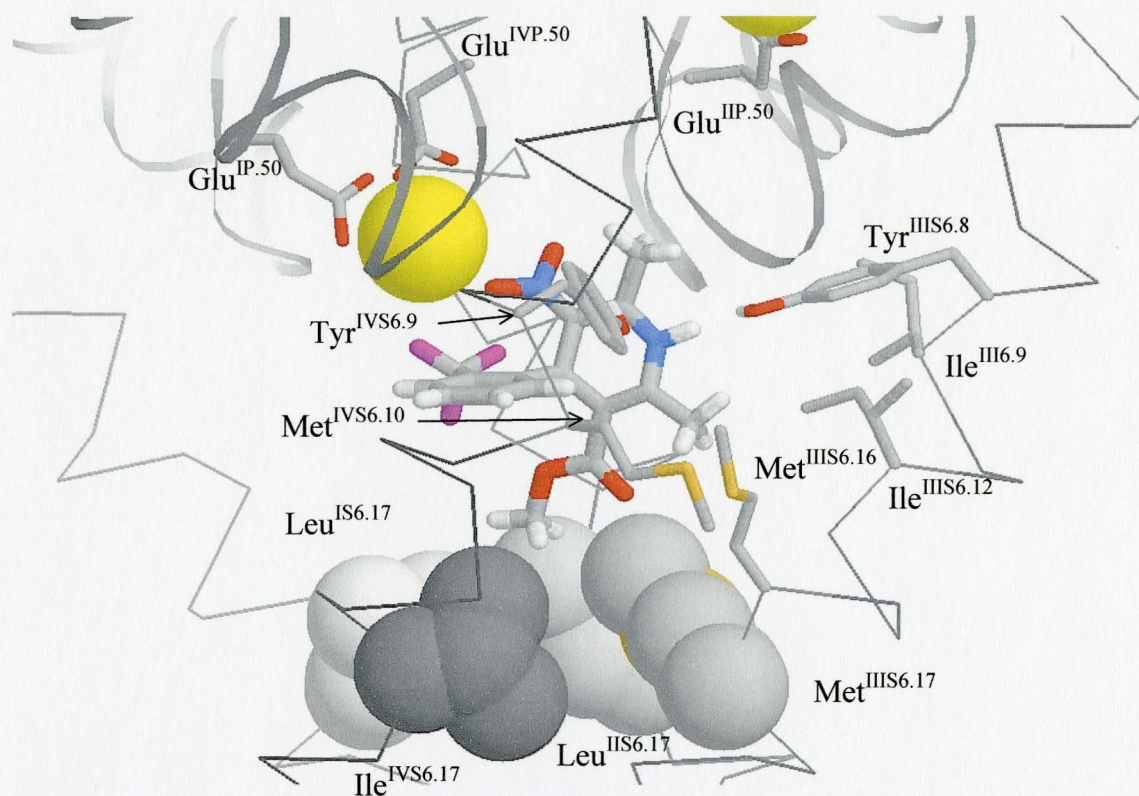


Fig.3.18 *A*. Side view of MC-minimized model of antagonist R-Bay K 8644 bound in portside-down mode in the pore of LCC. S5 segments are not shown for clarity. DHP-sensing residues, as well as the conserved acidic residues of selectivity filter, are shown as sticks. The ions are shown as yellow spheres. R-Bay is presented by sticks, with gray carbon atoms, white hydrogens, red oxygens, blue nitrogens and purple fluorines. The NH group of the ligand approaches hydroxy groups of Tyr^{IIS6.8} and Tyr^{IVS6.9}, while interaction with Tyr^{IVS6.9} stabilizes the portside-down orientation. The bracelet of hydrophobic residues near the S6 crossing is spacefilled. Antagonist R-Bay, approaching the gate by the hydrophobic methyl group would stabilize its closed conformations.

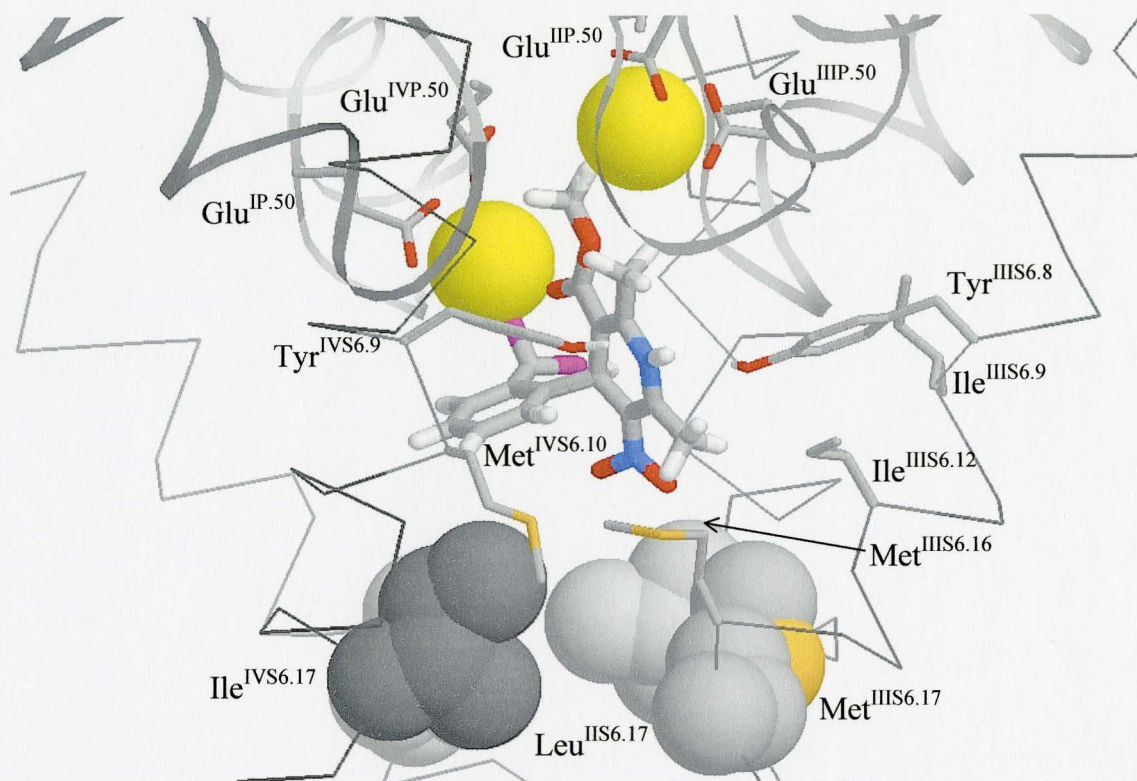


Fig.3.18 *B*. Side view of MC-minimized model of agonist S-Bay K 8644 bound in portside-down mode in the pore of LCC (See Fig. 3.18 *A* for other details). Agonist S-Bay approaching the hydrophobic gate by the hydrophilic group NO_2 would destabilize its closed conformations and, therefore, stabilize the open conformation.

3.5. Ca^{2+} permeation through agonist-bound pore

We took the lowest-energy conformation of LCC with S-Bay K 8644 bound inside the pore, found at the previous step of the modeling, as the starting structure for simulation of ion passage along the pore. In that conformation, Ca^{2+} ion chelated by Glu^{IP50} and $\text{Glu}^{\text{IVP50}}$ interacts simultaneously with one oxygen and two fluorine atoms of S-Bay K 8644. When another Ca^{2+} ion, arriving from outside the pore, replaces the first ion at its binding site of Glu^{IP50} and $\text{Glu}^{\text{IVP50}}$, the latter ion moves down the pore and eventually reaches the channel gate. We simulated this passage from selectivity filter to the gate along the hydrophilic face of the agonist. Several models of channel with hydrated ion at different levels of the pore were MC-minimized (Fig 3.19). The hydration shell of Ca^{2+} is comprised of approximately seven water molecules (Varadi, 1999). The positions and orientations of these water molecules, interacting with the ion in our models, were determined by special procedure in ZMM, which finds available unoccupied space around the ion. At different levels of the pore, the ligand and channel provide electronegative atoms, which may replace some of those water molecules. At least two electronegative atoms of agonist interact with the ion at every step of the passage. These favorable interactions facilitate ion passage through the pore.

At the selectivity filter, the ion is coordinated by four oxygens of Glu^{IP50} and Glu^{IVP50}, one oxygen of C=O group and one fluorine of CF₃ group of the agonist, and one water molecule (Fig 3.19 A). At the next level below, the coordination sphere of the ion is comprised of four electronegative atoms of Ser^{IS6.13}, Asn^{IIS6.13} and three water molecules. (Fig 3.19 B). Moving further down the pore, the ion approaches the hydrophobic bracelet, interacting with two oxygens of NO₂ group of agonist and five water molecules (Fig 3.19 C). The hydrophilic interactions with the ligand help the ion enter the gate, in the next minimized conformation, shown in Fig 3.19 D, the ion surrounded by hydration shell of seven water molecules is inside the bracelet of S6.17 hydrophobic residues.

In all models, water molecules comprising the hydrophobic shell of the ion do not overlap with any residues or ligand atoms. At the level of hydrophobic gate, the sidechains of S6.17 residues can move enough to accommodate the ion and surrounding seven water molecules. Overall, the formation of the ligand-receptor-hydrated ion complexes does not distort the geometry of the channel at any level of the pore, showing that there is enough space for the ion surrounded by hydration shell to permeate the pore with an agonist bound inside. Ser^{IS6.13}, Asn^{IIS6.13}, which provide favorable hydrophilic contacts to permeating ion, is highly conserved among Ca²⁺ and Na⁺ channels. Their role in modulation of ion passage through the pore can be tested experimentally by mutating them to some hydrophobic residues.

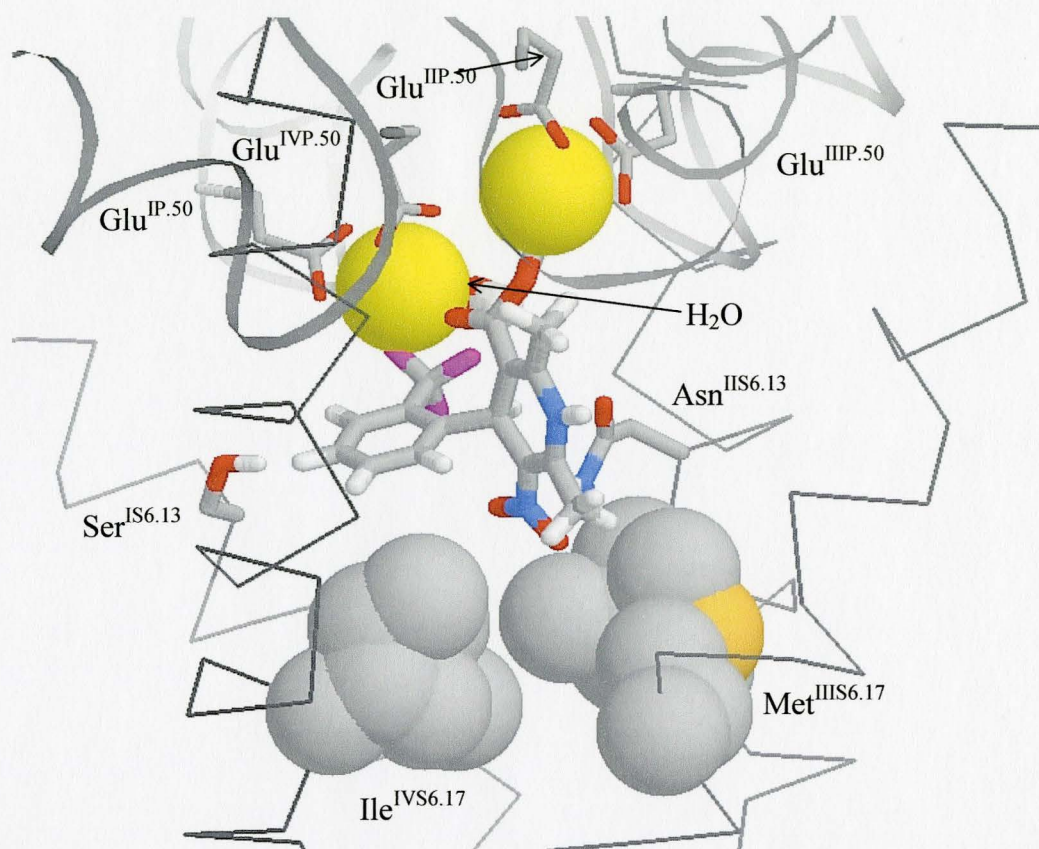


Fig.3.19 A. MC-minimized model of agonist S-Bay K 8644, bound in portside-down mode in the pore of LCC. The agonist, Ca²⁺-bound waters and polar residues involved in Ca²⁺ binding are shown as sticks. Ca²⁺ coordinates four oxygens in Glu^{IP50} and Glu^{IVP50}, one oxygen and two fluorine atoms in DHP, and one water molecule

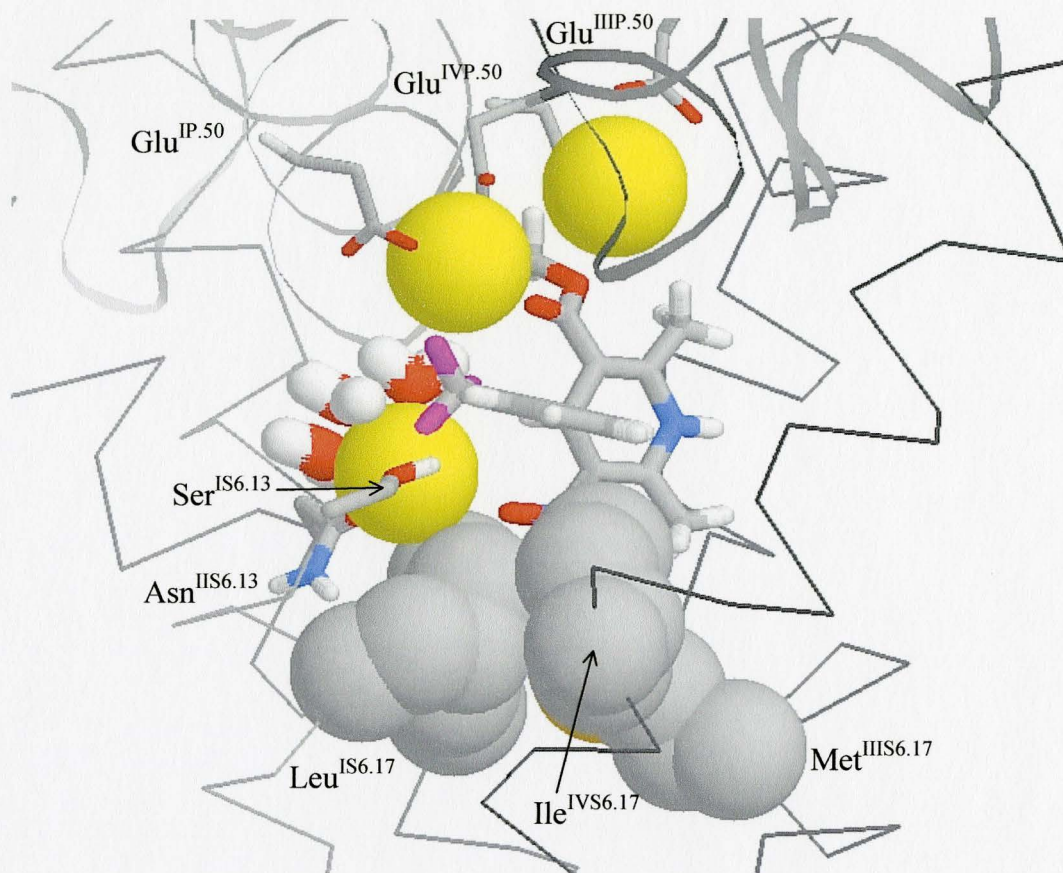


Fig.3.19B. MC-minimized model of agonist S-Bay K 8644, bound in portside-down mode in the pore of LCC (See Fig.3.19 A for other details). Ca^{2+} coordinates four electronegative atoms in Ser^{IS6.13}, Asn^{IIS6.13} and DHP and three waters.

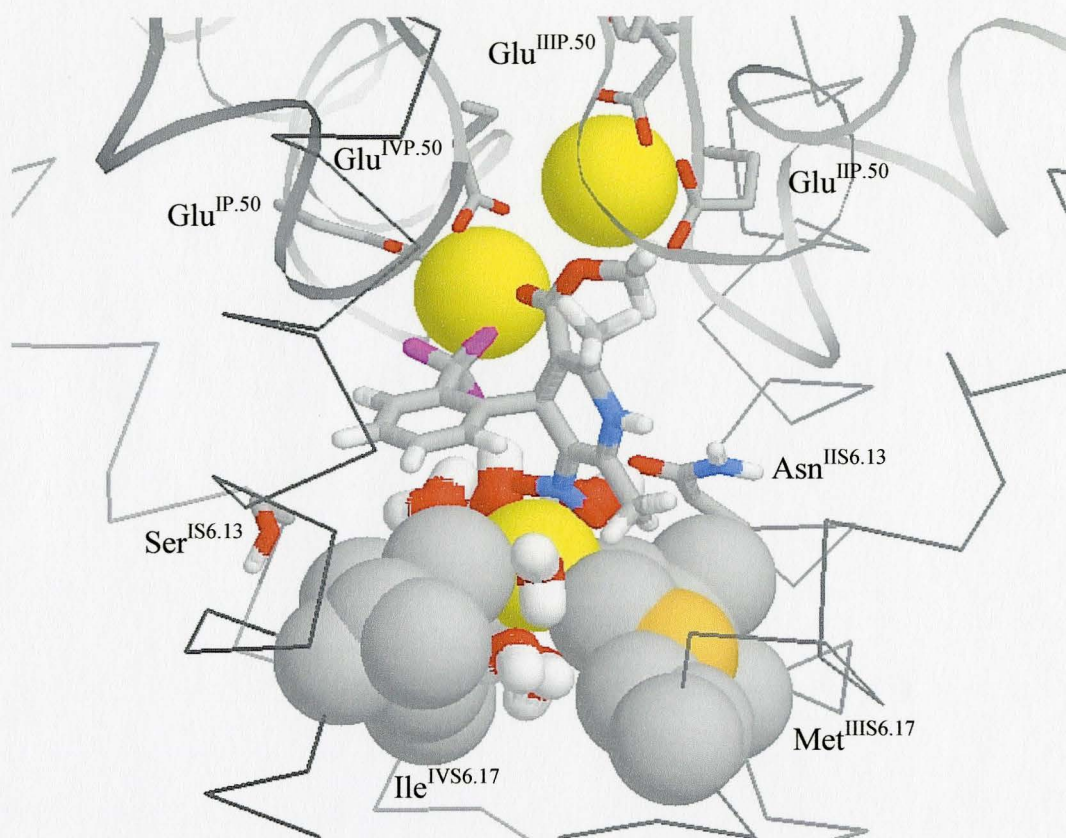


Fig.3.19 C. MC-minimized model of agonist S-Bay K 8644, bound in portside-down mode in the pore of LCC (See Fig.3.19 A for other details). Ca²⁺ coordinates two oxygens in the ligand's NO₂ group and five waters at the extracellular face of the hydrophobic bracelet.

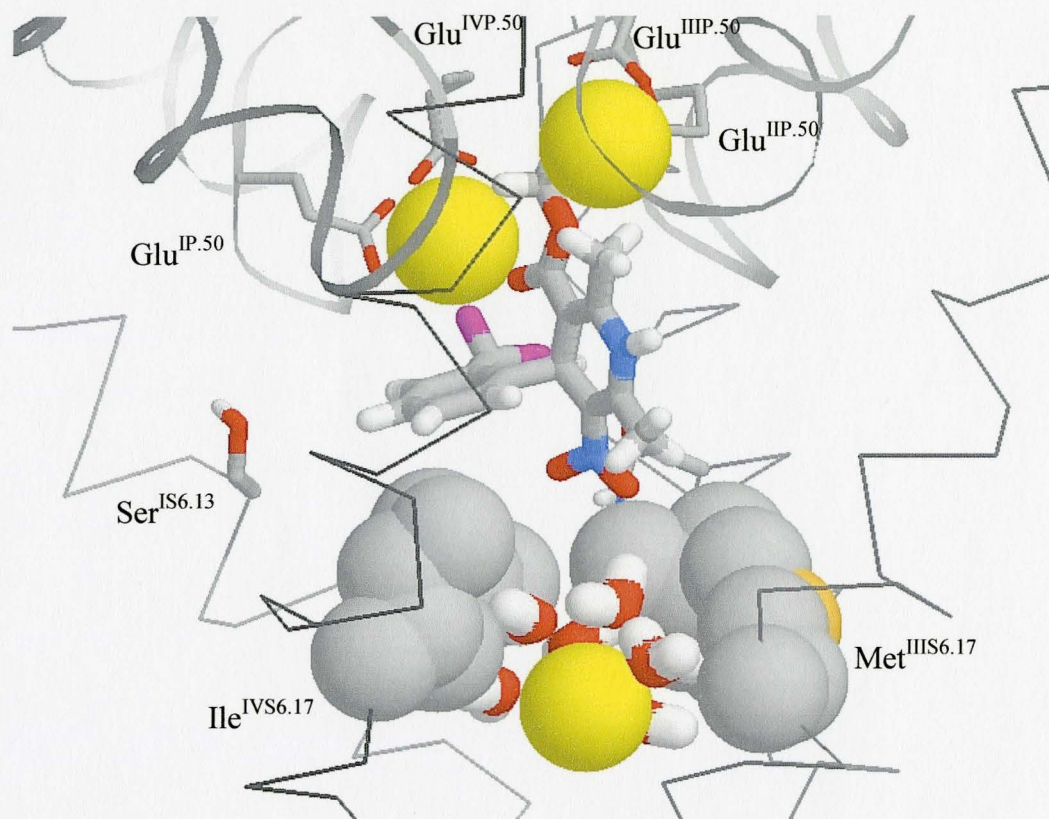


Fig.3.19 *D*. MC-minimized model of agonist S-Bay K 8644, bound in portside-down mode in the pore of LCC (See Fig.3.19 *A* for other details). Ca²⁺ coordinates seven waters inside the hydrophobic bracelet.

Chapter 4. Discussion

The main objective of the current project was to build a model of DHP-binding site of L-type Ca^{2+} channel, which would satisfy available experimental data and suggest explanation for the structure-activity relationships. While the modeling of alpha-helical TM S5 and S6 segments was based on available information about 3D structure of KcsA, we had to use different methods for the modeling of flexible P-loops that form the pore of the channel and contain the selectivity filter. The shaping of P-loops around some rigid LCC drug could provide necessary data about the approximate size and form of the channel pore. (S,S)-(+)-tetrandrine was chosen for this study, because it has a relatively inflexible structure, which would not change during minimization studies, but would force P-loops to adopt some new conformation, different from that of KcsA loops.

There are several data indicating that TD may bind in the region of selectivity filter. First, it competes for the LCC drug diltiazem binding site (King et al. 1989), which is composed of several residues of pore-facing segments IIIS6 and IVS6 (Kraus et al. 1998). On its way to the pore TD should be accommodated inside the selectivity filter region. Second, the presence of TD increases the affinity of some DHP drugs to the channel. The binding of TD into the selectivity filter of LCC with DHP

bound inside the pore below would prevent the DHP drug from leaving its binding site, and, therefore, increases the time of DHP-LCC interaction. These considerations suggest that TD may have its either permanent or transient binding site in the region of the selectivity filter and can be used for the modeling.

In order to find most probable low-energy conformations of TD we performed a thorough computational analysis, starting with more than 200 possible structures of TD. Energy minimization studies, based on the systematic varying of torsion angles, yielded 10 MECs with energies equal or less than 10 kcal/mol. The simple superposition of these conformations showed that seven MECs have the roughly triangular form, similar to X-Ray structure, acquired by Gilmore et al. (1975). More interestingly, the structure of three other MECs was significantly different, with the main TD cycle assuming the quadrangular shape. This alternative structure might also be involved in LCC-drug interaction and required to be taking into consideration during further studies.

TD molecule has several nucleophilic atoms, which can interact with Ca^{2+} ions. The experimental spectroscopic studies of other blockers of LCC, have already shown the formation of the complexes of these drugs with Ca^{2+} ions in non-polar milieu (Ananthanarayanan et al., 1993, Tetrault and Ananthanarayanan, 1993, Belciug and Ananthanarayanan, 1994). Basing on these earlier studies, we have undertaken several NMR experiments to investigate the interaction of TD with Ca^{2+} ions. The results have

shown the formation of 1:1 complex of the drug with Ca^{2+} ion. The modeling of this drug-ion interaction showed the possible structure of the complex formed.

Then we attempted to determine whether one or both families of TD conformations are present in solution, and which of them is stabilized by interaction with Ca^{2+} ions. The NOE spectra of TD alone have yielded the distances between TD protons. These distances were used as constraints during SR MCM, applied to all 10 low-energy MECs of TD. Our results have shown, that while majority of these distances corresponded to both triangular and quadrangular-shaped families of TD conformers, the rest was satisfied either only in the triangular, or only in quadrangular conformation. In particular, nine proton-proton distances, derived from NOE spectra of TD, corresponded to only triangular conformation, and six other distances, derived from the same spectra, corresponded only to the square-shaped TD. This situation is possible only if both families of conformers are present in solution simultaneously.

The same procedure was repeated for the Ca^{2+} - bound TD. Similarly, the distances have been derived and SR MCM search was performed with 10 starting MECs of TD. Again most constraints were satisfied in both conformations. However, there were four distances, which could be satisfied only in triangle conformation, and none of those NOE-derived constraints corresponded to the quadrangular conformation only. Thus we have determined the presence of only triangle-shaped TD conformers in the solution in the presence of Ca^{2+} , which allows us to conclude that the interaction with Ca^{2+} ion

stabilizes the triangular conformation of the drug. The most preferred Ca^{2+} binding site is located in the center of main TD cycle, where triangular-shaped TD has a depression, which size corresponds to the size of Ca^{2+} ion. The ion bound there interacts with three oxygens and form favorable van der Waals contacts with several protons. This binding would prevent conformational rearrangement of the main TD cycle and therefore, transition from the triangular conformation to quadrangular one. The NMR-derived information about the conformation of Ca^{2+} -bound TD in non-polar solution was then used during the modeling of selectivity filter of the channel with TD.

Our modeling studies on TD docking in the selectivity filter region of LCC showed that only small changes on P-loops conformation were required to accommodate TD- Ca^{2+} complex inside the region. While we did not attempt detailed modeling studies of P-loops, the TD docking allowed us to conclude about the general topology of the selectivity filter, including positions of Ca^{2+} ions. In the optimal chelation mode, four ions asymmetrically chelated at two levels of selectivity filter interact with TD nucleophilic atoms. Interestingly, the asymmetry of nucleophilic atoms of TD matched the asymmetric chelation of the ions.

The same chelation pattern was optimal in terms of energy in the case of nifedipine docking into the selectivity filter. For these studies, we used the approximate geometry of P-loops, acquired during TD docking. The modeling data showed that while

the general organization of the channel was kept as in KcsA template, the flexible loops, shaped around TD, can easily accommodate nifedipine on its way to the binding site, located in the pore below the selectivity filter.

Several alignments of TM S6 segments of LCC have been studied. During the docking of nifedipine into the model based on alternative alignment, proposed by Huber et al. (2000), the drug failed to interact with most of the DHP-sensing residues. Both suggested DHP-binding sites, inside the pore and in III/IV interface, were found unpromising for further modeling. In contrast, the docking of DHP into LCC model based on the alignment proposed by Lipkind et al (2000), where DHP-sensing residues of LCC and LA-sensing residues of Na⁺ channel face the pore, resulted in drug forming the maximum number of favorable contacts with conserved residues, mutations of which have been shown to affect the DHP binding.

There are two locations, which were considered as candidates for DHP binding. The first is inside the pore, and the second is in the interface between TM segments III S5-IV S5 and IV S6. Most of DHP-sensing residues are located in TM segments III S6 and IV S6 of LCC. The binding of DHP inside the pore would imply the involvement of not only those segments, but also of TM segments IS6 and IIS6 into the binding. The experimental data indicate that IS6 segment is important for the tissue-specific DHP binding in cardiac and vascular smooth muscle (Welling et al., 1997). Several photolabelling studies suggest DHP interaction with several residues of IS6

segment (Kalasz et al., 1993). Experiments on transferring of some IS6 residues to the chimeric DHP-sensing channel demonstrated increasing of channel inhibition by DHP ligand (Lacinova et al., 1999).

Now, if we consider experimental data which have been used to conclude about location of DHP binding site in the interface between IIIS5-IVS5-IVS6, we see that mutations of only two residues of IIIS5 segment were shown to affect DHP binding. Among them, the mutation of Thr^{IIIS5.16} to a large residue was shown to completely cancel the binding of DHP, while mutation of the same Thr^{IIIS5.16} to Ala residue of similar size had little effect on DHP binding (Huber et al., 2000). The possible explanation for this fact may be that introducing of a large residue into this region affects the DHP binding indirectly, by distorting the complementarity of S6 and S5 segments, which would result in conformational changes in DHP binding site even if its located inside the pore. Thus, taking into account the involvement of IS6 segment into the DHP binding, the location of the binding site inside the pore seems more probable. The results of our modeling studies also support this conclusion.

Our studies have shown that the most preferable orientation of DHP inside the pore is when the portside group of the drug faces down the pore, and the NH-group is oriented towards interface III/IV. This binding mode is stabilized by favorable contacts of DHP phenyl ring with Tyr^{IVS6.9}, and the coordination of NH-group of DHP by hydroxyl groups of Tyr^{IVS6.9} and Tyr^{IIIS6.8}. Mutations of these tyrosines to phenylalanines

decreased DHP affinity by about 12- and 3.5-fold, respectively (Peterson et al., 1996), supporting our conclusion about hydroxyls involvement in DHP binding. Mutation of these Tyr to Ala decreased the affinity even further (Peterson et al., 1996), indicating that the aromatic ring of tyrosine may also be important for interaction with DHP. Since in our model the interaction of DHP ring with aromatic group of Tyr^{IVS6.9} stabilizes the portside-down mode of DHP binding, we suggest that if this residue would be mutated to Ala, the channel would not discriminate between the portside-up and portside-down modes.

In our model, we propose that the channel gating is realized at the level of the crossing of S6 segments. The bracelet of hydrophobically conserved residues Leu^{IS6.17}, Leu^{IIS6.17}, Met^{IIIS6.17} and Ile^{IVS6.17} above the crossing may comprise “the gate”, regulating the ion current through the channel. The permeation of the hydrated Ca²⁺ ion through such hydrophobic bracelet is difficult since it is coupled with detaching of one or several water molecules, depending on the size of the bracelet. Thus, even slight changes in the size of the gate would result in regulation of the current. The modification of the size of the bracelet can be caused either by changes in conformation of the sidechains of hydrophobic residues, as was proposed by Zhorov and Ananthanarayanan (1996), or by small motions of S6 segments, which were detected for the KcsA by Perozo et al (1999).

In the portside-down mode, the enantiomers of Bay K 8644 approach the gate by the substituent group on the portside. Antagonist (R)-Bay K has a hydrophobic methoxy group at its portside. The favorable interaction of this group with the bracelet of hydrophobic residues would result in stabilizing of closed conformation of the gate. In contrast, the portside group of agonist (S)-Bay K is hydrophilic NO_2 . In the hydrophobic region near the gate, this group may interact with hydrated Ca^{2+} ion, thus facilitating its permeation through the gate.

While the blocking of LCC by DHP antagonists always seemed easily explained by simple pore-occluding mechanism, the paradoxical action of DHP agonists, which are also bound inside the pore, remained a mystery. In our studies, we have demonstrated that the hydrated ion can permeate through the agonist-occupied pore of LCC. At all levels of the pore, the channel and the drug provide several electronegative atoms, which interact with the ion and facilitate its permeation. As the rate of water displacement from Ca^{2+} by the residues or the drug (10^8 per second) is much faster than the rate of ion permeation (10^6 per second), the current amplitude does not change in the presence of even large pore-occluding agonists. Finally, we have shown that the sidechains of gate-forming residues can move enough to accommodate the hydrated ion.

Among the residues, which have been shown to interact with the permeating Ca^{2+} ion, Ser^{IIS6.13}, Asn^{IIS6.13} are highly conserved among Ca^{2+} channels. We

suggest that the mutations of them to some bulky hydrophobic residues would result in distortion of the ion current in the presence of agonist.

After the current project was already concluded, some novel experimental data became available. The study of nifedipine analog with ammonium group, attached by alkyl linkers of different length, has shown that the binding domain of the drug is located about 11-14 Å deep in the membrane, underneath the selectivity filter (Peri et al., 2000), supporting the location of DHP binding site inside the pore of the channel, proposed in this study. The attachment of permanently charged trimethylammonium group by octamethylene spacer to the port and starboard sides of DHP demonstrated that the portside-down mode is seven times more preferable than the portside-up binding mode, in complete agreement with our predictions.

Another study has shown the presence of a new DHP-sensing residue, Ser^{IIP.47}, the mutation of which seriously affected the DHP action (Yamaguchi et al., 2000). In our model, this residue interacts with DHP ligands, providing significant contribution to the energy of LCC interaction with pore-bound DHP (see Table 3.12 for partitioned energies of ligand-receptor interaction).

Although the homology modeling approach is shown to be very helpful for our understanding of the unknown 3D organization of many proteins, it is necessary to acknowledge several limitations of this method. First, none of the known methods of

energy minimization can guarantee that the best found conformation represents the global minimum of energy of the protein under investigation. The MCM method, realized in ZMM program that was used in current study, is very effective for the search of the best local minimum in a wide area around the starting point. During several modeling simulations, we varied the starting conformations of the drug bound to the channel, and most of the resulting conformations represented the same local minimum of energy, indicating that we may have found the lowest-energy conformation.

Another important limitation of our modeling is that all calculations were conducted in vacuum; therefore we did not take into consideration the hydrophobic effects. When this problem will be addressed in further modeling studies of LCC, we expect to determine more precisely the magnitudes of the energy of ligand-receptor interactions, which could be compared with those derived from binding experiments. However, the aim of the current study was to perform only initial modeling in order to get clues to the previously unknown location of DHP binding site in LCC and determine the best geometry for ligand-receptor interactions.

The modeling of LCC selectivity filter is also just a rough estimation of the geometry of the P-loops and locations of chelated Ca^{2+} ions. As we mentioned before, we understand that the precise and detailed modeling of this region would require additional experimental data unavailable now.

There are several other approximations in the homology modeling approach, for example, the electrostatic parameters in the force field based on Coulomb equations may sometimes result in an overestimation of electrostatic force. However, in spite of all these limitations, the molecular modeling can be successfully employed when this approach is the only way to determine the unknown protein structure or figure out some mechanisms of protein action.

In conclusion, our model of DHP-binding site of LCC, based on X-Ray structure of KcsA, is in complete agreement with most experimental data, both with those available in the beginning of our study, and with some novel recently released data. The data on Ca^{2+} titration by TD derived from NMR experiments provided necessary information about drug- Ca^{2+} ion complex which may be formed in the region of cell membrane. This information was used for the modeling of selectivity filter of LCC.

We have provided an explanation for the structure-activity relationship paradoxes, such as the opposite effects on the channel by enantiomers of the same drug. Several suggestions for further mutational studies can be made based on our model. The mutation of hydrophobic IS6.17 and IS5.17 residues, forming the part of hydrophobic bracelet of LCC, would affect the channel gating. The conserved residues IS5.13 and IS6.13, which interact with permeating Ca^{2+} ion, may be mutated to some large residues, which would decrease or eliminate the agonist effect on the channel. As the portside-down DHP binding mode has been already shown to be more preferable (Peri et al.,

2000), it would be interesting to check how the aromatic ring of Tyr^{IVS6.9} contributes to stabilization of this binding mode, for example by mutation of this residue to Ala. In addition, the role of conserved acidic residues IP.54, IIP.51, IIP.54 and IVP.54, which are suggested to form the upper part of selectivity filter, is also yet to be studied. All these mutational experiments, along with the model of LCC presented in current study, will help us to understand better the three-dimensional organization of L-type Ca²⁺ channel and its modulation by the ligands.

Chapter 5. Bibliography

- Abagyan, R., and Argos, P. 1992. Optimal Protocol and Trajectory Visualization for Conformational Searches of Peptides and Proteins. *J.Mol.Biol.* 225:519-32
- Almers, W. and McCleskey, E. W. 1984. Non-selective conductance in calcium channels of frog muscle: calcium selectivity in a single-file pore. *J. Physiol. (Lond)*, 353: 585-608
- Ames, J. B., Ishima, R., Tanaka, T., Gordon, J. I., Stryer, L. and Ikura, M. 1997. Molecular mechanics of calcium-myristoyl switches. *Nature (London)* 389, 198–202
- Ananthanarayanan, V. S. 1991. Peptide hormones, neurotransmitters, and drugs as Ca^{2+} ionophores: implications for signal transduction. *Biochem Cell Biol.* 69(2-3):93-5
- Ananthanarayanan, V. S., S. Tetreault, and A. Saint-Jean. 1993. Interaction of calcium channel antagonists with calcium: spectroscopic and modeling studies on diltiazem and its Ca^{2+} complex. *J Med Chem.* 36(10):1324-32
- Ananthanarayanan, V. S., Belciug, M. P., Zhorov, B. S. 1996. Interaction of oxytocin with Ca^{2+} : II. Proton magnetic resonance and molecular modeling studies of conformations of the hormone and its Ca^{2+} complex. *Biopolymers*, 40(5): 445-64

- Bahinski, A., A. Yatani, G. Mikala, S. Tang, S. Yamamoto, and A. Schwartz. 1997. Charged amino acids near the pore entrance influence ion-conduction of a human L-type cardiac calcium channel. *Mol. Cell. Biochem.* 166:125-134
- Baker, O. S., H. P. Larsson, L. M. Mannuzzu, and E. Y. Isacoff. 1998. Three transmembrane conformations and sequence-dependent displacement of the S4 domain in shaker K⁺ channel gating. *Neuron.* 20(6):1283-94
- Bangalore, R., N. Baidur, A. Rutledge, D. J. Triggle, and R. S. Kass. 1994. L-type calcium channels: asymmetrical intramembrane binding domain revealed by variable length, permanently charged 1,4-dihydropyridines. *Mol Pharmacol.* 46(4):660-6
- Bean, B. P. 1989. Multiple types of calcium channels in heart muscle and neurons. Modulation by drugs and neurotransmitters. *Ann N Y Acad Sci.* 560:334-45
- Belciug, M.-P. and V. S. Ananthanarayanan. 1994. Interaction of calcium channel antagonists with calcium: structural studies on nifedipine and its Ca²⁺ complex. *J. Med. Chem.* 37:4392-4399.
- Bezannilla, F., E. Perozo, D. M. Papazian, and E. Stefani. 1991. Molecular basis of gating charge immobilization in Shaker potassium channels. *Science.* 254(5032):679-83
- Bezannilla, F. 2000. The voltage sensor in voltage-dependent ion channels. *Physiol Rev.* 80(2):555-92
- Bezprozvanny, I., R. H. Scheller, and R. W. Tsien. 1995. Functional impact of syntaxin on gating of N-type and Q-type calcium channels. *Nature.* 378(6557):623-6

- Bodi, I., H. Yamaguchi, M. Hara, M. He, A. Schwartz, and G. Varadi. 1997. Molecular studies on the voltage dependence of dihydropyridine action on L-type Ca^{2+} channels. Critical involvement of tyrosine residues in motif IIS6 and IVS6. *J. Biol. Chem.* 272:24952-24960
- Braunewell KH, Gundelfinger ED. 1999. Intracellular neuronal calcium sensor proteins: a family of EF-hand calcium-binding proteins in search of a function. *Cell Tissue Res.*, 295(1):1-12
- Brodersen DE, Etzerodt M, Madsen P, Celis JE, Thogersen HC, Nyborg J, Kjeldgaard M. 1998. EF-hands at atomic resolution: the structure of human psoriasin (S100A7) solved by MAD phasing. *Structure*, 15;6(4):477-89
- Burgess, D. L., J. M. Jones, M. H. Meisler, and J. L. Noebels. 1997. Mutation of the Ca^{2+} channel beta subunit gene *Cchb4* is associated with ataxia and seizures in the lethargic (lh) mouse. *Cell.* 88(3):385-92
- Burgoyne RD, Weiss JL. 2001. The neuronal calcium sensor family of Ca^{2+} -binding proteins/ *Biochem J.* 1;353(Pt 1):1-12
- Canti, C., K. M. Page, G. J. Stephens, and A. C. Dolphin. 1999. Identification of residues in the N terminus of alpha1B critical for inhibition of the voltage-dependent calcium channel by Gbeta gamma. *J Neurosci.* 19(16):6855-64
- Catterall, W. A. 1995. Structure and function of voltage-gated ion channels. *Annu Rev Biochem.* 64:493-531
- Cha, A., G. E. Snyder, P. R. Selvin, and F. Bezanilla. 1999. Atomic scale movement of

- the voltage-sensing region in a potassium channel measured via spectroscopy. *Nature*. 402(6763):809-13
- Chuang, R. S., H. Jaffe, L. Cribbs, E. Perez-Reyes, and K. J. Swartz. 1998. Inhibition of T-type voltage-gated calcium channels by a new scorpion toxin. *Nat Neurosci*. 1(8):668-74
- Cockcroft, V. B., D. J. Osguthorpe, E. A. Barnard, A. E. Friday, and G. G. Lunt. 1990. Ligand-gated ion channels. Homology and diversity. *Mol Neurobiol*. 4(3-4):129-69
- Corpet F. 1988. Multiple sequence alignment with hierarchical clustering. *Nucl. Acids Res.* 16:10881-10890
- Cox, J. A., Malnoe, A. and Stein, E. A. 1981. Regulation of brain cyclic nucleotide phosphodiesterase by calmodulin. *J. Biol. Chem.* 256, 3218–3222
- Davare, M.A., M.C.Horne and J.W.Hell. 2000. Protein phosphatase 2A is associated with class C L-type calcium channels (Cav1.2) and antagonizes channel phosphorylation by cAMP-dependent protein kinase. *J Biol Chem* 275(50):39710-7
- De Jongh, K. S., C. Warner, and W. A. Catterall. 1990. Subunits of purified calcium channels. Alpha 2 and delta are encoded by the same gene. *J Biol Chem*. 265(25):14738-41
- DePover, A., M. A. Matlib, S. W. Lee, G. P. Dube, I. L. Grupp, G. Grupp, and A. Schwartz. 1982. Specific binding of [3H]nitrendipine to membranes from coronary arteries and heart in relation to pharmacological effects.

- Paradoxical stimulation by diltiazem. *Biochem Biophys Res Commun.*
108(1):110-7
- Doring, F., V. E. Degtiar, M. Grabner, J. Striessnig, S. Hering, and H. Glossman. 1996. Transfer of L-type calcium channel IVS6 segment increases phenylalkylamine sensitivity of $\alpha 1A$. *J Biol Chem.* 271(20):11745-9
- Doyle D.A., J.M. Cabral, R.A. Pfuetzner, A. Kuo, J.M. Gulbis, S.L. Cohen, B.T. Chait, and R. MacKinnon 1998. The structure of potassium channel: molecular basis of K^+ conduction and selectivity. *Science.* 280:69-77
- East JM. 2000. Sarco(endo)plasmic reticulum calcium pumps: recent advances in our understanding of structure/function and biology. *Mol.Membr.Biol.*, 17(4):189-200
- Fan, I. Q., B. Chen, and J. D. Marsh. 2000. Transcriptional regulation of L-type calcium channel expression in cardiac myocytes. *J Mol Cell Cardiol.*32(10):1841-9
- Felix, R., C. A. Gurnett, M. De Waard, and K. P. Campbell. 1997. Dissection of functional domains of the voltage-dependent Ca^{2+} channel $\alpha 2\delta$ subunit. *J Neurosci.* 17(18):6884-91
- Felix, R. 2000. Channelopathies: ion channel defects linked to heritable clinical disorders. *J Med Genet.* 37(10):729-40
- Ferry, D. R., and H. Glossmann. 1982. Evidence of multiple receptor sites within the putative calcium channel. *Naunyn Schmiedebergs Arch Pharmacol.*
321(1):80-3
- Ferry, D. R., A. Goll, C. Gadow, and H. Glossmann. 1984. (-)-3H-desmethoxyverapamil

- labelling of putative calcium channels in brain: autoradiographic distribution and allosteric coupling to 1,4-dihydropyridine and diltiazem binding sites. *Naunyn Schmiedebergs Arch Pharmacol.* 327(2):183-7
- Ghazi, A., C. Berrier, B. Ajouz, and M. Besnard. 1998. Mechanosensitive ion channels and their mode of activation. *Biochimie.* 80(5-6):357-62
- Gilmore, C. J., R. F. Bryan, and S. M. Kupchan. 1976. Conformation and reactivity of the macrocyclic tumor-inhibitory alkaloid tetrandrine. *J Am Chem Soc.* 98(7):1947-52
- Gregg, R. G., A. Messing, C. Strube, M. Beurg, R. Moss, M. Behan, M. Sukhareva, S. Haynes, J. A. Powell, R. Coronado, and P. A. Powers. 1996. Absence of the beta subunit (cchb1) of the skeletal muscle dihydropyridine receptor alters expression of the alpha 1 subunit and eliminates excitation-contraction coupling. *Proc Natl Acad Sci U S A.* 93(24):13961-6
- Go, N., Sheraga, H.A. 1970. Ring closure and local conformational deformations of chain molecules. *Macromolecules,* 3:178-187
- Goldmann, S. and J. Stoltefuss. 1991. 1,4-Dihydropyridines - effects of chirality and conformation on the calcium-antagonist and calcium agonist activities. *Angew. Chem. Int. Ed.* 30:1559-1578
- Govyryn, V. A. and B. S. Zhorov. 1994. Ligand-receptor interactions in molecular physiology. Nauka, St.Petersburg, 240 pp. (*in Russian*)
- Grabner, M., Wang, Z., Hering, S., Striessnig, J., Glossmann, H. 1996. Transfer of 1,4-dihydropyridine sensitivity from L-type to class A (BI) calcium channels.

Neuron, 16(1): 207-18

He, M. I. Bodi, G. Mikala, and A. Schwartz. 1997. Motif III5 of L-type calcium channels is involved in the dihydropyridine binding site. A combined radioligand binding and electrophysiological study. *J. Biol. Chem.* 272:2629-2633

Heizmann CW, Cox JA. 1998. New perspectives on S100 proteins: a multifunctional Ca(2+)-, Zn(2+)- and Cu(2+)-binding protein family. *Biomaterials*, 11(4):383-97

Hering, S., Aczel, S., Grabner, M., Doring, F., Berjukow, S., Mitterdorfer, J., Sinnegger, M. J., Striessnig, J., Degtiar, V. E., Wang, Z., Glossmann, H. 1996. Transfer of high sensitivity for benzothiazepines from L-type to class A (BI) calcium channels. *J Biol Chem.*, 271(40): 24471-5

Herlitze, S., D. E. Garcia, K. Mackie, B. Hille, T. Scheuer, and W. A. Catterall. 1996. Modulation of Ca²⁺ channels by G-protein beta gamma subunits. *Nature*. 380(6571):258-62

Herlitze, S., G. H. Hockerman, T. Scheuer, and W. A. Catterall. 1997. Molecular determinants of inactivation and G protein modulation in the intracellular loop connecting domains I and II of the calcium channel alpha1A subunit. *Proc Natl Acad Sci U S A*. 94(4):1512-6

Herzig, S., H. Lullmann, and H. Sieg. 1992. Frequency- and potential-dependency of the negative inotropic action of various dihydropyridine and non-dihydropyridine calcium antagonists. *Pharmacol Toxicol.* 71(3 Pt 1):229-

35

- Hess, P., J. B. Lansman, Tsien, R. W. 1984. Different modes of Ca channel gating behavior favored by dihydropyridine Ca agonists and antagonists. *Nature* 311:538-544
- Hess, P. 1990. Calcium channels in vertebrate cells. *Annu.Rev.Neurosci.*13:337-56
- Hille, B. 1992. Ionic channels of excitable membranes. Sunderland, Mass.:Sinauer Associates, 607 pp.
- Hille, B. 1994. Modulation of ion-channel function by G-protein-coupled receptors. *Trends Neurosci.* 17(12):531-6
- Hockerman, G.H., B.Z. Peterson, B.D. Johnson, and W.A. Catterall. 1997. Molecular determinants of drug binding and action on L-type calcium channels. *Annu. Rev. Pharmacol. Toxicol.* 37:361-396
- Houdusse A, Cohen C. 1996. Structure of the regulatory domain of scallop myosin at 2 Å resolution: implications for regulation. *Structure*, 15;4(1):21-32
- Hovius, R., Vallotton, P., Wohland, T., and H. Vogel. 2000. Fluorescence techniques: shedding light on ligand-receptor interactions. *Trends. Pharmacol. Sci.* 21(7):266-73
- Huber, I., E. Wappl, A. Herzog, J. Mitterdorfer, H. Glossmann, T. Langer, and J. Striessnig 2000. Conserved Ca²⁺-antagonist-binding properties and putative folding structure of a recombinant high-affinity dihydropyridine-binding domain. *Biochem. J.* 347:829-836

- Hymel, L., J. Striessnig, H. Glossmann, and H. Schindler. 1988. Purified skeletal muscle 1,4-dihydropyridine receptor forms phosphorylation-dependent oligomeric calcium channels in planar bilayers. *Proc Natl Acad Sci U S A.* 85(12):4290-4
- Ikeda, S. R. 1996. Voltage-dependent modulation of N-type calcium channels by G-protein beta gamma subunits. *Nature.* 380(6571):255-8
- Isom, L. L., D. S. Ragsdale, K. S. De Jongh, R. E. Westenbroek, B. F. Reber, T. Scheuer, and W. A. Catterall. 1995. Structure and function of the beta 2 subunit of brain sodium channels, a transmembrane glycoprotein with a CAM motif. *Cell.* 83(3):433-42
- Jahn, H., W. Nastainczyk, A. Rohrkasten, T. Schneider, and F. Hofmann. 1988. Site-specific phosphorylation of the purified receptor for calcium-channel blockers by cAMP- and cGMP-dependent protein kinases, protein kinase C, calmodulin-dependent protein kinase II and casein kinase II. *Eur J Biochem.* 178(2):535-42
- James P, Inui M, Tada M, Chiesi M, Carafoli E. 1989. Nature and site of phospholamban regulation of the Ca²⁺ pump of sarcoplasmic reticulum. *Nature* 2;342(6245):90-2
- Jay, S. D., A. H. Sharp, S. D. Kahl, T. S. Vedvick, M. M. Harpold, and K. P. Campbell. 1991. Structural characterization of the dihydropyridine-sensitive calcium channel alpha 2-subunit and the associated delta peptides. *J Biol Chem.* 266(5):3287-93

- Johnson, B. D., G. H. Hockerman, T. Scheuer, and W. A. Catterall. 1996. Distinct effects of mutations in transmembrane segment IVS6 on block of L-type calcium channels by structurally similar phenylalkylamines. *Mol Pharmacol.* 50(5):1388-400
- Jones, S. W., and K. S. Elmslie. 1997. Transmitter modulation of neuronal calcium channels. *J Membr Biol.* 155(1):1-10
- Jones, L. P., P. G. Patil, T. P. Snutch, and D. T. Yue. 1997. G-protein modulation of N-type calcium channel gating current in human embryonic kidney cells (HEK 293). *J Physiol.* 498(Pt 3):601-10
- Kalasz, H., T. Watanabe, H. Yabana, K. Itagaki, K. Naito, H. Nakayama, A. Schwartz, and F.L. Vaghy. 1993. Identification of 1,4-dihydropyridine binding domains within the primary structure of the α_1 subunit of the skeletal muscle L-type calcium channel. *FEBS Lett.* 331:177-181.
- Katz, A. M. 1996. Calcium channel diversity in the cardiovascular system. *J Am Coll Cardiol.* 28(2):522-9
- Kim, M.-S., T. Morii, L.-X. Sun, K. Imoto, and Y. Mori. 1993. Structural determinants of ion selectivity of brain calcium channels. *FEBS Lett.*, 318:145-148 .
- Kimball, S. D., D. M. Floyd, J. Das, J. T. Hunt, J. Krapcho, G. Rovnyak, K. J. Duff, V. . Lee, R. V. Moquin, C. F. Turk, and et al. 1992. Benzazepinone calcium channel blockers. 4. Structure-activity overview and intracellular binding site. *J Med Chem.* 35(4):780-93
- Kimball, S. D., J. T. Hunt, J. C. Barrish, J. Das, D. M. Floyd, M. W. Lago, V. G. Lee, S.

- H. Spergel, S. Moreland, S. A. Hedberg, and et al. 1993. 1-Benzazepin-2-one calcium channel blockers--VI. Receptor-binding model and possible relationship to desmethoxyverapamil. *Bioorg Med Chem.* 1(4):285-307
- Koch, S. E., I. Bodi, A. Schwartz, and G. Varadi. 2000. Architecture of Ca²⁺ channel pore-lining segments revealed by covalent modification of substituted cysteines. *J Biol Chem.* 275(44):34493-500
- Kraus, R., Reichl, E., Kimball, S. D., Grabner, M., Murphy, B. J., Catterall, W. A., Striessnig, J. 1996. Identification of benz(othi)azepine-binding regions within L-type calcium channel alpha1 subunits. *J Biol Chem.* 271(33): 20113-8
- Kraus, R. L., Sinnegger, M. J., Glossmann, H., Hering, S., Striessnig, J. 1998. Familial hemiplegic migraine mutations change alpha1A Ca²⁺ channel kinetics. *J Biol Chem.* 273(10): 5586-90
- Kraus, R. L., Hering, S., Grabner, M., Ostler, D., Striessnig, J. 1998. Molecular mechanism of diltiazem interaction with L-type Ca²⁺ channels. *J Biol Chem.*, 273(42): 27205-12
- Kupchan, S. M., A. J. Liepa, R. L. Baxter, and H. P. Hintz. 1973. New alkaloids and related artifacts from *Cyclea peltata*. *J Org Chem.* 38(10):1846-52
- Kwan, C. Y., H. W. Deng, and Y. Y. Guan. 1992. Tetrandrine is not a selective calcium channel blocker in vascular smooth muscle. *Zhongguo Yao Li Xue Bao.* 13(5):385-90
- Kwan, Y. W., R. Bangalore, M. Lakitsh, H. Glossmann, and R. S. Kass. 1995. Inhibition

- of cardiac L-type calcium channels by quaternary amlodipine: implications for pharmacokinetics and access to dihydropyridine binding site. *J Mol Cell Cardiol.* 27(1):253-62
- Lacinova, L., N. Klugbauer, M. Hu, and F. Hofmann. 1999. Reconstruction of the dihydropyridine site in a non-L-type calcium channel: the role of the IS6 segment. *FEBS Lett.* 451: 152-156
- Ladant, D. 1995. Calcium and membrane binding properties of bovine neurocalcin δ expressed in *Eschericia coli*. *J. Biol. Chem.* 270, 3179–3185
- Qi, X. F., B. S. Zhorov, and V. S. Ananthanarayanan. 2000. CD, ¹H NMR and molecular modeling studies of the interaction of Ca²⁺ with substance P and Ala⁷-substance P in a non-polar solvent. *J Pept Sci.* 6(2):57-83
- Langs, D. A., and D. J. Triggle. 1985. Conformational features of calcium channel agonist and antagonist analogs of nifedipine. *Mol Pharmacol.* 27(5):544-8
- Leao, R. M., J. S. Cruz, C. R. Diniz, M. N. Cordeiro, and P. S. Beirao. 2000. Inhibition of neuronal high-voltage activated calcium channels by the omega-phoneutria nigriverter Tx3-3 peptide toxin. *Neuropharmacology.* 39(10):1756-67
- Lee, K. S., E. Marban, and R. W. Tsien. 1985. Inactivation of calcium channels in mammalian heart cells: joint dependence on membrane potential and intracellular calcium. *J Physiol.* 364:395-411
- Lee, A., S. T. Wong, D. Gallagher, B. Li, D. R. Storm, T. Scheuer, and W. A. Catterall.

1999. Ca^{2+} /calmodulin binds to and modulates P/Q-type calcium channels. *Nature*. 399(6732):155-9
- Lee, A., T. Scheuer, and W. A. Catterall. 2000. Ca^{2+} /calmodulin-dependent facilitation and inactivation of P/Q-type Ca^{2+} channels. *J Neurosci*. 20(18):6830-8
- Lee, A., Wong, S. T., Gallagher, D., Li, B., Storm, D. R., Scheuer, T. and Catterall, W. A. 1999. Ca^{2+} /calmodulin binds to and modulates P/Q type calcium channels. *Nature (London)* 399, 155–159
- Letts, V. A., R. Felix, G. H. Biddlecome, J. Arikath, C. L. Mahaffey, A. Valenzuela, F. S. Bartlett, 2nd, Y. Mori, K. P. Campbell, and W. N. Frankel. 1998. The mouse stargazer gene encodes a neuronal Ca^{2+} -channel gamma subunit. *Nat Genet*. 19(4):340-7
- Liman, E. R., P. Hess, F. Weaver, and G. Koren. 1991. Voltage-sensing residues in the S4 region of a mammalian K^+ channel. *Nature*. 353(6346):752-6
- Li, Z. and H. A. Scheraga. 1987. Monte Carlo-minimization approach to the multiple-minima problem in protein folding. *Proc. Natl. Acad. Sci. U. S. A.* 84:6611-6615
- Lin, L. Z., H. L. Shieh, C. K. Angerhofer, J. M. Pezzuto, G. A. Cordell, L. Xue, M. E. Johnson, and N. Ruangrunsi. 1993. Cytotoxic and antimalarial bisbenzylisoquinoline alkaloids from *Cyclea barbata*. *J Nat Prod*. 56(1):22-9
- Lipkind, G.M. and H.A. Fozzard. 2000. KcsA crystal structure as framework for a molecular model of the Na^+ channel pore. *Biochemistry* 39:8161-8170.

- Llinas, R. R., M. Sugimori, and B. Cherksey. 1989. Voltage-dependent calcium conductances in mammalian neurons. The P channel. *Ann N Y Acad Sci.* 560:103-11
- Logothetis, D. E., S. Movahedi, C. Satler, K. Lindpaintner, and B. Nadal-Ginard. 1992. Incremental reductions of positive charge within the S4 region of a voltage-gated K⁺ channel result in corresponding decreases in gating charge. *Neuron.* 8(3):531-40
- Man in't Veld, A. J. 1989. Calcium antagonists in hypertension. *Am J Med.* 86(4A):6-14
- Masumiya, H., Y. Tanaka, H. Tanaka, and K. Shigenobu. 2000. Inhibition of T-type and L-type Ca²⁺ currents by aranidipine, a novel dihydropyridine Ca²⁺ antagonist. *Pharmacology.* 61(2):57-61
- McCleskey, E. W., A. P. Fox, D. H. Feldman, L. J. Cruz, B. M. Olivera, R. W. Tsien, and D. Yoshikami. 1987. Omega-conotoxin: direct and persistent blockade of specific types of calcium channels in neurons but not muscle. *Proc Natl Acad Sci U S A.* 84(12):4327-31
- McDonald, T. F., D. Pelzer, and W. Trautwein. 1984. Cat ventricular muscle treated with D600: characteristics of calcium channel block and unblock. *J Physiol.* 352:217-41
- McFerran, B. W., Graham, M. E. and Burgoyne, R. D. 1998. NCS-1, the mammalian homologue of frequenin is expressed in chromaffin and PC12 cells and regulates neurosecretion from dense-core granules. *J. Biol. Chem.* 273, 22768–22772

- Meador WE, Means AR, Quioco FA. 1992. Target enzyme recognition by calmodulin: 2.4 Å structure of a calmodulin-peptide complex. *Science*, 28;257(5074):1251-5
- Meador WE, Means AR, Quioco FA. 1993. Modulation of calmodulin plasticity in molecular recognition on the basis of x-ray structures. *Science*, 10;252(5140):1718-21
- Mikala, G., A. Bahinski, A. Yatani, S. Q. Tang, and A. Schwartz. 1993. Differential contribution by conserved glutamate residues to an ion-selectivity site in the L-type Ca²⁺ channel pore. *FEBS Lett.* 335:265-269
- Milani, D., A. Malgaroli, D. Guidolin, C. Fasolato, S. D. Skaper, J. Meldolesi, and T. Pozzan. 1990. Ca²⁺ channels and intracellular Ca²⁺ stores in neuronal and neuroendocrine cells. *Cell Calcium.* 11(2-3):191-9
- Mitterdorfer, J., M. J. Sinnegger, M. Grabner, J. Striessnig, and H. Glossmann. 1995. Coordination of Ca²⁺ by the pore region glutamates is essential for high-affinity dihydropyridine binding to the cardiac Ca²⁺ α₁ subunit. *Biochemistry.* 34: 9350–9355
- Moreno CS, Park S, Nelson K, Ashby D, Hubalek F, Lane WS, Pallas DC. 2000. WD40 repeat proteins striatin and S/G(2) nuclear autoantigen are members of a novel family of calmodulin-binding proteins that associate with protein phosphatase 2A. *J Biol Chem*, 25;275(8):5257-

- Newcomb, R., B. Szoke, A. Palma, G. Wang, X. Chen, W. Hopkins, R. Cong, J. Miller, L. Urge, K. Tarczy-Hornoch, J. A. Loo, D. J. Dooley, L. Nadasdi, R. W. Tsierl, J. Lemos, and G. Miljanich. 1998. Selective peptide antagonist of the class E calcium channel from the venom of the tarantula *Hysterocrates gigas*. *Biochemistry*. 37(44):15353-62
- Nonner, W., L. Catacuzzeno, and B. Eisenberg. 2000. Binding and Selectivity in L-Type Calcium Channels: A Mean Spherical Approximation. *Biophys. J.* 79: 1976-1992
- Nunoki, K., V. Florio, and W. A. Catterall. 1989. Activation of purified calcium channels by stoichiometric protein phosphorylation. *Proc Natl Acad Sci U S A.* 86(17):6816-20
- Ophoff, R. A., G. M. Terwindt, M. N. Vergouwe, R. van Eijk, P. J. Oefner, S. M. Hoffinan, J. E. Lamerdin, H. W. Mohrenweiser, D. E. Bulman, M. Ferrari, J. Haan, D. Lindhout, G. J. van Ommen, M. H. Hofker, M. D. Ferrari, and R. R. Frants. 1996. Familial hemiplegic migraine and episodic ataxia type-2 are caused by mutations in the Ca²⁺ channel gene CACNL1A4. *Cell*. 87(3):543-52
- Opie, L. H. 1988. Calcium channel antagonists. Part IV: Side effects and contraindications drug interactions and combinations. *Cardiovasc Drugs Ther.* 2(2):177-89
- Palczewski, K., T. Kumasaka, T. Hori, C. A. Behnke, H. Motoshima, B. A. Fox, I. Le Triong, D. C. Teller, T. Okada, R. E. Stenkamp, M. Yamamoto, and M.

- Miyéno. 2000. Crystal structure of rhodopsin: A G protein-coupled receptor. *Science*. 289(5480):739-45
- Papazian, D. M., L. C. Timpe, Y. N. Jan, and L. Y. Jan. 1991. Alteration of voltage-dependence of Shaker potassium channel by mutations in the S4 sequence. *Nature*. 349(6307):305-10
- Pelton, J.T., and L.R.McLean. 2000. Spectroscopic methods for analysis of protein secondary structure. *Anal Biochem* . 277(2):167-76
- Perez-Reyes, E., L. L. Cribbs, A. Daud, A. E. Lacerda, J. Barclay, M. P. Williamson, M. Fox, M. Rees, and J. H. Lee. 1998. Molecular characterization of a neuronal low-voltage-activated T-type calcium channel. *Nature*. 391(6670):896-900
- Peri, R., S. Padmanabhan, A. Rutledge, S. Singh, and D. J. Triggle. 2000. Permanently charged chiral 1,4-dihydropyridines: molecular probes of L-type calcium channels. Synthesis and pharmacological characterization of methyl(omega-trimethylalkylammonium) 1,4-dihydro-2,6-dimethyl-4-(3-nitrophenyl)-3,5-pyridinedicarboxylate iodide, calcium channel antagonists. *J. Med. Chem.* 43:2906-14
- Perozo, E., D.M. Cortes, and L.G. Cuello. 1998. Three-dimensional architecture and gating mechanism of a K⁺ channel studied by EPR spectroscopy. *Nature Struct. Biol.* 5:459-469
- Perozo, E., D.M. Cortes, and L.G. Cuello. 1999. Structural rearrangements underlying K⁺-channel activation gating. *Science* 285:73-78.

- Peterson, B.Z. and W.A. Catterall. 1995. Calcium binding in the pore of L-type calcium channels modulates high affinity dihydropyridine binding. *J. Biol. Chem.* 270:18201–18204
- Peterson, B.Z., T.N. Tanada, and W.A. Catterall. 1996. Molecular determinants of high affinity dihydropyridine binding in L-type calcium channel. *J. Biol. Chem.* 271:52930-5296
- Peterson, B.Z., B.D. Johnson, G.H. Hockerman, M. Acheson, T. Scheuer, and W.A. Catterall. 1997. Analysis of the dihydropyridine receptor site of L-type calcium channels by alanine-scanning mutagenesis. *J. Biol. Chem.* 272:18752-18765
- Peterson, B. Z., C. D. DeMaria, J. P. Adelman, and D. T. Yue. 1999. Calmodulin is the Ca^{2+} sensor for Ca^{2+} -dependent inactivation of L-type calcium channels. *Neuron*. 22(3):549-58
- Peterson, B. Z., DeMaria, C. D. and Yue, D. T. 1999. Calmodulin is the Ca^{2+} sensor for Ca^{2+} -dependent inactivation of L-type calcium channels. *Neuron* 22, 549–558
- Ragsdale, D. S., J. C. McPhee, T. Scheuer, and W. A. Catterall. 1994. Molecular determinants of state-dependent block of Na^+ channels by local anesthetics. *Science*. 265:1724-8
- Randall, A., and R. W. Tsien. 1995. Pharmacological dissection of multiple types of Ca^{2+} channel currents in rat cerebellar granule neurons. *J Neurosci*. 15(4):2995-3012

- Reuter, H. 1974. Localization of beta adrenergic receptors, and effects of noradrenaline and cyclic nucleotides on action potentials, ionic currents and tension in mammalian cardiac muscle. *J Physiol.* 242(2):429-51
- Reuter, H., and H. Scholz. 1977. The regulation of the calcium conductance of cardiac muscle by adrenaline. *J Physiol.* 264(1):49-62
- Roguin, A., and Y. Edoute. 1999. [Mibefradil--a T-type calcium channel blocker]. *Harefuah.* 136(2):167-9
- Ruth, P., A. Rohrkasten, M. Biel, E. Bosse, S. Regulla, H. E. Meyer, V. Flockerzi, and F. Hofmann. 1989. Primary structure of the beta subunit of the DHP-sensitive calcium channel from skeletal muscle. *Science.* 245(4922):1115-8
- Schafer BW, Heizmann CW. 1996. The S100 family of EF-hand calcium-binding proteins: functions and pathology. *Trends Biochem.Sci.*, 21(4):134-40
- Seydl, K., D. Kimball, H. Schindler, and C. Romanin. 1993. The benzazepine/benzothiazepine binding domain of the cardiac L-type Ca^{2+} channel is accessible only from the extracellular side. *Pflugers Arch.* 424(5-6):552-4
- Silverstein, R.M., Bassler, G.C., and T.C.Morrill. 1991. Spectrometric identification of organic compounds. 5th edition. John Wiley & Sons. 418 pp.
- Sobieszek A, Babiychuk EB, Ortner B, Borkowski J. 1997. Purification and characterization of a kinase-associated, myofibrillar smooth muscle myosin light chain phosphatase possessing a calmodulin-

targeting subunit. *J Biol Chem*, 14;272(11):7027-33

- Striessnig, J., B. J. Murphy, and W. A. Catterall. 1991. Dihydropyridine receptor of L-type Ca^{2+} channels: identification of binding domains for [3H](+)-PN200-110 and [3H]azidopine within the alpha 1 subunit. *Proc Natl Acad Sci U S A*. 88(23):10769-73
- Strynadka NC, Cherney M, Sielecki AR, Li MX, Smillie LB, James MN. 1997. Structural details of a calcium-induced molecular switch: X-ray crystallographic analysis of the calcium-saturated N-terminal domain of troponin C at 1.75 Å resolution. *J Mol Biol*, 17;273(1):238-55
- Takahashi, M., M. J. Seagar, J. F. Jones, B. F. Reber, and W. A. Catterall. 1987. Subunit structure of dihydropyridine-sensitive calcium channels from skeletal muscle. *Proc Natl Acad Sci U S A*. 84(15):5478-82
- Tanabe, T., K. G. Beam, J. A. Powell, and S. Numa. 1988. Restoration of excitation-contraction coupling and slow calcium current in dysgenic muscle by dihydropyridine receptor complementary DNA. *Nature*. 336(6195):134-9
- Tetreault, S., and V. S. Ananthanarayanan. 1993. Interaction of calcium channel antagonists with calcium: structural studies on verapamil and its Ca^{2+} complex. *J Med Chem*. 36(8):1017-23
- Toyoshima C, Nakasako M, Nomura H, Ogawa H. 2000. Crystal structure of the calcium pump of sarcoplasmic reticulum at 2.6 Å resolution. *Nature*, 8;405(6787):647-55
- Triggle, D. J. 1997. Cardiovascular T-type calcium channels: physiological and

- pharmacological significance. *J Hypertens Suppl.* 15(5):S9-15
- Triggle, D. J. 1999. The pharmacology of ion channels: with particular reference to voltage-gated Ca²⁺ channels. *Eur J Pharmacol.* 375(1-3):311-25
- Tsien, R. W., P. Hess, E. W. McCleskey, and R. L. Rosenberg. 1987. Calcium channels: mechanisms of selectivity, permeation, and block. *Annu Rev Biophys Biophys Chem.* 16:265-90
- Tsien, R. W., A. P. Fox, P. Hess, E. W. McCleskey, B. Nilius, M. C. Nowycky, and R. L. Rosenberg. 1987. Multiple types of calcium channel in excitable cells. *Soc Gen Physiol Ser.* 41:167-87
- Uchida, K., and P. M. Iuvone. 1999. Intracellular Ca²⁺ concentrations in cultured chicken photoreceptor cells: sustained elevation in depolarized cells and the role of dihydropyridine-sensitive Ca²⁺ channels. *Mol Vis.* 5:1
- Varadi, G., Mori, Y., Mikala, G., Schwartz, A. 1995. Molecular determinants of Ca²⁺ channel function and drug action. *Trends Pharmacol Sci.* 16(2): 43-9
- Varadi, G., M. Strobeck, S. Koch, L. Caglioti, C. Zucchi, and G. Palyi. 1999. Molecular elements of ion permeation and selectivity within calcium channels. *Crit. Rev. Biochem. Mol. Biol.* 34:181-214
- Wallner, M., P. Meera, M. Ottolia, G. J. Kaczorowski, R. Latorre, M. L. Garcia, E. Stefani, and L. Toro. 1995. Characterization of and modulation by a beta-subunit of a human maxi KCa channel cloned from myometrium. *Receptors Channels.* 3(3):185-99
- Wang, G., and J. R. Lemos. 1995. Tetrandrine: a new ligand to block voltage-dependent

Ca²⁺ and Ca²⁺-activated K⁺ channels. *Life Sci.* 56(5):295-306

Wang, T. J., J. C. Ausiello, and R. S. Stafford. 1999. Trends in antihypertensive drug advertising, 1985-1996. *Circulation.* 99(15):2055-7

Wei, X. Y., Luchowski, E.M., Rutledge, A., Su, C.M., and D.J. Triggle. 1986. Pharmacologic and radioligand binding analysis of the actions of 1,4-dihydropyridine activator-antagonist pairs in smooth muscle. *J Pharmacol Exp Ther.* 239(1):144-53

Wei, X. Y., E. Perez-Reyes, A. E. Lacerda, G. Schuster, A. M. Brown, and L. Birnbaumer. 1991. Heterologous regulation of the cardiac Ca²⁺ channel alpha 1 subunit by skeletal muscle beta and gamma subunits. Implications for the structure of cardiac L-type Ca²⁺ channels. *J Biol Chem.* 266(32):21943-7

Weiner, S.J., P.A. Kollman, D.A. Case, U.C. Singh, C. Ghio, G. Alagona, S. Profeta, and P. Weiner. 1984. A new force field for molecular mechanical simulation of nucleic acids and proteins. *J. Am. Chem. Soc.* 106:765-784.

Weiss, S. 2000. Measuring conformational dynamics of biomolecules by single molecule fluorescence spectroscopy. *Nat Struct Biol.* 7(9):724-9

Welling, A., A. Ludwig, S. Zimmer, N. Klugbauer, V. Flockerzi, and F. Hofmann. 1997. Alternatively spliced IS6 segments of the α_{1C} gene determine the tissue-specific dihydropyridine sensitivity of cardiac and vascular smooth muscle L-type Ca²⁺ channels. *Circ. Res.* 81:526-532.

Wiser, O., M. K. Bennett, and D. Atlas. 1996. Functional interaction of syntaxin and

- SNAP-25 with voltage-sensitive L- and N-type Ca^{2+} channels. *Embo J.* 15(16):4100-10
- Yamaguchi, S., Y. Okamura, T. Nagao, and S. Adachi-Akahane. 2000. Serine residue in the IIS5-S6 linker of the L-type Ca^{2+} channel alpha 1C subunit is the critical determinant of the action of dihydropyridine Ca^{2+} channel agonists. *J. Biol. Chem.* 275:41504-11
- Yamamoto Y, Sokawa Y, Maekawa S. 1997. Biochemical evidence for the presence of NAP-22, a novel acidic calmodulin binding protein, in the synaptic vesicles of rat brain. *Neurosci Lett.*, 14;224(2):127-30
- Yang, J., P.T. Ellinor, W.A. Sather, J-F. Zhang, and R.W. Tsien. 1993. Molecular determinants of Ca^{2+} selectivity and ion permeation in L-type Ca^{2+} channels. *Nature.* 366:158-161.
- Yellen, G. 1999. The bacterial K^+ channel structure and its implications for neuronal channels. *Current Opin. Neurobiol.* 9:267-273
- Zamponi, G. W., and T. P. Snutch. 1998. Modulation of voltage-dependent calcium channels by G proteins. *Curr Opin Neurobiol.* 8(3):351-6
- Zhorov, B.S. 1981. Vector method for calculating derivatives of energy of atom-atom interactions of complex molecules according to generalized coordinates. *J.Struct.Chem.* 22:4-8
- Zhorov, B. S. and Brovtyna, N. B. 1993. Conformational analysis of d-tubocurarine: implications for minimal dimensions of its binding site within ion channels. *J Membr Biol.* 135: 19-26

- Zhorov, B. S. 1993. Comparison of lowest energy conformations of dimethylcurine and methoxyverapamil: evidence of ternary association of calcium channel, Ca^{2+} , and calcium entry blockers. *J Membr Biol.* 135(2):119-27
- Zhorov, B.S. and V.S. Ananthanarayanan. 1996. Structural model of a synthetic Ca^{2+} channel with bound Ca^{2+} ions and dihydropyridine ligands. *Biophys. J.* 70:22-37
- Zhorov, B. S., and V. S. Ananthanarayanan. 1998. Signal transduction within G-protein coupled receptors via an ion tunnel: a hypothesis. *J Biomol Struct Dyn.* 15(4):631-7
- Zhorov, B. S., and V. S. Ananthanarayanan. 2000. Homology models of mu-opioid receptor with organic and inorganic cations at conserved aspartates in the second and third transmembrane domains. *Arch Biochem Biophys.* 375(1):31-49
- Zhorov, B. S., and P. D. Bregestovski. 2000. Chloride channels of glycine and GABA receptors with blockers: Monte Carlo minimization and structure-activity relationships. *Biophys J.* 78(4):1786-803
- Zhorov, B.S., E. Folkman, and V.S. Ananthanarayanan. 2001. Homology modeling of L-type calcium channel with agonists and antagonists. *Arch Biochem Biophys.* (accepted for publication)
- Zuhlke, R. D., and H. Reuter. 1998. Ca^{2+} -sensitive inactivation of L-type Ca^{2+} channels depends on multiple cytoplasmic amino acid sequences of the $\alpha_1\text{C}$ subunit. *Proc Natl Acad Sci U S A.* 95(6):3287-94